VARIABILITY OF THE STRATIFIED FLOW IN THE PASSAGES CONNECTING GREEN BAY AND LAKE MICHIGAN

by

Erik S. Gottlieb

A dissertation submitted in partial fulfillment
of the requirements for the degree of
Doctor of Philosophy
(Oceanic Science)
in The University of Michigan
1992

Doctoral Committee:

Associate Professor Guy Meadows, Co-Chair
James Saylor, Physical Scientist, Great Lakes Environmental Research Laboratory (GLERL), Co-Chair
Assistant Professor Giles Brereton
Professor Donald Portman
Alan Bratkovich, Oceanographer, GLERL

ACKNOWLEDGEMENTS

I would like to thank all members of my committee for their advice and suggestions, and to the scientists and staff at the Great Lakes Environmental Research Laboratory for their support. I would like to give special thanks to Gerry Miller, Terry Miller and Ron Muzzi for their technical expertise, and to John Grimes and Dave Morse for their help in the field. Finally, I want to acknowledge my parents and my wife for their unconditional and unending support.

TABLE OF CONTENTS

ACKNOWLEDGEMENTS ii

LIST OF FIGURES v

LIST OF TABLES viii

CHAPTER

I. INTRODUCTION 1

Purpose of Investigation
Physical Characteristics of Green Bay and the Passages
Brief Description of Present Investigation

II. PREVIOUS INVESTIGATIONS AND THEORETICAL CONSIDERATIONS 8

Investigations of Green Bay
Laboratory Investigations
Non-Rotating Theoretical Investigations
Rotating Theoretical Investigations
Other Related Investigations
Conceptual Framework for Present Investigation

III. PRESENTATION AND DESCRIPTION OF THE CURRENT, TEMPERATURE, WATER LEVEL AND METEOROLOGICAL OBSERVATIONS 28

Description of Data Set and Processing Techniques
Averaged Data from the 1977 and 1989 Stratified Seasons
1989 XBT Transects and Related Raw Data
Samples of the Raw Data from 1977 and 1989

IV. ANALYSIS OF THE STRATIFIED VOLUME EXCHANGES 57

Volume Transport Computations and Results
Spectral and Cospectral Analyses
Joint Occurrence Distributions and Scatter Plots

V. DISCUSSION OF THE STRATIFIED VOLUME EXCHANGES 74

VI. CONCLUSIONS 82

APPENDIX 85

BIBLIOGRAPHY 90

LIST OF FIGURES

Figure

1.1 Surface map of Green Bay, Lake Michigan 5

1.2 Bathymetric map of the Green Bay mouth region..... 6

1.3 Bathymetric map of the northern Green Bay region 7

2.1 Schematic diagram of an ocean estuary 8

2.2 Schematic diagram of two-layer exchange with a sinusoidal net barotropic current component 13

2.3 Idealized vertical profiles of interface shape with varying magnitudes of two-layer exchange flows 16

2.4 As in Fig. 2.3, but with varying component of barotropic flow 17

2.5 Box-flow model for single-layer exchange 19

2.6 Schematic diagram of Kelvin wave propagation out of a channel.....21

2.7 Conceptual model of the expected effects of rotation on the currents and temperatures observed during the stratified season in the passages connecting Green Bay and Lake Michigan 26

2.8 Conceptual model of a two-layered density structure with a tilted thermocline across the bay mouth.....26

2.9 Conceptual model of the effects of Ekman transport on the water surface level and thermocline depth in the region of the bay mouth 27

3.1 Map indicating mooring numbers.....28

3.2 40-hour low-pass filtered currents and temperatures in Deaths Door, Rock Island, St. Martin Island, and Poverty Island Passages during the 1977 stratified season 44

3.3 40-hour low-pass filtered temperatures, lower-layer currents, and winds during the 1977 and 1989 stratified seasons 45

LIST OF FIGURES (CONTINUED)

Figure

3.4 40-hour low-pass filtered currents in Deaths Door and Rock Island Passages, and computed volume transports through all major passages in Green Bay during 1989.....46

3.5 XBT temperatures during July 22 and Oct. 10, 1989 along a transect through Deaths Door Passage.....47

3.6 Raw hourly currents and temperatures in Deaths Door Passage, and meteorological data from the same times as the XBT transects shown in Fig. 3.5.....48

3.7 Raw hourly currents in Rock Island and St. Martin Island Passages, and temperatures in all three passages from the same times as the XBT transects shown in Fig. 3.5.....49

3.8 Raw hourly water levels in Green Bay and Lake Michigan from the same times as the XBT transects shown in Fig. 3.5.....50

3.9 Raw hourly currents and temperatures in Deaths Door, Rock Island, and Poverty Island Passages, and meteorological data during July 14-26 and Aug. 7-19, 1977.....51

3.10 Raw hourly currents and temperatures in Deaths Door and Rock Island Passages, and meteorological data during July 26 to Aug. 19, 1989.....52

3.11 Raw hourly thermistor chain recordings from Rock Island Passage during July 26 to Aug. 11, 1989.....53

3.12 As in Fig. 3.10, during Sep. 25 to Oct. 7, 1989.....54

3.13 As in Fig. 3.11, during Sep. 13-29.....55

3.14 As in Fig. 3.7, showing currents and temperatures from two locations within Deaths Door Passage.....56

4.1 Power spectra and cospectra for the 12.0 and 20.0 m velocities from Deaths Door Passage during 1989.....60

4.2 As in Fig. 4.1, for the 20.0 m temperature and 29.8 m velocity.....60

LIST OF FIGURES (CONTINUED)

Figure

4.3 Scatter plots from Deaths Door Passage during 1977 and 1989 69

4.4 As in Fig. 4.3, from Rock Island Passage.....70

4.5 As in Fig. 4.3, from Poverty and St. Martin Island Passages.....71

4.6 Joint occurrence distributions of lower-layer velocity vs. cross-mouth density difference for the top depth level during 1977 and 1989.....72

4.7 As in Fig. 4.6, for the middle and bottom depth levels during 1989.....73

LIST OF TABLES

Table

3.1 Mooring number, location, depth, and time of each station along the XBT transect 34

3.2 Monthly averages of the raw temperatures from each mooring and depth level during July, Aug., and Sept. of 1989 36

4.1 Start and stop dates, number of points, and number of subseries for each of the raw time series records used in the spectral analysis..... 60

4.2 Mean, trend, and percent of total variance accounted for by low, semidiurnal, 1st mode, and 2nd mode frequencies for each along-channel velocity component series..... 61

4.3 Results of cospectral analysis for each along-channel velocity component series during 1989 61

4.4 Joint occurrence distributions of unidirectional and opposing flow directions observed through Deaths Door and Rock Island Passages..... 64

CHAPTER I

INTRODUCTION

Purpose of Investigation

Green Bay is a long, narrow, shallow gulf connected to the northwestern side of Lake Michigan (Fig. 1.1). The bay contains less than two percent of the total water volume contained in the lake, but about one third of the total Lake Michigan watershed drains into the bay. During this century, agricultural runoff, municipal waste water discharges, and industrial pollution (most notably from paper mills) have adversely affected water quality in the very shallow southern waters of the bay. Despite flushing by cleaner Lake Michigan waters and the recent implementation of the Lower Green Bay and Fox River Remedial Action Plan, water quality remains poor (Great Lakes Reporter, 1989).

During the stratified season (usually from late spring to mid-autumn), warm and polluted Fox River water enters Green Bay at the city of Green Bay, WI (Fig. 1.1), and circulates and mixes with the cooler and cleaner waters in the bay. Fox River water has been traced as far as 40 km away from the river mouth (Modlin and Beeton, 1970), but more typically is mixed with cooler Lake Michigan-originating water by lunar tide and seiche motions. These motions also influence the waters exchanged between Green Bay and Lake Michigan. Thus, knowledge of the response of the bay's waters and the Lake Michigan exchange waters to the forces acting on them are needed to determine the loading, transport, and fate of toxic contaminants within the bay's aquatic environment. Or in other words, mixing and flushing of the waters within Green Bay help determine the fate of pollutants within the bay.

To aid evaluation of the sources, transport, and fate of contaminants in Green Bay, and to help prioritize and allocate research, remedial actions, and regulatory efforts, the United States Environmental Protection Agency initiated the Green Bay/Fox River Mass Balance Study (U.S.E.P.A., 1989). The mass balance approach is based on the law of conservation of mass, where "the quantities of contaminants entering the system, less quantities stored or transformed within the system, must equal the quantities leaving the system". As previously mentioned, a major route via which contaminants leave Green Bay is through the bay mouth and out into Lake Michigan, and thus knowledge of water volume exchange rates between the bay and lake are required for mass balance modelling. The present investigation was undertaken as part of the Mass Balance Study to measure and record the currents flowing into and out of the bay mouth, and to compute directly the water volume exchange rates occurring between Green Bay and Lake Michigan.

Using current meters and other instrumentation, the flow through the passages connecting the bay and Lake Michigan (Fig. 1.2), and also through the passages connecting the northern and southern halves of the bay (Fig. 1.3), was measured during 1977 and again during 1988-1989. Comparison with meteorological and water level data will demonstrate how atmospheric forcing, tidal forcing, and both surface and internal (thermocline) seiching affect the exchange of waters through the bay mouth passages and the subsequent flushing of the bay. Thus, the main goals of the present investigation are:

1) Identify the important bay/lake water volume exchange processes, and help reveal the underlying hydrodynamics during the stratified season.

2) Describe the variability in the stratified volume exchange, and relate it to variability in atmospheric forcing, water levels, and internal density structure.

3) Estimate the average magnitude of the stratified water volume exchange.

This information will be required by Green Bay mass balance modelers, and will be of general interest to hydrodynamicists, limnologists, and physical oceanographers.

Physical Characteristics of Green Bay and the Passages

Green Bay is 193 km long and 22 km wide, averages 15.8 m deep, is 4250 km^2 in surface area, and has a volume of 67 km^3, as described by Mortimer (1978). The bathymetry within the bay is generally characterized by broad central plains edged by steeply sloped coasts (see Fig. 1.3 for example), and the bay's northern and southern extremes are comprised of broad shallows. The bay is divided into northern and southern halves by Chambers Island (Figs. 1.1 and 1.3), and thus exchange of waters between the halves is confined to the passages on either side of the island (Fig. 1.3). The western Chambers Island passage is about 10 km wide and averages 22 m deep, while the eastern passage is much more constricted in both width and depth.

The exchange of waters between Green Bay and Lake Michigan is mostly confined to the four main passages (see Fig. 1.1) located across the mouth of Green Bay. Currents through the narrow Sturgeon Bay canal (Fig. 1.1) can be strong at times, but transport insignificant amounts of water (Saylor, 1964). The present investigation will focus on the Green Bay mouth region (Fig. 1.2), where the complicated bathymetry can be described generally as a series of islands separated by meandering passages which have very steeply sloped sides. Going from south to north (Figs. 1.1 and 1.2), Deaths Door Passage is relatively deep and narrow, Rock Island Passage is the deepest and widest, St. Martin Island Passage is shallow and narrow, and Poverty Island Passage is shallow and wide. These passages range from 24 to 44 m in depth, from 2.2 to 4.0 km in width, and are 0.52 km^2 in cross-sectional area along a transect defined by Mortimer (1978); this area is roughly equivalent to that across the Chambers Island passages. Specific physical dimensions of each passage are listed in the Appendix.

Due to its relatively shallow depth, strong thermal stratification of the waters within Green Bay is maintained throughout the spring, summer, and autumn months. During this stratified season, a sharp thermocline separates the bay's waters into upper

(above the thermocline) and lower (below) layers. A thermocline also exists in Lake Michigan, and due to the greater depths the lower-layer water is much colder (and denser) in the lake than in the bay. Thus, below the thermocline there exists a horizontal pressure gradient component that drives the colder and denser lower-layer lake water into Green Bay, and to compensate upper-layer water from the bay exits into Lake Michigan. This process is called "two-layer" or "estuarine" exchange, and is the main focus of the present investigation.

Brief Description of Present Investigation

The present investigation will utilize data collected during 1977 (Miller and Saylor, 1985) and 1989 (Gottlieb, Saylor, and Miller, 1990), and will be limited to the season when thermal stratification is present. Even though wintertime currents can remain quite active under the ice (Gottlieb *et al.*, 1990), intense summertime stratification causes two-layered currents and water temperatures within the passages, resulting in the most dynamically complex exchange processes observed throughout the year. Also, the present investigation will be limited mostly to the mouth region passages (Figs. 1.1 and 1.2); the Chambers Island flanking passages were the subject of a separate investigation (Miller and Saylor, 1992).

While oceanic passages have been the subject of frequent and sometimes extensive field investigations - Drake Passage and the Strait of Gibraltar are the most notable examples - similar investigations in smaller fresh water passages are lacking. However, the dynamics of two-layered volume exchanges have been the subject of extensive theoretical and some laboratory investigations, and representative examples of these investigations are described in Chapter II. Chapter III includes a graphical presentation of some of the current meter and meteorological data, a description of the observed two-layered exchanges and other phenomena, and volume transport values computed using the current meter data, and in Chapter IV the observations are compared with the theories.

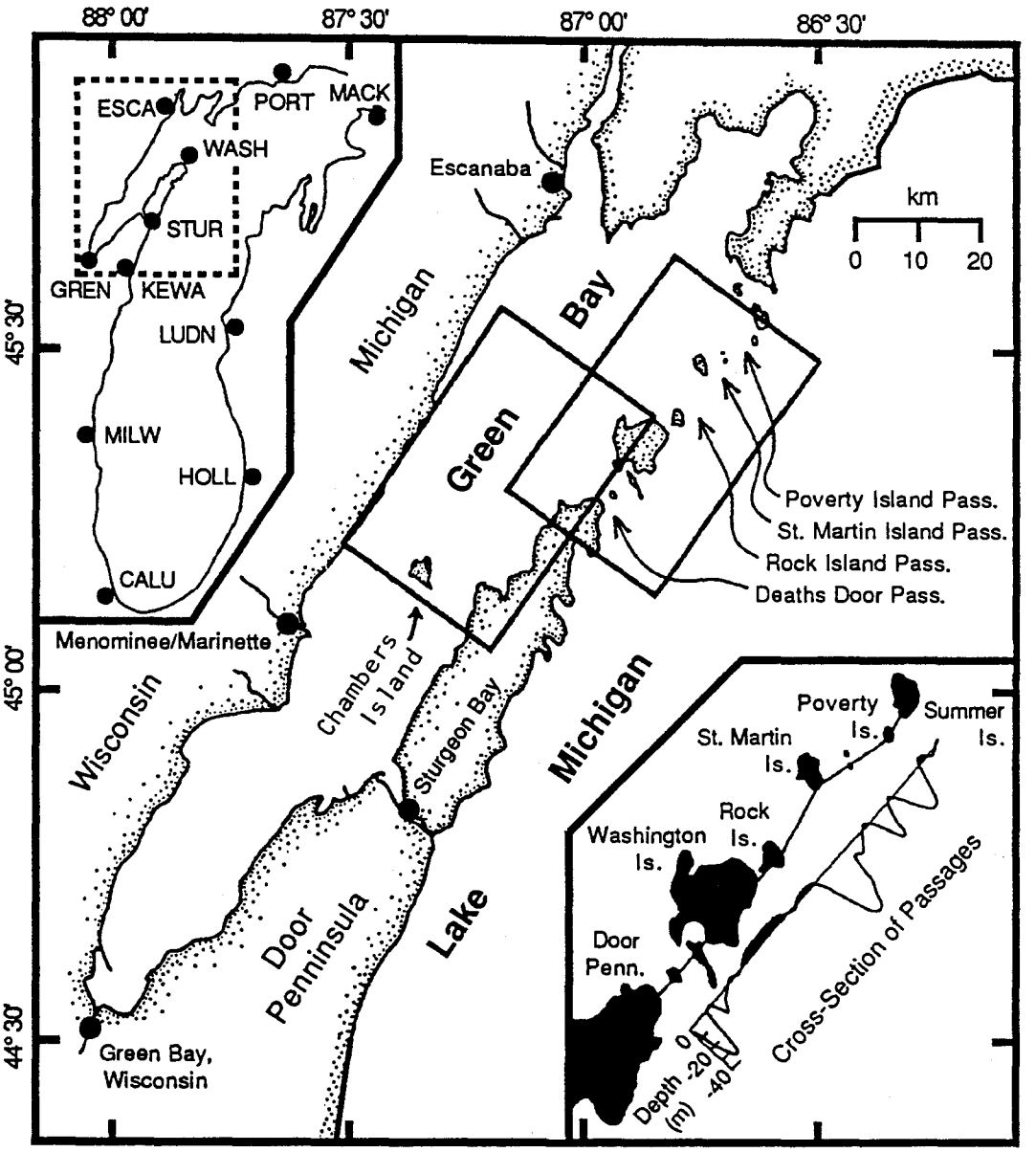

Figure 1.1. Surface map of Green Bay (map area outlined within dashed inset box), located on the northwestern side of Lake Michigan, showing major cities and rivers. Enlarged bathymetric maps covering the areas outlined within the right and left inset rectangles are presented in Figs. 1.2 and 1.3, respectively. The right inset rectangle outlines the Green Bay mouth region, where volume exchange flows between Green Bay and Lake Michigan occur through the four main passages. Exchange flows between the north and south halves of the bay occur through the passages on either side of Chambers Island (located in the center of the bay, see also Fig. 1.3). The lower inset figure shows a slightly enlarged surface map of the bay mouth region and a bathymetric transect across the mouth (additional transects are shown in the Appendix). The upper inset figure shows the locations of water level gauges around Green Bay and Lake Michigan. The gauge locations are Ludington (LUDN), Holland (HOLL), Calumet Harbor (CALU), Milwaukee (MILW), Kewaunee (KEWA), Sturgeon Bay ship canal (STUR), Detroit Harbor on Washington Island (WASH), city of Green Bay (GREN), Escanaba (ESCA), Port Inland (PORT), and Mackinaw City (MACK).

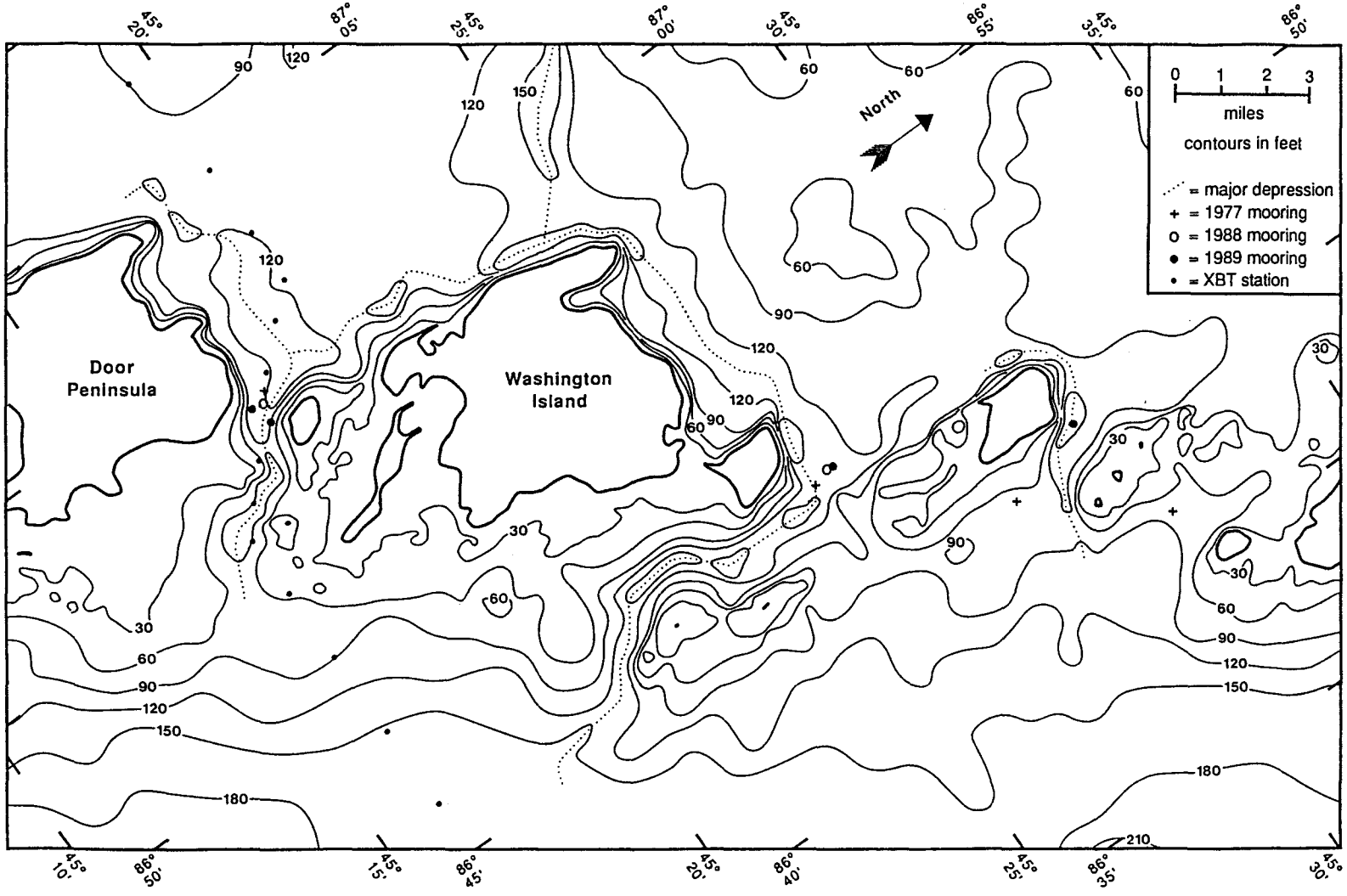

Figure 1.2. Bathymetric map of the Green Bay mouth region (see Fig. 1.1) indicating locations of current meter moorings (mooring numbers shown in Fig. 3.1) from the 1977 and 1989 stratified seasons, and an XBT transect (station locations and times listed in Table 3.1) collected in July and October, 1989. All significant volume exchange flows between Green Bay and Lake Michigan occur through these narrow and meandering passages.

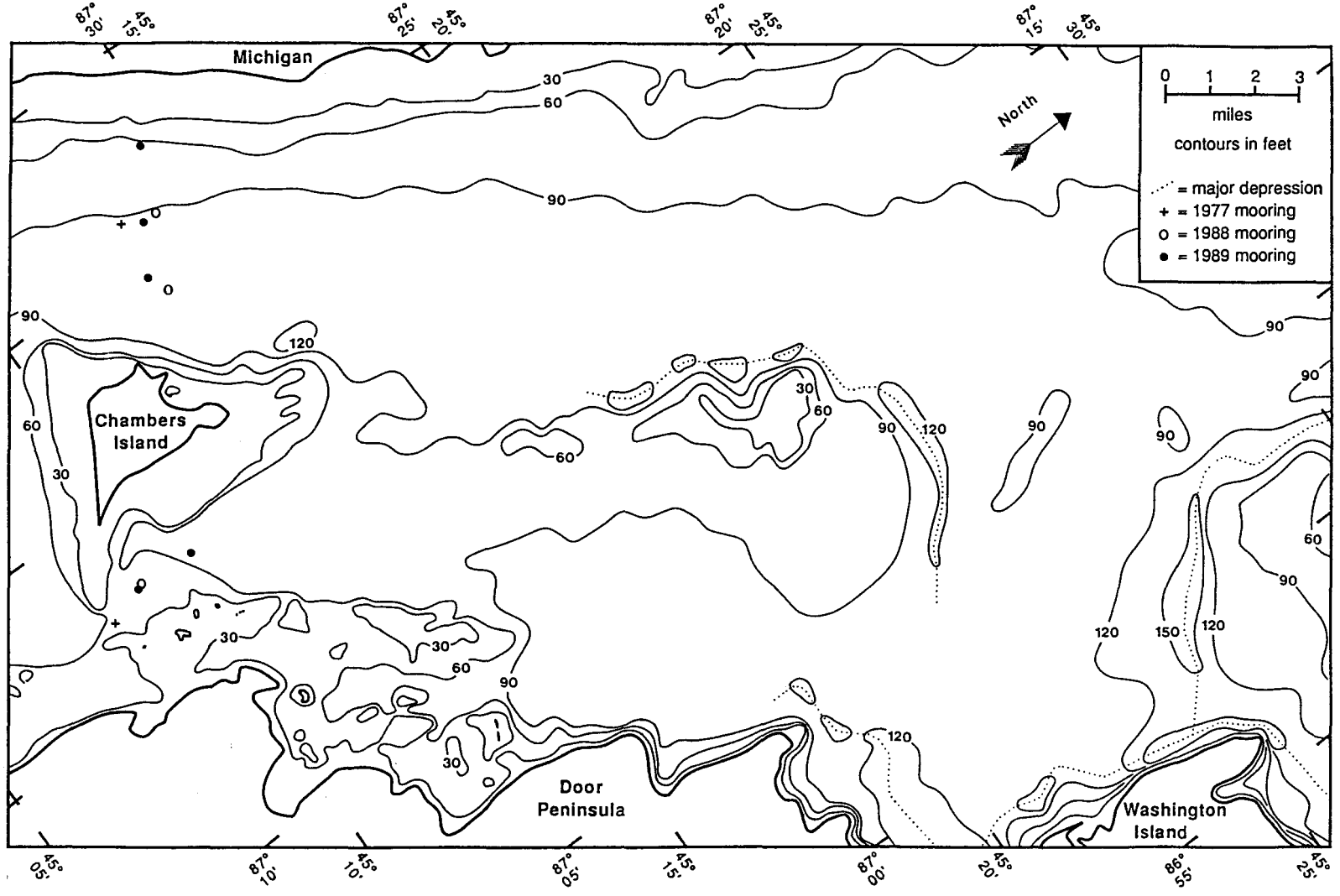

Figure 1.3. Bathymetric map of the northern Green Bay region (see Fig. 1.1) indicating locations of current meter moorings (mooring numbers shown in Fig. 3.1) from the 1977 and 1989 stratified seasons. Volume exchange flows between the northern and southern halves of Green Bay mostly occur through the wide passage to the west of Chambers Island, and are the subject of a separate investigation by Miller and Saylor (1992).

CHAPTER II

PREVIOUS INVESTIGATIONS AND THEORETICAL CONSIDERATIONS

Investigations of Green Bay

The waters in Green Bay generally are two-layered during the stratified season, with cool, clean, dense Lake Michigan-originating water underlying warm, polluted, and less dense riverine water. This situation is analogous to an ocean estuary (Fig. 2.1), where salty and dense ocean water (O) and fresh and less dense riverine water (R) enter the estuary (E) and mix with each other. Given a steady inflow of riverine water, the exchange flow at the transition (T) will be two-layered, with a surface layer outflow of the ocean-riverine water mixture, and a compensating deep layer inflow of ocean water. The two-layer exchange flow is significantly influenced by the forces of wind, barometric pressure, tides, internal pressure (density) gradients, friction, and, if certain conditions are satisfied, Coriolis force. Thus, two-layer exchange flows generally are complicated, and have been the subject of many field, theoretical, laboratory, and numerical investigations.

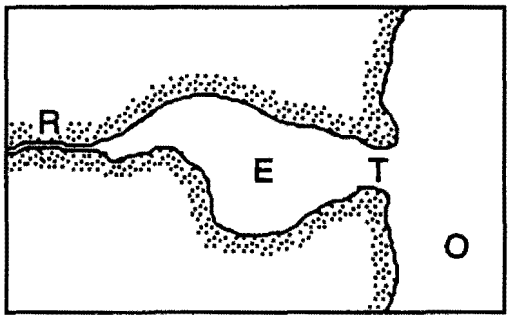

Figure 2.1. Schematic diagram of an ocean estuary, showing ocean (O), estuary (E), rivers (R), and the mouth or transition (T). The direct analogy with the present investigation (Fig. 1.1) is Lake Michigan (O), Green Bay (E), the Fox and other rivers (R), and the passages connecting the bay and lake (T). Under ordinary conditions, two-layer exchange of O and E waters occurs at T. Redrawn from Stommel and Farmer (1953).

Investigations of two-layer flow phenomena in Green Bay are relatively scarce. Modlin and Beeton (1970), using a simple estuarine mixing model described in Ketchum

(1951), performed a volumetric analysis of conductivity-traced river water in Green Bay during August 1969. They computed "flushing rates" – the length of time it takes one day's accumulation of river water to move through an estuary – of 225 days (from the Fox River mouth to Sturgeon Bay, see Fig. 1.1) and 36 days (from Sturgeon Bay to Deaths Door Passage), totaling 261 days from the head to the mouth of the bay. They also computed values of 100, 400, 760, and 8,350 m^3/s for the lakeward transport of water across transects located progressively nearer to the bay mouth, thus showing that flushing of the southern end of the bay is mostly dependent upon river discharge, whereas the larger transports nearer to the mouth are driven by very large volumes of inflowing lake water.

Oscillatory motions, such as tides and seiches, are common in many ocean and lake basins, and influence surface levels, thermocline depth, and estuarine mixing. In subsequent chapters it will be seen that tidal currents are a major constituent of the flow occurring through the passages connecting Green Bay and Lake Michigan. A detailed description of tidal motions, tidal resonance, and co-oscillations of the bay-lake system is provided by Mortimer (1965). Mortimer (1978) provides a comprehensive study of all other water motions in Green Bay, including river discharges, surface seiches, wind-driven gyres, and estuarine mixing. He listed seven characteristic "large-lake" motions (excluding tides) to be expected in the bay:

1) wind-driven surface drift
2) gradient currents produced by the wind-induced surface or thermocline tilt
3) upwelling and downwelling of the thermocline
4) internal Kelvin wave response to certain thermocline perturbations
5) internal Poincaré wave response to certain thermocline perturbations
6) surface seiches
7) gradient currents associated with bay-lake density differences

All seven motions are expected to influence the currents through the bay's mouth to some extent, but the last one is of particular importance to the two-layer exchange flows. These density gradient exchange flows are, in Mortimer's words, "mainly inward- and outward-going currents in the mouth, sometimes running concurrently in different directions at different levels or through different passages, but also affecting the open Bay particularly the

deeper regions." In his conclusions, Mortimer noted that repeated cross-sectional temperature (density) transects and continuous recordings of vertical profiles of temperature, flow, and other variables of interest would be a required part of any meaningful experimental investigation.

Besides several unpublished two- and three-dimensional models (Wang *et al*, 1991), the most comprehensive numerical model of Green Bay is a two-dimensional, time-dependent, vertically integrated hydrodynamical model presented by Heaps, Mortimer, and Fee (1982). The model is useful for investigating forcing by wind and surface disturbances propagating between the bay and Lake Michigan, but cannot be used for determining the vertical structure of the currents and temperatures. Also, the large vertical current shears observed in the mouth passages (a shear of 60 cm/s over 30 m depth was noted by Miller and Saylor, 1985) dictate the need for a multi-layer numerical grid in order to model the important role of stratification.

The first comprehensive investigation utilizing current meter recordings was Miller and Saylor (1985), part of which involved instrumenting the four main mouth passages (see 1977 moorings in Fig. 1.2) with current meter moorings (two meters per mooring, placed at 12 m depth and 5 m above the bottom) from May to September. They observed large volumes (3,300 m^3/s) of cold lake water entering the bay through the mouth near the bottom and extending far into the bay, thus maintaining stratification and promoting flushing. Monthly-averaged currents were strongest through Deaths Door and Rock Island Passages, and revealed a persistent pattern of bayward flow along the passage floor and lakeward flow above 12 m depth through all passages. The pattern was strongest during July and mostly reversed (i.e., lakeward flow near the bottom) during September at which time the thermocline was weakening and deepening.

For the cold inflowing lake water, Miller and Saylor (1985) estimated volume transport values of 2,100, 800, and 350 m^3/s through Rock Island Passage, Deaths Door Passage, and the combined northern two passages, respectively. Using the total of these

volume transport values they computed an "emptying time" – the basin volume divided by the inflowing or outflowing volume transport – of 219 days for Green Bay. Even though this value compared well with the Modlin and Beeton (1970) value, the definitions of emptying, residence, and flushing times can be disparate and must be compared with caution, as described in Modlin and Beeton (1970), Mortimer (1978), and Miller and Saylor (1985).

The most comprehensive field study to date was accomplished during the summer of 1989, and some of the results have been published in Gottlieb, Saylor, and Miller (1990). Part of the investigation involved instrumenting three of the four main passages (see 1989 moorings in Fig. 1.2) with current meter moorings (configured as in Saylor and Miller, 1985, with an additional meter placed at 20 m depth) from May to October; additionally, Rock Island Passage was instrumented with a thermistor chain mooring, and an XBT transect (see Fig. 1.2) was collected in Deaths Door Passage during July and October. The present investigation will involve a thorough description, analysis, and comparison of the data collected during both the 1977 and 1989 field investigations.

Laboratory Investigations

Despite their limitations, laboratory investigations have been very successful in representing some oceanographic and limnetic flow phenomena, one of which is two-layer estuarine exchange flows. Stommel and Farmer (1952 and 1953) expanded single-layer theories (given by Ippen, 1950) to include two layers, and devised laboratory experiments to test the theories. Stommel and Farmer (1952) describe how a channel acts to <u>control</u> single-layer flow in the special case when the Froude number $F=u^2/gD=1$ where u is the mean flow velocity, D is the channel depth, and g is the gravitational acceleration. In this case, the fluid surface is configured as a stationary wave occupying the channel, and the flow through the channel is said to be <u>hydraulically controlled</u> (i.e., "choked", or

"constricted"). A good explanation of hydraulic control is given by Whitehead (1974), describing non-rotating, frictionless flow past constrictions such as dams and weirs:

> In the case of flow over a dam, the height of water over the dam is found to "control" (i.e., to be sufficient information to calculate) the height of water in the upstream basin as well as the velocity and transport of water over the dam. This is so because of ... a simple rule: the speed of outflow is just the shallow-water wave speed based on the water height above the dam. Thus the dam "controls" the flow by blocking changes in downstream level from propagating upstream as waves.

In the case of two-layer exchange flow, Stommel and Farmer (1952) define the "interfacial Froude number" by the equation

$$F_i = \left[1 + \left(\frac{u_1 D_1}{u_2 D_2}\right)^2 \left(\frac{n}{1-n}\right)^3 \right]^{-1} \qquad (1)$$

where the subscripts 1 and 2 denote the upper and lower layers, respectively, and $n = D_1/D = D_1/(D_1 + D_2)$. As in the single-layer case, the two-layer flow is hydraulically controlled and the interface is a stationary internal wave when $F_i = 1$. This type of control is realized in estuarine transitions where the transition is abrupt, river discharge is relatively low, and mixing between layers is negligible.

Stommel and Farmer (1953) describe how a control (as just described) acts to limit the amount of sea water available for mixing within a two-layered estuary. Referring to Fig. 2.1, if there are no tides in the ocean O, if the estuary E is sufficiently deep, if there is no mixing of the two layers within E, and if the river discharge R is not too large, then the lower layer in E will be stagnant, the upper layer will be entirely fresh, and there will be a two layered exchange flow through T. Now,

> Suppose that some agency for vertical mixing of the two layers exists in the estuary E and that the amount of mixing is progressively increased. The upper layer is now somewhat brackish, the discharge of both layers through T is increased, and the interface is nearer to the mid-depth. Increased mixing in E decreases the salinity difference of the two layers at T and increases the discharge; but there is a point beyond which increased mixing has no further effect on either the discharges through or the salinities at T.

Such an estuary is termed "overmixed" by Stommel and Farmer (1953), since the salinity in the estuary is determined by the controlling action of the transition rather than any diffusive or turbulent mixing processes within the estuary as described by Ketchum (1951). Overmixing occurs only in estuaries in which there is vertical stratification, hydraulically controlled two-layer exchange at the transition, and sufficient mixing in the estuary. Overmixing is a special limiting case of the generalized maximal two-layer exchange theory to be described in a subsequent section.

In any stratified estuarine transition (e.g., the channels connecting Green Bay and

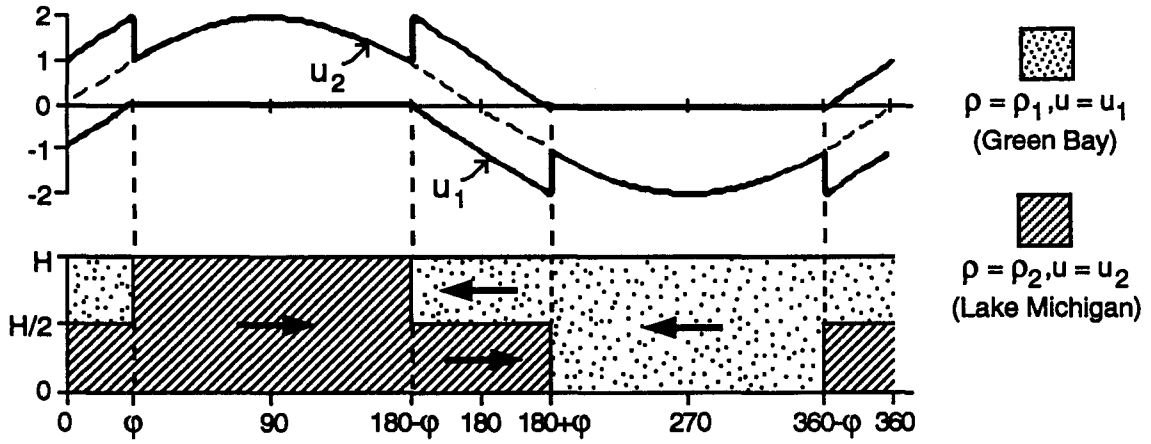

Figure 2.2. Schematic diagram of two-layer exchange through an idealized estuary mouth, with a sinusoidal net barotropic current component. Shown are the densities and velocities (+ is into Green Bay) of the waters occupying the mouth. For the barotropic component shown, the exchange is mostly single-layer. Redrawn from Stigebrandt (1977).

Lake Michigan) it is important to distinguish clearly between the baroclinic (that due to tilting of isopycnals, e.g., the thermocline) and barotropic (that due to tilting of the water surface level) components of the currents through the transition. Surface level tilting which drives barotropic currents through channels is caused commonly by tidal and meteorological forcing. Stigebrandt (1976) shows how the two-layer exchange capacity of an estuarine transition can be enhanced by the effect of fluctuating barotropic currents. Fig. 2.2 shows how for a simple sinusoidal water level fluctuation, the exchange through the transition is usually single-layer, and sometimes two-layer. During the single-layer exchanges the velocity is relatively large, and thus the transports through the transition in

either layer are greater than if the exchange had been entirely two-layer. Stigebrandt also notes how internal waves are generated at some transitions, and thus can be an important factor (among other factors) affecting the exchanges and mixing of the two layers.

Laboratory investigations incorporating the effects of rotation (Coriolis force) are described in Whitehead *et al.* (1974), Stern *et al.* (1982), and Whitehead (1986). Whitehead (1986) investigates a homogeneous (single-layer), rotating, barotropic, steady, inviscid fluid flowing through a rectangular channel, and notes that the channel width w does not need to approach the Rossby radius for rotational effects to be felt. Rather, a novel width scale $B = (2g\Delta\zeta)^{1/2}/f$, where $\Delta\zeta$ is the difference in free surface height at the ends of the channel and f is the rotation frequency, is found such that rotation influences the flow in the channel when $B/w<1$, and is insignificant when $B/w>1$. Also, the mean flow velocity $\bar{u}$ in the channel is predicted by the equations:

$$\bar{u} = g\Delta\zeta/fw \qquad \text{for } B/w<1 \qquad (2)$$

$$\bar{u} = (2g\Delta\zeta)^{1/2} - \tfrac{1}{2}fw \qquad \text{for } B/w>1 \qquad (3)$$

While Rossby radii usually are a measure of the deviation of local vorticity from upstream vorticity, B is instead a measure of the velocity due to Bernoulli's law times the inverse of the cross-channel velocity shear (the cross-channel shear scales as the inertial time scale f^{-1}). Also, the velocity computed from Equation (2) is identical to that computed for the case of "geostrophic control", as will be shown in a subsequent section.

The Whitehead *et al.* (1974) investigation involves the simplest possible rotational dynamics applied to two-layer estuarine exchange: Bernoulli's law in the along-channel direction, geostrophic balance in the cross-channel direction, and conservation of potential vorticity in the flow. In this case, the effect of rotation is to tilt the interface up to the right (looking into the estuary in the Northern Hemisphere) and, if the rotation is strong enough, actually confine the inflowing sea water to the right side of the channel. Stern *et al.* (1982) further describes the effects of rotation on two-layer flows:

> When light rotating fluid spreads over heavier fluid in the vicinity of a vertical wall (coast) a boundary jet forms, the leading edge or nose of which propagates along the coast. A certain fraction of the boundary transport is not carried by the nose but is deflected backwards (detrained) and left behind the propagating nose. Laboratory observations suggest that the nose slows down and stagnates, whereupon the trailing flow separates from the coast and an intermittent boundary current is formed.

This phenomenon will be discussed in a subsequent section.

Non-Rotating Theoretical Investigations

To date, Armi (1986), Armi and Farmer (1986), and Farmer and Armi (1986) provide the most comprehensive and generalized theoretical framework for studying maximal two-layer exchange through a constriction with barotropic net flow. Armi and Farmer (1986) investigate the internal hydraulics of two-layer flow between two reservoirs connected by a channel with vertical walls, constant depth, and slowly varying width, using the fully nonlinear, frictionless, quasi-steady one-dimensional shallow water equations with the rigid lid approximation. They show that

> ... maximal two-layer exchange with a net barotropic flow requires the presence of two controls, one at the narrowest section and a second or 'virtual' control lying to one side of the narrowest section. The two controls are connected by a subcritical (laminar) region, but are separated from subcritical conditions in the reservoirs by supercritical (turbulent) flow and stationary internal bores (internal hydraulic jumps).

Subcritical, critical, and supercritical flows occur at points in the channel for which $G^2 < 1$, $G^2 = 1$, and $G^2 > 1$, respectively, with the "composite Froude number" G given by

$$G^2 = F_1^2 + F_2^2 = \frac{u_1^2}{g'y_1} + \frac{u_2^2}{g'y_2} \qquad (4)$$

where the subscripts 1 and 2 denote the upper and lower layers, respectively, u is flow speed, y is layer thickness, and $g' = g(\rho_2 - \rho_1)/\rho_2$ is reduced gravity. Many of Armi and Farmer's (1986) results are conveniently plotted in the Froude-number plane (F_1,F_2), thus revealing the locations of the control points as well as the regions of subcritical and supercritical flow.

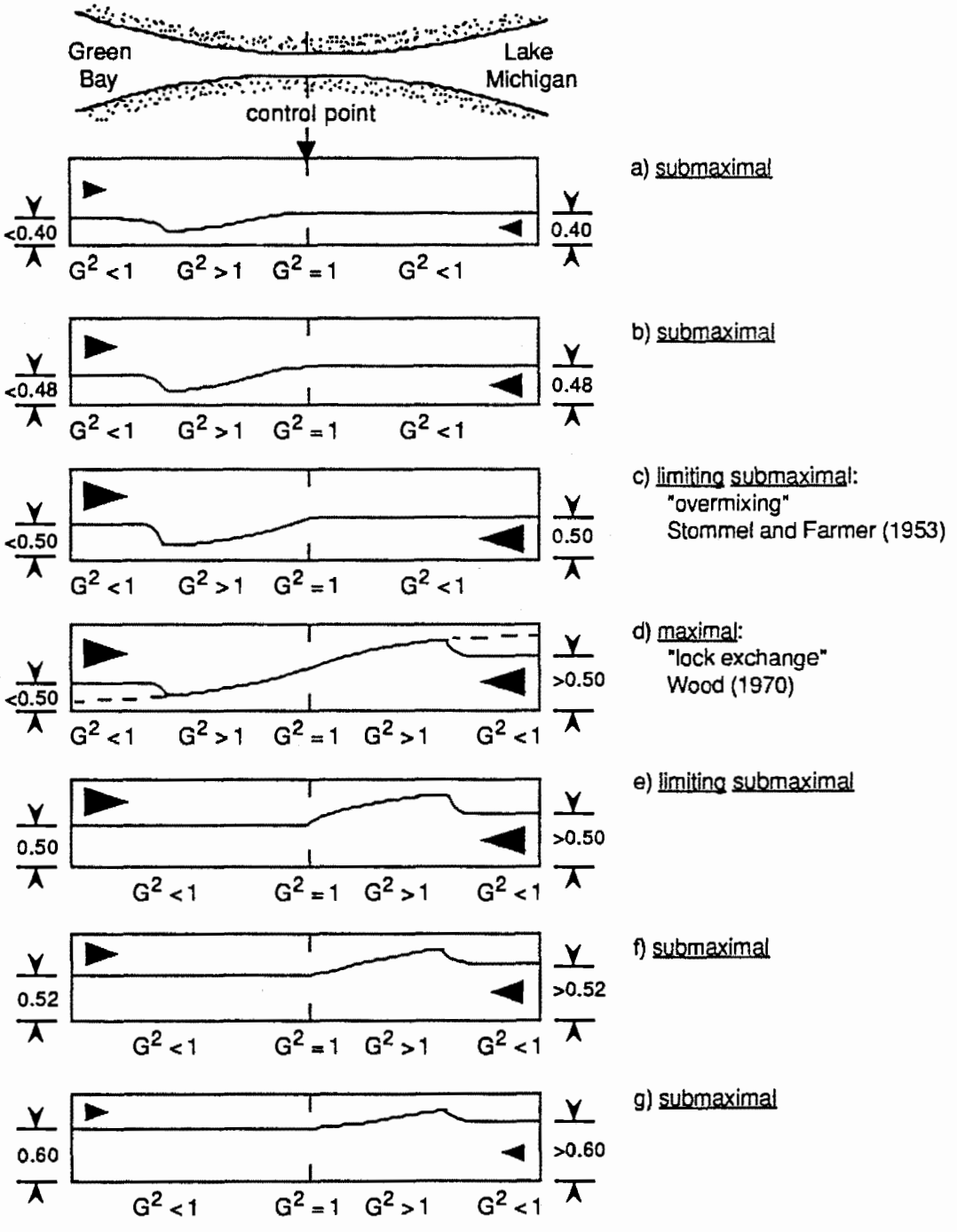

Figure 2.3. Plan view of idealized passage connecting Green Bay and Lake Michigan, and idealized vertical profiles of interface shape with varying magnitudes of two-layer exchange flows (arrowheads). Only the "lock exchange" flow (d) is the maximal two-layer exchange flow. See text for further explanation. Redrawn from Armi and Farmer (1986).

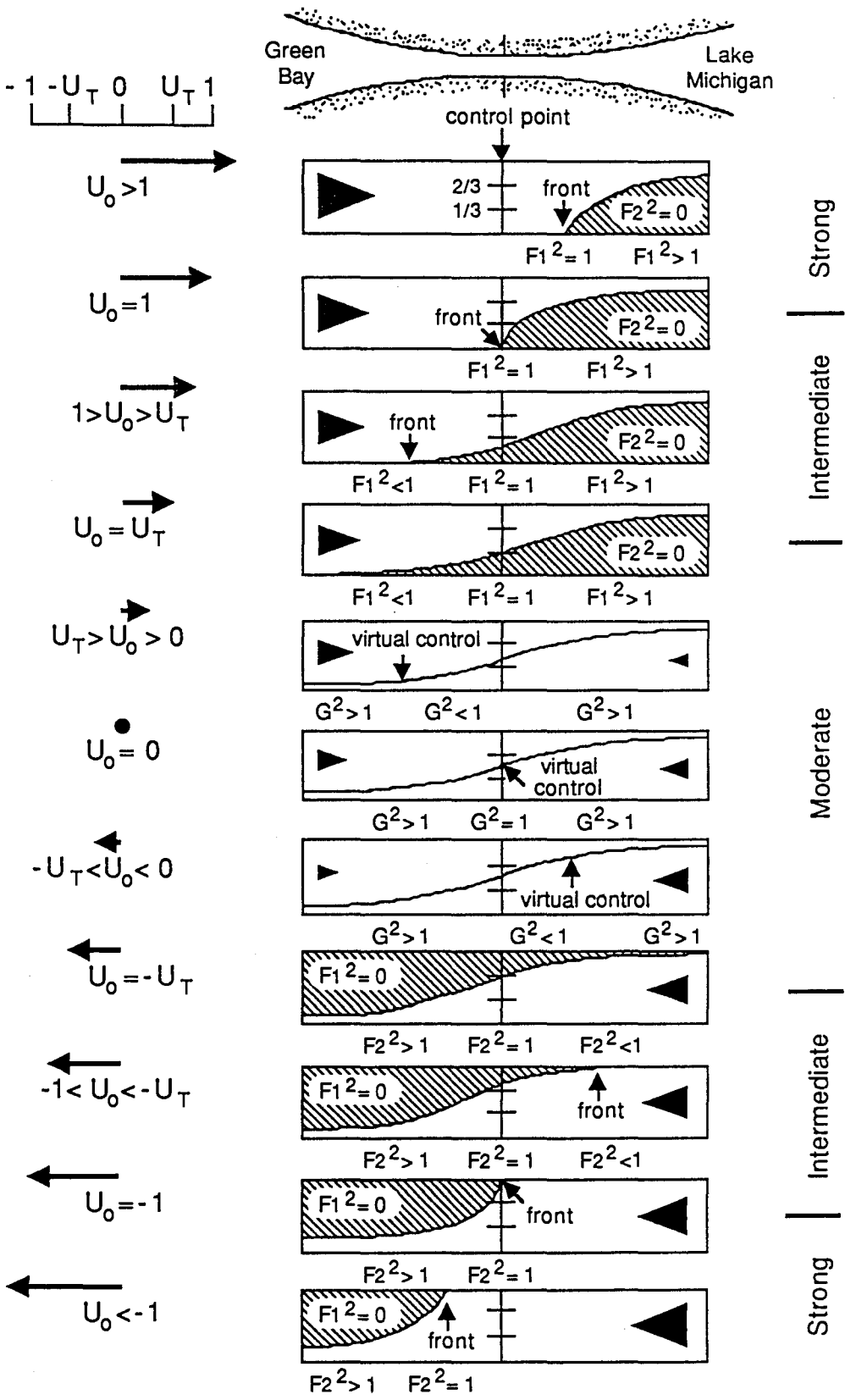

Figure 2.4. As in figure 2.3, but with varying component of barotropic flow U_O (indicated on left side of the figure). Motionless layers are shaded. See text for further explanation.

Profiles of the interface shape in the absence of a net barotropic flow for varying layer thicknesses are shown in Fig. 2.3. The narrowest point in the channel is the control point, at which the flow is critical ($G^2 = 1$), and the points where the interfaces are the most steeply sloped are stationary bores, which separate supercritical ($G^2 > 1$) flow in the channel from subcritical ($G^2 < 1$) conditions in the reservoir. The two-layer exchange is maximal only for the case (Fig. 2d) where the interface heights in the estuary and ocean are lower and higher, respectively, than the interface height at the constriction (i.e., the case where supercritical flow occurs on both sides of the control point); the exchange is submaximal in all other cases. Also, it is assumed that mixing of the fluids in the estuarine reservoir is complete and occurs away from the channel region, which is equivalent to the more theoretical condition of large reservoirs containing homogeneous (ρ_1 and ρ_2) fluids.

The previously-described Stommel and Farmer (1953) example of "mixing progressively increasing up to, but not beyond, the point of overmixing" now can be easily understood with the progression of interface profiles (Fig. 2.3a to d) corresponding to progressive states of mixing in an estuary. Increased mixing in the estuary leads to increased lower-layer thickness in the estuary and increased exchange (Figs. 2.3a and b) up to the point (overmixing) where the lower layer thickness in the estuary is just less than half the depth (Figs. 2.3c and d). Stommel and Farmer (1953) incorrectly assumed that the lower-layer thickness must stay less than half the depth, and thus mixing beyond the point of "overmixing" leads to increased lower layer thickness but decreased exchange (Figs. 2.3e to g). It is important to note again that the maximal exchange rate (Fig. 2.3d) occurs only when supercritical flow and bores exist on both sides of the control point.

As anticipated from Fig. 2.2, adding a net barotropic component to the two-layer exchange flow has a pronounced effect on the interface shape. Fig. 2.4 shows the effect of a varying net barotropic flow U_O from both directions (into and out of the estuary). If the outflowing barotropic component is great enough ($U_O \geq U_T$) the inflowing lower layer is arrested, and a further increase ($1 \geq U_O > U_T$, or "intermediate" flow) forces the

motionless lower layer back out of the estuary, and for an even further increase ($U_O > 1$, or "strong" flow) the control point is occupied entirely by the outflowing upper layer. The converse situation occurs if the barotropic component is inflowing ($U_O \leq -U_T$). The leading or trailing edge of the motionless layer is a "front", and in a real lake or ocean would be subjected to dynamics not investigated by Armi and Farmer. For the case of "moderate" flow, a second control point ($G^2 = 1$) or "virtual" control exists on the upstream (with respect to U_O) side of the control point at the constriction; the control points coalesce for $U_O = 0$, and the virtual control disappears for $U_O \geq U_T$ and $U_O \leq -U_T$.

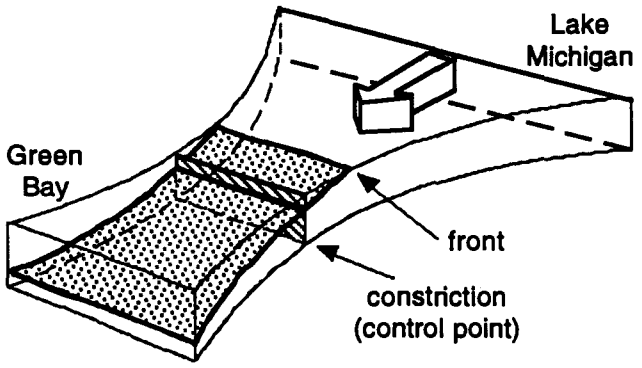

Figure 2.5. Box-flow model for single-layer exchange. Shown is an intermediate flow (Fig. 2.4) with stationary upper layer. Redrawn from Armi and Farmer (1986).

The intermediate and strong exchange flows shown in Fig. 2.4 are referred to as "box flows" ($U_O \leq -U_T$) and "inverted box flows" ($U_O \geq U_T$), a model for which is shown in Fig. 2.5; a familiar example of an inverted box flow is a frictionless salt wedge at the mouth of an estuary. In the box model, the walls and floor of the constriction form three sides of the box and the interface forms the fourth, so that the interface height determines both the flow rate U_O and volume exchange through the constriction. The importance of distinguishing between box flows and gravity currents is noted by Armi and Farmer (1986):

> Box flows are steady with respect to the contraction. Gravity currents can only be considered steady in a coordinate frame that moves along with the front. This distinction is important since, in contrast to gravity currents, the frontal boundary for box flows is stationary and the interface shape behind the front is determined by the flow rate and channel width.

Finally, Armi and Farmer note that a periodically-fluctuating barotropic flow component always tends to increase the maximal two-layer exchange through a constriction.

The case of maximal two-layer exchange over a sill is investigated by Farmer and Armi (1986). They find that the sill primarily controls the lower layer, and only indirectly affects the upper layer. Compared to the corresponding constriction example, the interface over the sill crest is deeper, the lower layer flows more rapidly, but the two-layer exchange is significantly less. The geometry and bathymetry of the passages connecting Green Bay and Lake Michigan (Fig. 1.2) suggests that Armi and Farmer (1986) is more relevant than Farmer and Armi (1986) to the present investigation. Bathymetric features (e.g., ridges, rises, sumps, and sills) could influence the lower-layer inflow of Lake Michigan water, as described in Farmer and Armi (1986), but this phenomenon will not be examined in the present investigation.

In a later investigation, Armi and Farmer (1987) extend the concept of maximal two-layer exchange to include all such naturally occurring flows. Even though the Armi and Farmer (1986) investigation assumed inviscid and quasi-steady flows, any two-layer exchange flow is maximal if the control region is bounded on either side by supercritical flows and bores; all other flows are submaximal. Furthermore, anytime the two-layer exchange is maximal then (1) the exchange is fully determined by the processes occurring in the control region and (2) the exchange is the greatest that can occur. This is so because the supercritical flows and bores at both ends of the channel isolate the governing processes within the channel from outside processes in the adjoining basins. In conclusion, Armi and Farmer (1987) note that time-dependent effects (e.g., tides) can drastically influence two-layer exchange through a channel (by shifting locations of the controls, filling and draining of sumps within the control region, generation of internal bores, etc.). However, if the control is bounded on both sides by supercritical flows, then the exchange is maximal.

Rotating Theoretical Investigations

Gill (1976 and 1977), Shen (1981), Toulany and Garrett (1984), Whitehead (1986), Wright (1987), and Hermann *et al.* (1989) have investigated the effect of earth's rotation (the Coriolis effect, herein referenced to the Northern Hemisphere) on single-layer

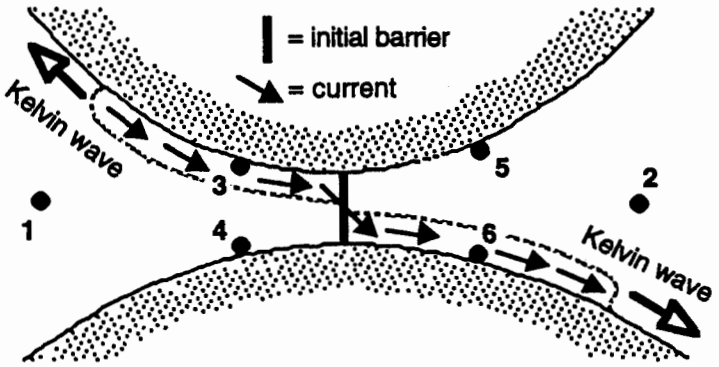

Figure 2.6. Schematic diagram of Kelvin wave propagation out of a channel connecting two reservoirs initially separated by a barrier, and with the initial water surface level higher at point 1 than at point 2. See text for further explanation. Redrawn from Pratt (1990).

flow through a channel. Pratt (1991) provides a compact, comprehensive, critical summary of these investigations, and describes the differences between "geostrophic control" and "rotating critical (hydraulic) control" in a channel connecting two reservoirs containing a homogeneous fluid. Pratt argues that "the steady flows described by existing hydraulic theories are not geostrophically controlled in any limit, nor does the transport relation given by geostrophic control place any bound on the value predicted by hydraulic theories", as described herein.

The idea of geostrophic control is easily described by reference to the situation shown in Fig. 2.6, where an idealized barrier dams the narrowest section of a vertical-walled channel connecting two reservoirs, the fluid density and depth H are uniform throughout the channel and both reservoirs, and there exists a motionless initial state with a mean fluid surface level difference $\Delta\zeta = \zeta_1 - \zeta_2$, where subscripts denote the numbered locations shown in Fig. 2.6. Now, suppose the barrier is suddenly removed. If $\zeta_1 > \zeta_2$, a flow into the ζ_2 reservoir will be initiated by two Kelvin waves propagating in opposite

directions away from the barrier and, if the rotation is sufficiently strong, each Kelvin wave will be "trapped" against its respective right-hand shoreline (see Fig. 2.6).

By definition, a trapped Kelvin wave induces significant motions only along the wall or shoreline it is trapped against, so a good assumption is that $\zeta_4 = \zeta_1$ and $\zeta_5 = \zeta_2$. If the width-averaged along-channel velocity $\bar{u} = \frac{g(\zeta_4-\zeta_3)}{fw} = \frac{g(\zeta_6-\zeta_5)}{fw}$ is geostrophically balanced and the along-channel momentum balance is $u_t - fv = -g\zeta_x - \lambda u$ (where w is the constant channel width and λ is a friction coefficient), then applying the limit of steady, frictionless motion in a channel with negligible cross-channel velocity ($v \ll u$) results in an expression for the volume transport Q through the channel:

$$Q = Hw\bar{u} = gH\Delta\zeta/f \qquad (5)$$

Furthermore, it can be argued (Toulany and Garrett, 1984) that the cross-straight surface level difference cannot exceed the value $\Delta\zeta$, and thus Equation (5) imposes an upper bound on the transport through the channel. Thus, any flow governed by Equation (5) is said to be geostrophically controlled.

A different approach is to use rotating hydraulic theory, where the flow is assumed to be initially steady and the non-linear equations of motion are solved using advection terms. This approach yields solutions for the surface level elevations which are either "symmetric" in which case $\Delta\zeta = 0$ and Equation (5) yields $Q = 0$, or "asymmetric" in which case the flow at the narrowest point in the channel is hydraulically controlled (i.e., $F^2 = 1$ and the Kelvin wave speed is zero at the control point). Because (e.g., Armi and Farmer, 1986) a control region isolates (via supercritical flow and a bore) the processes influencing surface levels at either end of the channel, it is clear that the transport through the channel can depend on ζ_1 or ζ_2 but not both, as it does in Equation (5). Therefore, Pratt suggests that geostrophically controlled flow cannot be achieved in any limit of rotating hydraulic theory, despite the fact that the equations of hydraulics would appear to be more general due to the inclusion of nonlinear advective terms.

Pratt explains the conditions under which geostrophic control holds. Referring to the previously described situation depicted in Fig. 2.6, after the barrier at the channel center is removed (at time t = 0) the linearized shallow water equations may be used (Gill, 1976) to obtain a solution valid to $O(\Delta\zeta^2/H^2)$ if $\Delta\zeta/H \ll 1$, schematically represented in Fig. 2.6. The removal of the barrier generates Kelvin waves that propagate out of the channel in opposite directions, leaving behind a coastal boundary current on each side of the channel, and a current cross-over region (which is a potential vorticity front) at the channel center. In this situation, the steady coastal boundary current is geostrophically controlled in that Equation (5) holds, and this solution would be valid for all time were it not for weak nonlinear effects.

Hermann *et al.* (1989) have investigated the nonlinear situation and found that the vorticity front is actually advected downstream with the geostrophic flow, leaving behind a symmetric flow which is subcritical rather than geostrophically controlled. Thus, geostrophic control is a temporary state occurring after Kelvin waves have propagated out of the channel (i.e., for $t \gg f^{-1}$) but before the vorticity front has been advected out (i.e., for $t \ll t_a$, where the advective time scale $t_a = H\Delta/f\Delta\zeta$ and $\Delta \approx 5w$). Pratt briefly comments on control in the ocean (also applicable to Lake Michigan and Green Bay):

> Hydraulically controlled flows are generally associated with small values of the minimum width-to-basin width ratio and O(1) values of $\Delta\zeta/H$. In the ocean $\Delta\zeta/H$ is typically very small, and the corresponding flows will tend to be completely subcritical rather than hydraulically controlled. For internal flows, where $\Delta\zeta$ measures the difference in interface or isopycnal level, $\Delta\zeta/H$ can be O(1) and hydraulic control is more likely.

Finally, Pratt notes a discrepancy between Wright (1987) who shows that geostrophic control is inapplicable for the case of finite reservoirs, and Whitehead (1986, described in a previous section) who experimentally verifies geostrophic control in a laboratory channel connecting finite reservoirs. Pratt resolves this paradox with a figure from Whitehead's experiment (Pratt's Fig. 4) showing how the flow separates from one wall of

the channel. This flow separation phenomenon is neglected by Wright (1987), and presently has not been observed or explained in any other investigations. In summary, geostrophic control in a channel connecting infinite homogeneous reservoirs occurs if both $\Delta\zeta/H$ is small and the time scale is in the range $f^{-1} < t < t_a$. Two-layer exchange flows, for which $\Delta\zeta/H$ is usually O(1), thus are more likely to be hydraulically controlled. For finite reservoirs, geostrophic control can occur if a peculiar separation phenomenon observed by Whitehead (1986) exists.

Other Related Investigations

Other investigations related to the present investigation will be noted but not described here. Non-rotating studies include Garrett and Toulany (1982), Clarke (1990), and Tang (1990). Rotating studies include Garrett and Petrie (1981), Lawrence (1990), Oguz *et al.* (1990), and Farmer and Møller (1990). The latter is an ongoing combined field and modeling investigation in a sea strait that has roughly the same physical dimensions as the passages connecting Green Bay and Lake Michigan, but to date the results are still preliminary and have not been extensively analyzed. However, some of the field data analysis and presentation techniques in Farmer and Møller (1990) are useful for the present investigation.

Conceptual Framework for Present Investigation

In anticipation of the observations to be presented in the following chapter, Figs. 2.7 and 2.8 show a conceptual model describing the effects of earth's rotation (Coriolis effect) on the two-layer exchange flows between Green Bay and Lake Michigan. If rotation effects are dominant, then a geostrophic balance between the thermocline tilt and lower-layer currents (as described in Fig. 2.7) would be expected. However, since other forces (e.g., friction) may be important, the balance may be something other than geostrophic. For the previously described pressure-driven lower-layer Lake Michigan-

water inflow, rotation results in tilting of the internal density (temperature) structure and thermocline, observed as relatively warm temperatures at the southern extreme of the bay mouth, and cold at the northern extreme (Fig. 2.7).

If lower-layer currents and thermocline tilt are geostrophically balanced (Fig. 2.7), then the scaled along-channel equation of motion is:

$$fV = (1/\rho)\,\Delta P/\Delta X \qquad (6)$$

where V is along-channel velocity component, $\Delta P/\Delta X$ is the cross-channel pressure gradient, $\rho = 1000$ kg/m^3, and $f = 10^{-4}$ s^{-1}. The magnitude of $\Delta P/\Delta X$ can be estimated using a two-layer model with a tilted thermocline (Fig. 2.8), where the relative pressures below the thermocline at the south and north ends of the mouth are $P_S = \rho_1 gH$ and $P_N = \rho_1 g(H-h) + \rho_2 gH$, respectively. Using the values $\rho_2-\rho_1 = 1.0$ kg/m^3, $\Delta X = 10$ km $= 10000$ m, $h = 20$ m (these values will be justified in Chapter III) yields $\Delta P/\Delta X = (P_N-P_S)/\Delta X = gh(\rho_2-\rho_1)/\Delta X = 0.02$ kg/m^{2}s^2. Thus, equation (6) gives a geostrophically-balanced thermocline tilt of $h/\Delta X = 2.0$ m/km for a current magnitude of $V = 0.2$ m/sec $= 20$ cm/sec. In Chapter IV joint occurrence distributions of thermocline tilt vs. current magnitude will be presented, and in Chapter V the scale analysis will be extended to include friction, non-linear, and time dependent terms.

Ekman transport (the net movement of upper-layer water at some angle to the right of the wind) produces water level differences which are mirrored by thermocline depth level differences, as shown in Fig. 2.9. For the prevailing southwest (northeastward) winds observed during the stratified season, the wind-driven transport of the upper-layer waters in both Green Bay and Lake Michigan causes an elevated water surface level and downwelled thermocline in the northeastern corner of the bay, and a depressed water level and upwelled thermocline outside of the bay mouth in the lake. The result is a baroclinic pressure field driving lower-layer water from the lake into the bay, and a barotropic pressure field driving water at all depths out of the bay and into the lake, as shown in Fig. 2.9. Conversely, for a northeast (southwestward) wind these pressure fields are

oppositely directed, so that lower-layer water is upwelled and driven out of the bay and into the lake.

Finally, it is informative to compare the internal density gradient computed above with a typical water surface level perturbation $\Delta\zeta'$ and resulting internal surface (thermocline) level perturbation $(\rho/\Delta\rho)\Delta\zeta'$ computed at the bay and lake coasts using a storm surge model (Schwab, 1978). For a typical wind stress of 1 dyne/cm^2 (corresponding to a wind speed of 400 cm/s) over the lake and bay surfaces, Schwab (1978) indicates values of $\Delta\zeta' = 3$ and 5 cm respectively for the lake and bay coasts. Using $\rho/\Delta\rho = 1000$ yields respective values of $(\rho/\Delta\rho)\Delta\zeta' = 30$ and 50 m, so that the difference between the thermocline depths in the bay and lake would be about 20-30 m. Assuming that this difference occurs over a horizontal distance of about 10 km yields a thermocline tilt of about 2.0 m/km, which is near the value computed using Equation (6). Thus, it may be difficult to determine which terms or balances dominate in the equations of motion, as will be seen in Chapter V.

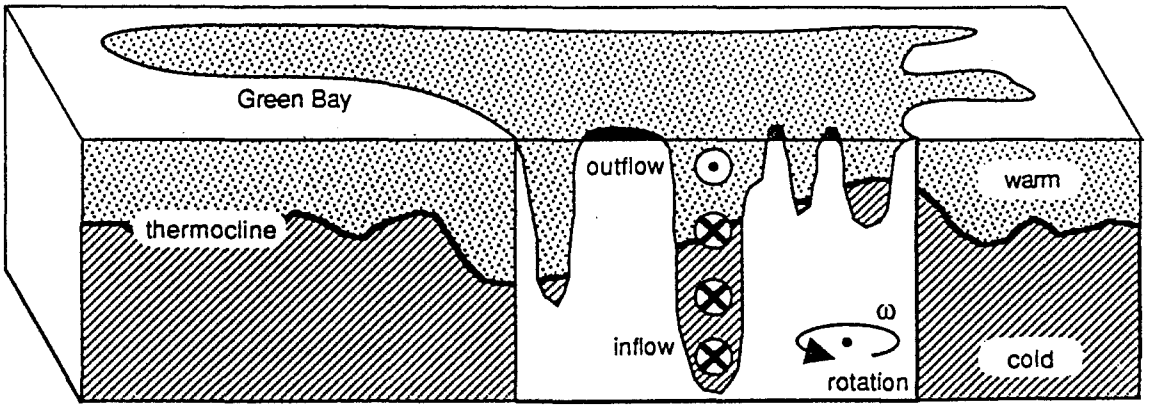

Figure 2.7. Conceptual model used to describe the effects of earth's rotation on the currents and temperatures observed during the stratified season in the passages connecting Green Bay and Lake Michigan. During stratification, very cold and dense water (hatched) below the thermocline (thick line) in Lake Michigan is driven by the internal pressure force through the passages and into Green Bay. To compensate, warm water (stippled) exits the bay above the thermocline, resulting in two-layer exchange with lower-layer inflow and upper-layer outflow. After an initial adjustment period the thermocline becomes tilted upward towards the north (upper diagram) in order to balance the internal pressure force and the inflowing currents.

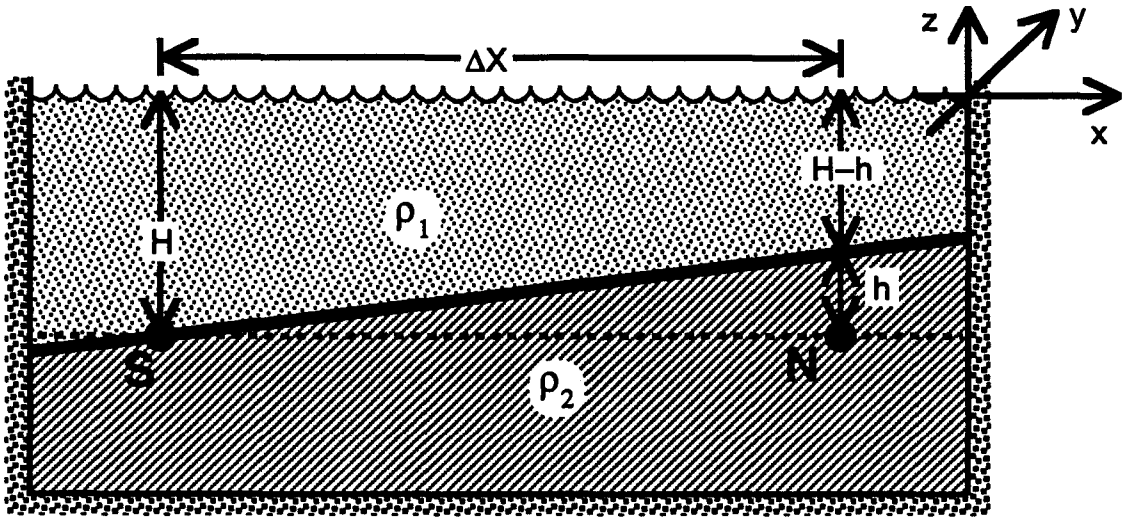

Figure 2.8. Conceptual model of a two-layered density structure with a tilted thermocline across the bay mouth (see Fig. 2.7). Below the thermocline, the pressure difference between the north (N) and south (S) ends of the mouth is proportional to the horizontal thermocline tilt h/ΔX. See text for further description.

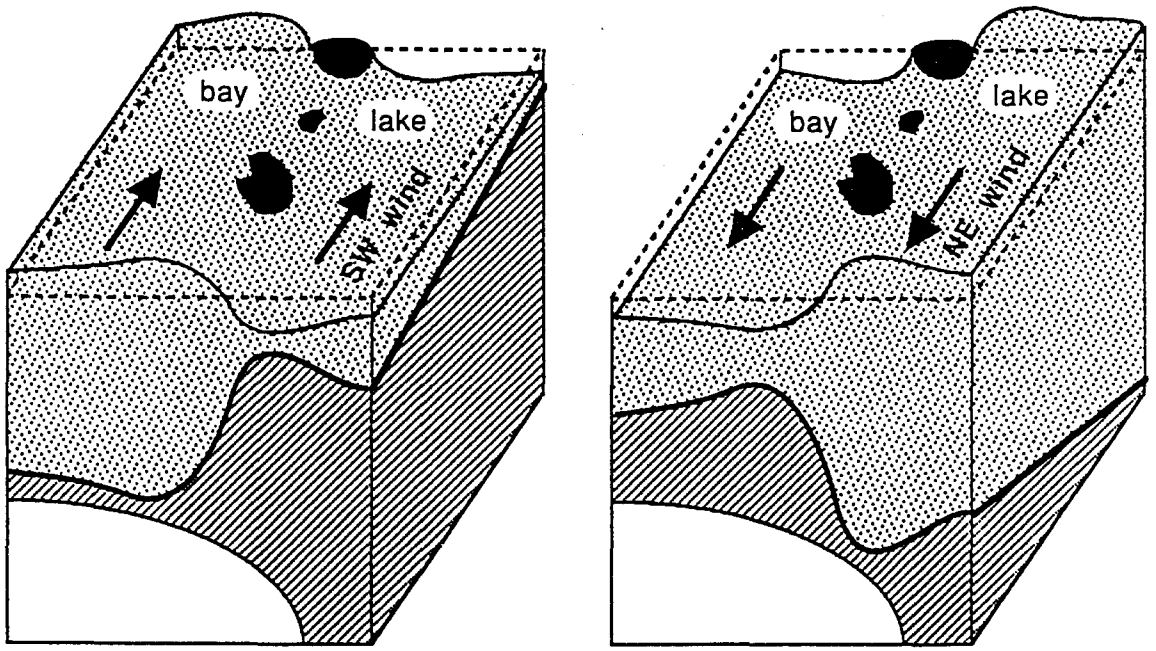

Figure 2.9. Ekman transport, the net movement of upper-layer water at some angle to the right of the wind direction, affects the internal pressure force within the mouth of Green Bay (the surface areas in the diagrams represent the area in Fig. 1.2). During the stratified season, the prevailing internal pressure force is directed into the bay, and prevailing winds are from the southwest. For a southwest wind (left diagram), the induced transport in the bay and lake produces a water level increase in the bay and decrease in the lake. To compensate, the thermocline upwells in the lake and downwells in the bay, thus enhancing the internal pressure force. Conversely, a northeast wind (right diagram) produces a downwelled thermocline in the lake and upwelled in the bay, thus suppressing the internal pressure force. For a complete description of Ekman dynamics and wind-driven water mass redistributions, see Bennett (1978), Csanady (1975), Gill (1982) Jacobs (1974), Kraus and Turner (1967), McCormick and Meadows (1988), Mohammed-Zaki (1980), Mortimer (1974), Munk and Anderson (1948), Pollard, et. al., (1973), and Price and Weller (1986).

CHAPTER III

PRESENTATION AND DESCRIPTION OF THE CURRENT, TEMPERATURE, WATER LEVEL, AND METEOROLOGICAL OBSERVATIONS

Description of Data Set and Processing Techniques

Complete descriptions of all current meter and meteorological data collected during 1977-1978 and 1988-1989 have been presented in Miller and Saylor (1985) and Gottlieb *et al.* (1990), respectively. Other data collected during the 1989 stratified season included time series of thermistor chain temperatures, Lake Michigan and Green Bay water levels, and an XBT transect (see Fig. 1.2) sampled in July and October. All time series data described herein, which includes the current meter, thermistor chain, meteorological, and water level gauge records, were processed in an identical manner. Time series data processing consisted of averaging (if necessary) to an hourly interval (herein referred to as the "raw" data, unless otherwise noted), 40-hour low-pass filtering (with a Cosine-Lanczos filter, as described in Mooers and Smith, 1968), and then averaging again ("averaged" data) to a 12-hour interval (current velocities) or a 3- or 4-hour interval (all other data).

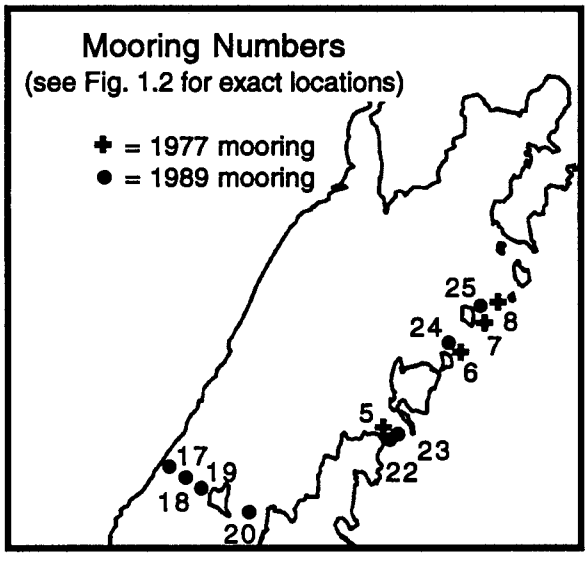

Figure 3.1. Map indicating mooring numbers.

The current meter data, consisting of current velocities and water temperatures recorded at 15-minute intervals, were collected by vector-averaging current meters (VACMs) suspended on the taut-line moorings numbered in Fig. 3.1. Moorings from 1977 held two VACMs (at 12 m depth, and 5 m above the bottom) and most 1989 moorings held three VACMs (at 12 and 20 m depth, and 5 m above the bottom). All current velocity vectors presented herein have been rotated into their respective passage axes, so that the currents may be described as flowing into or out of northern Green Bay (Fig. 1.3); rotation angles are 55, 40, 25, and 0° for Deaths Door, Rock Island, St. Martin Island, and Poverty Island Passages, respectively. Herein, data from each VACM will be referred to by mooring number (Fig. 3.1) and depth in parentheses; for example, 24(20.0) refers to the VACM at 20 m depth on mooring number 24.

Meteorological data recorded hourly at the city of Green Bay (Fig. 1.1), consisting of wind velocity, air temperature, and barometric pressure, were obtained from the National Climate Data Center. The 1977 meteorological data were recorded at 3-hour intervals, linearly interpolated to 1-hour intervals, and then processed as raw data. Wind velocities recorded at Sheboygan, Wisconsin and a buoy in northern central Lake Michigan compared well with those recorded at the city of Green Bay (Gottlieb *et al.*, 1990), and for the present investigation it will be assumed that the recorded winds represent the actual winds at the Green Bay mouth region. Water levels recorded hourly by permanent gauges around Lake Michigan and at the city of Green Bay, and at temporary gauges at Escanaba and Washington Island (see Fig. 1.1 for gauge locations), were obtained from the National Ocean Survey branch of the National Oceanic and Atmospheric Administration.

Averaged Data from the 1977 and 1989 Stratified Seasons

Current velocities and water temperatures from Deaths Door, Rock Island, St. Martin Island, and Poverty Island Passages are presented in Fig. 3.2. Currents from the

upper and lower levels in Deaths Door Passage opposed each other during mid-May to mid-September, indicating two-layer exchange flow with cool Lake Michigan inflow along the bottom (lower layer) and warm Green Bay outflow near the surface (upper layer). Major two-layer exchange events occurred during May 22-25, June 14 to July 7, July 12-22 and Aug. 12-16, and events of shorter duration but equal magnitude occurred persistently from mid-July to early September. Almost all of the two-layer exchange events were separated by much weaker but persistent "inverse" two-layer exchange events, i.e., Lake Michigan inflow near the surface and Green Bay outflow along the bottom.

The flow directions (inflowing or outflowing) of the currents in Rock Island and Deaths Door Passages (Fig. 3.2) were mostly unidirectional at the bottom level, and were more frequently opposed in direction at the top level (percent occurrence distributions of the flow directions are presented in the following chapter in Table 4.4). Compared to Deaths Door Passage, two-layer exchange events in Rock Island Passage were weaker and rarer, but lower-layer inflow of Lake Michigan water was strong and persistent in both passages. Rock Island Passage is less constricted (see Appendix) and less sheltered (see Fig. 1.2) than Deaths Door Passage so the surface currents there are more subject to direct wind forcing, which is consistent with the observed weaker two-layer flows and the occurrences of opposing upper-layer flows. Due to its much larger cross-sectional area, currents through Rock Island Passage produce two to three times greater volume transport than currents of comparable magnitude through Deaths Door Passage, as will be seen in the following section.

The maximum temperature difference (about 12°C) between the upper and lower layers in Deaths Door and Rock Island Passages (Fig. 3.2) occurred from late June to early September, indicating complete development of the thermocline. The upper-level temperature record from Deaths Door Passage shows a relatively warm period during late May which was related to the observed large outflow of Green Bay water there. The notable temperature dip seen in the record during July 7-12 correlated with a gap between

two major exchange events, indicating that the passage was flooded with Lake Michigan water during that time. Upper-level temperatures in Rock Island Passage were similar to those in Deaths Door Passage, but in the former the late-May warming trend was weaker and the noted temperature dip was not as pronounced. From late July to mid-August in both Deaths Door and Rock Island Passages, the periodicity observed in the upper-layer temperature fluctuations was also observed in the lower-layer inflow events, indicating that the inflow events were associated with thermocline oscillations.

On Sept. 9 mooring 5 was struck by a ship and sunk, and thus only bottom temperature (Fig. 3.2) was recorded thereafter. Also on Sept. 9, the strongest filtered current speed (almost 40 cm/s) of the entire season was observed at 6(41.3) in Rock Island Passage during a brief but very intense lower-layer inflow event. Corresponding to this event was the initiation of decreasing temperature difference between the upper and lower layers in the passage, thus marking the onset of autumnal thermocline degradation. During Sept. 12-29 a pronounced warming trend and a rare, strong, lower-layer outflow event were simultaneously recorded at 6(41.3), and during Oct. 9-23 a cooling trend in both layers occurred coincident with a strong lower-layer inflow and weaker but persistent upper-layer inflow in the passage. The water column was nearly isothermal by early November, after which time the upper- and lower-level currents and temperatures were identical (i.e., the flow was barotropic) in all passages.

Fig. 3.2 also shows currents and temperatures from St. Martin Island and Poverty Island Passages. Currents recorded at 7(18.8) near the bottom of St. Martin Island Passage show the previously-described lower-layer inflow events that occurred June 14 to July 7 and July 12-22. However, currents recorded at 8(24.0) near the bottom of Poverty Island Passage do not show those events. Rather, currents at both levels in Poverty Island Passage were very weak and exhibited the most omni-directional behavior observed in any of the passages. Also, in Poverty Island Passage prior to thermocline degradation the upper- and lower-level current directions were much more random than in

either Deaths Door or Rock Island Passages (scatter plots of upper vs. lower layer flow are presented in the following chapter), indicating that the response to forcing was more complicated in this passage.

During mid- to late June (Fig. 3.2), the upper-level warming trend observed in the southern passages (Deaths Door and Rock Island) corresponded with an upper-level cooling trend in the northern passages (St. Martin and Poverty Island), thus indicating a long-term, large-scale, horizontal temperature (density) gradient across the mouth of Green Bay. The upper panel of Fig. 3.3 shows joint occurrences of a strong horizontal temperature gradient across the bay mouth, and lower-layer inflow events recorded in Rock Island Passage (joint occurrence distributions of cross-mouth density difference vs. lower-layer velocity are presented in the following chapter in Figs. 4.6 and 4.7). All of the major lower-layer inflow events and even some of the shorter ones occurred during periods of relatively cold upper-level temperatures in St. Martin and Poverty Island Passages, warmer temperatures in Rock Island Passage, and persistently warmest temperatures in Deaths Door Passage, i.e., periods when the thermocline surface across the mouth was tilted up towards the north (Figs. 2.7 and 2.8). Thus, lower-layer inflow of Lake Michigan water occurs very frequently during periods when the thermocline tilts up towards the northern end of the bay mouth.

For the 1989 stratified season, joint occurrences of lower-layer inflow events and thermocline tilting events are revealed in the lower panel of Fig. 3.3, which shows temperatures at both the top and middle depth levels in Deaths Door (22 and 23), Rock Island (24), and St. Martin Island (25) Passages, and bottom-level currents in Deaths Door Passage. These joint occurrences, which are consistent with geostrophy (Figs. 2.7 and 2.8), were evident but certainly not as obvious an influence on the exchange as they were in 1977. Comparison of the upper-level (12 m) temperatures in Fig. 3.3 shows that the average temperature difference between the north (moorings 8 and 25) and south (5 and 22) ends of the bay mouth during the 1989 season was about half of that during the

1977 season. However, geostrophically-consistent exchanges were observed during 1989, seen (Fig. 3.3) as a number of relatively short but recurrent periods of jointly occurring lower-layer inflow and tilted thermocline, for example May 27 to June 1, July 1-8, July 16-20, July 24-29, Aug. 1-7, Aug. 8-15, and others.

Lower-layer inflow events and temperatures in Deaths Door Passage revealed an eight-day periodicity during mid-July to early August, 1989, and this same periodicity also was observed in the winds during the same dates (Fig. 3.3). The calculated theoretical period of a longitudinal, first-mode, standing internal wave in the Green Bay basin is about eight days (Gottlieb *et al.*, 1990). The similar periodicities observed in the wind, lower-layer inflow, and temperatures across the bay mouth are consistent with near-resonant meteorological forcing of an internal seiche in Green Bay, as described briefly in Gottlieb *et al.* (1990). This phenomenon will not be analyzed in the present investigation, and will herein be referred to as the 8-day thermocline oscillation in Green Bay.

1989 XBT Transects and Related Raw Data

An opportunity to investigate the relationship between thermocline position and two-layer exchange is provided by the two XBT transects through Deaths Door Passage collected during July and October. The station number, position, depth, and time for each XBT station are listed in Table 3.1, and the temperatures along the transects are shown in Fig. 3.5. In the present section, the temperature transects will be described, and then compared with the associated raw time series data.

In the July transect the thermocline was found at about the same depth range (15-20 m) in both the bay and the lake, and was slightly elevated (to 10-15 m) in the passage. Below the thermocline however, temperatures were 3 to 4°C cooler in the lake than at comparable depths in the bay, thus providing the pressure (density) gradient that drives the lower-layer inflow. By October, the transect (Fig. 3.5) shows that the thermocline was highly degraded but stratification remained significant. Temperatures were 3 to 4°C

cooler in the lake at nearly all depth levels, resulting in very steeply sloped isotherms within the passage. The wave-like shapes of the 9, 10, and 10.2°C isotherms indicate internal waves, vertical overturning, or some other internal hydraulic phenomenon.

XBT Station Number	Latitude (degrees N)	Longitude (degrees W)	Distance from last (km)	Chart Depth (m)	Trace Depth (m)	Trace Time (EST)
09 (34)	45.328 (45.325)	87.070 (87.078)	2.6 (2.6)	30.9	30.9 (32.7)	1739 (2026)
10 (33)	45.328 (45.325)	87.037 (87.037)	1.7 (1.7)	36.4	35.8 (37.1)	1751 (2016)
11 (32)	45.328 (45.325)	87.010 (87.012)	1.2 (1.2)	35.8	35.8 (35.2)	1801 (2010)
12 (31)	45.318 (45.318)	86.997 (86.997)	0.9 (0.9)	38.8	42.1 (39.6)	1807 (2004)
13 (30)	45.310 (45.307)	86.980 (86.980)	1.2 (1.2)	35.5	38.4 (38.4)	1814 (1956)
(29)	(45.298)	(86.965)	(0.9)	34.5	(36.5)	(1757)
14 (28)	45.288 (45.288)	86.948 (86.948)	1.1 (1.1)	18.2	39.0 (25.8)	1824 (1751)
15 (27)	45.280 (45.278)	86.932 (86.933)	0.9 (0.9)	28.8	28.3 (27.7)	1827 (1748)
17 (26)	45.272 (45.272)	86.920 (86.922)	0.9 (0.9)	27.3	18.3 (30.2)	1849 (1740)
(25)	(45.272)	(86.898)	(1.1)	13.9	(20.1)	(1734)
18	45.272	86.892	1.4	17.6	20.1	1905
19 (24)	45.272 (45.272)	86.857 (86.858)	1.7 (2.1)	26.7	30.8 (31.5)	1911 (1715)
20	45.272	86.815	2.1	46.7	42.7	1923
21	45.272	86.775	2.0	48.5	50.3	1928
(23)	(45.272)	(86.755)	(5.0)	48.5	(49.0)	(1704)
22	45.272	86.738	1.8	48.5	50.9	1938

Table 3.1. Number, location, depth, and time of each station along the XBT transect collected during July 22 (no parentheses) and October 10 (parentheses), 1989. XBT station number 29 was located near mooring 23. See Fig. 1.2 for transect location map, and Fig. 3.5 for vertical temperature profiles.

To aid interpretation of the XBT transects, Fig. 3.6 shows raw water level and meteorological records, and current velocity and temperature records from the three depth levels in Deaths Door Passage. At around the time of the July XBT collection the observed currents, temperatures, and water levels (Fig. 3.6) exhibit a prominent 12.4-hour (1.93 cpd) oscillation, which is the period of the semidiurnal tide. Some of these tidal currents also show a strong baroclinic component. For example, during July 16-19 the inflowing tidal currents were strong at the bottom, weaker at the middle, and very weak at the top level. The baroclinic pressure gradient was enhanced by wind-induced upwelling of cold Lake Michigan water at the Green Bay mouth in response to the observed mostly-southerly winds (Fig. 3.6), as described in Fig. 2.9. Subsequently during July 19-21, the baroclinic pressure gradient was suppressed by wind-induced downwelling of the thermocline in Lake Michigan (Fig. 2.9) in response to the observed

very strong northeast winds (Fig. 3.6). The resulting currents observed during July 20-24 were mostly barotropic.

The observed currents (Fig. 3.6) at around the time of the XBT transect (July 22) were weak but flowed into Green Bay at all depth levels, and also showed a small baroclinic component with increased flow near the bottom. The effect of the semidiurnal tidal oscillation (Fig. 3.5) was notable during periods when the tidal currents were mostly barotropic (e.g., June 20-24 in Fig. 3.6), i.e., the flooding (inflowing) currents were associated with the warming portion of the tidal temperature oscillation, and the ebbing (outflowing) currents with the cooling portion. This association between inflowing Lake Michigan water and warming temperatures in the passage is inconsistent with the two-layer estuarine exchange model (Figs. 2.3 and 2.4), in which inflowing currents should carry cooler Lake Michigan water and thus should be associated with cooling temperatures. However, these observations are consistent when interpreted as a semidiurnal internal waveform, as will be described Chapter V.

During October (Fig. 3.6) the 2- to 4-day period variability observed in the water levels was associated with the observed barometric pressure fluctuations. During the first half of October bottom level currents were very strong and almost entirely into Green Bay, as indicated by the observed (Fig. 3.5) steeply-sloped isotherms. Also, the temperatures in Deaths Door Passage showed the thermocline to be persistent but weakening, observed as a general decrease in the temperature difference between the top and bottom levels. Two notable warming events observed on Oct. 7 and 11 at the bottom level did not obviously correspond with any fluctuations in the meteorological or water level records, indicating the persistent influence of the baroclinic pressure gradients (i.e., stratification). During the collection time of the XBT transect, the observed currents showed lower-layer inflow and weak but mostly outward flow at the middle and top levels, consistent with an intermediate-type exchange (Fig. 2.4) of Lake Michigan water flowing in and under a retarded outflow of Green Bay water.

Raw currents in Rock and St. Martin Island Passages and the raw temperatures in each passage at each depth level during July and October are shown in Fig. 3.7. Top- and middle-level temperatures and currents in Rock Island Passage were warming and outflowing during July 14-17 and 20-24, and cooling and inflowing during July 17-20, consistent with a two-layer exchange model. The tidal signal in the temperature records was prominent at all levels in Deaths Door Passage, but only at the top levels in Rock and St. Martin Island Passages. The tidal signal was notably absent from the bottom-level temperature records in Rock and St. Martin Island Passages, indicating that the origin of this water was from an isothermal portion of the water column. Also, the waters in these passages were typically cooler (denser) than in Deaths Door Passage (see monthly averages in Table 3.2), indicating the influence of cold Lake Michigan water. Despite a thermocline tilted up to the north during July 20-24, currents at all levels in Rock Island Passage were mostly outflowing (joint occurrence distributions of cross-mouth density differences and lower-layer flow magnitudes for the season are presented in the following chapter in Figs. 4.6 and 4.7). In this case, the effects of earth's rotation (Fig. 2.7) must have been overwhelmed by other factors.

Passage and Mooring	Depth (m)	JUL	AUG	SEP	Passage and Mooring	Depth (m)	JUL	AUG	SEP
Deaths	12.0	13.54	15.99	15.94	Rock	12.0	12.35	14.82	15.59
Door	20.0	9.80	9.93	12.13	Island	20.0	7.81	8.79	11.03
22	22.5	8.08	7.67	9.70	24	39.2	5.52	5.91	6.56
Deaths	12.0	13.04	15.29	15.39	St. Martin	12.0	11.71	13.68	15.69
Door	20.0	9.42	9.88	11.70	Island	20.0	7.68	9.36	11.73
23	29.8	7.40	7.46	9.90	25	31.9	5.94	6.96	8.18

Table 3.2. Monthly averages of the raw temperatures (in °C) from each mooring and depth level during July, August, and September of 1989.

Fig. 3.8 shows raw and filtered water level records from gauges located inside Green Bay and around Lake Michigan (see Fig. 1.1 for gauge locations). The filtered levels during July revealed that large variability, especially noted at Milwaukee, Calumet, and Holland, was associated with strong winds (Fig. 3.6) shifting from south-southwesterly to northeasterly during July 18-20. A large dip in the Kewaunee level dur-

ing July 16-18 showed no apparent association with any other observed water level or meteorological fluctuation, but it must be cautioned that some observed large-amplitude water-level variations were due to local effects rather than large lake-level excursions, for example if the gauge was located within a harbor or canal. Water levels at all gauges during October revealed large-amplitude fluctuations, and water level fluctuations at the Washington Island, Escanaba, Port Inland, and Mackinaw City gauges were associated with barometric pressure fluctuations (Fig. 3.6), i.e. peaks in the filtered levels were associated with dips in the pressure.

Fig. 3.8 may be used to estimate the magnitude of the currents through the Green Bay mouth passages driven by water level excursions in either the bay or lake. A maximum averaged water level excursion of about 0.5 ft/day = 0.00015 km/day was observed at the bay mouth (Washington Island) during Oct. 5-7. Multiplying by half of the bay's surface area (2125 km^2) and dividing by the bay mouth's cross-sectional area (0.52 km^2) yields a value of 0.62 km/day = 0.7 cm/s, which is below the threshold value (1.0 cm/s) of the current meter rotor. Thus, currents through the bay mouth driven by water level excursions are typically two orders of magnitude less than the currents driven by other forcing mechanisms (tides, internal pressure differences, etc.), and cannot be measured using mechanical current meters.

Samples of the Raw Data from 1977 and 1989

Stratified exchange flows can be categorized into four groups based on the flow directions (into or out of the bay) of the two layers, and these groups are:

1) two-layer exchange — lower-layer inflow and upper-layer outflow
2) single-layer inflow — both layers inflowing
3) single-layer outflow — both layers outflowing
4) inverse two-layer exchange — lower-layer outflow and upper-layer inflow

The frequency of occurrence of the observed exchange flows within these four groups will be shown (Chapter IV) using scatter plots, but scatter plots do not reveal the vertical shear

(baroclinic) structure of the stratified exchange currents. In the present section, representative samples of the raw data records (which are too large to be shown in their entirety) help reveal the baroclinic structure, dynamic variability, and character of the stratified exchange flows.

Fig. 3.9 shows samples of the raw current and water temperature records from Deaths Door, Rock Island, and Poverty Island Passages during July 14-26 and Aug. 7-19. Single-layer inflow and two-layer exchange events were associated with south-southwesterly winds, and single-layer outflow and inverse two-layer exchange events with northeasterly to northwesterly winds, consistent with Fig. 2.9. During the periods July 14-22 and Aug. 12-16 the strong lower-layer inflow events observed in Rock Island Passage were associated with fluctuations in the bottom-level temperature difference between Deaths Door and Poverty Island Passages. The lower-layer inflow at 6(41.3) occurred during periods of relatively warm temperatures at 5(31.3) and cool at 8(24.0), compared with the temperatures during other periods (e.g., July 22-23, Aug. 7-11, and Aug. 16-19). Specifically, the lower-layer inflow at 6(41.3) occurred when the temperature difference between 5(31.3) and 8(24.0) exceeded about -3°C, i.e., the inflow occurred when $T_{5(31.3)} - T_{8(24.0)} > -3°C$. Conversely, during the periods July 22-23, Aug. 7-11, and Aug. 16-19 the temperature difference $T_{5(31.3)} - T_{8(24.0)}$ was less than -3°C, and was associated with lower-layer outflow at 6(41.3). These observations are consistent with geostrophy (Figs. 2.7 and 2.8).

The characteristics of the lower-layer currents observed during the stratified season are typified by those shown in Fig. 3.9. In Deaths Door and Rock Island Passage the magnitudes of the lower-layer inflowing currents were consistently larger than the outflowing current magnitudes. A strong lunar semidiurnal tidal signal in the current and temperature records, along with other various weaker signals of sub-daily periods were observed frequently in all passages (spectral peaks will be identified in the spectral analysis to be presented in Chapter IV). The amplitudes and frequencies of the sub-daily

oscillations showed large variability within different passages and at different depth levels. Because of the use of three depth levels rather than two, the 1989 observations provide a better opportunity to investigate these sub-daily oscillations and their influence on the two-layer exchange flows.

Raw currents and temperatures recorded in Deaths Door and Rock Island Passages at the bottom, middle, and top depth levels during the 1989 stratified season are shown in Fig. 3.10. The strongest cycle of the 8-day thermocline oscillation in Green Bay (introduced on pg. 33) was observed during the period from July 28 to Aug. 6. During this period the barometric pressure gradually dropped, and the wind reversed from northeasterly to southwesterly. The bottom- and middle-level currents responded by gradually reversing from weakly outflowing to strongly inflowing in Rock Island Passage, and by producing the largest two-layer exchange flows (Aug. 1-6) observed during the entire season in Deaths Door Passage. Also during Aug. 1-6, the Rock Island lower-layer inflow was steady, as compared to the Deaths Door lower-layer inflow in which an extremely large semidiurnal tidal signal was observed.

The low-pass filtered water temperatures observed across the bay mouth (Fig. 3.10) during Aug. 1-6 (the last half of strongest cycle of the 8-day Green Bay thermocline oscillation) were consistent with the expected effect of rotation (Figs. 2.7 and 2.8). This thermocline tilt was observed as a temperature difference between the middle levels in Deaths Door and Rock Island Passages, i.e., the inflow occurred when the temperature at 23(20.0) exceeded that at 24(20.0) by about 2°C. Also during Aug. 1-6 the temperatures at 23(20.0 m) revealed a very large-amplitude (up to 13°C) semidiurnal oscillation, while at 24(20.0 m) the oscillation was mostly absent. Furthermore, the semidiurnal temperature oscillation was observed at all depth levels within Deaths Door Passage, indicating that the range of the semidiurnal thermocline excursion was approaching the depth (about 30 m) of the passage. In this case, the warm temperatures in Deaths Door Passage may result from the large internal tidal range,

increased Green Bay outflow, rotation effects (Fig. 2.7), or a combination of these and possibly other mechanisms.

Thermistor chain recordings from Rock Island Passage showing the 8-day thermocline oscillation in Green Bay are presented in Fig. 3.11, where during the oscillation cycle from July 28 to Aug. 6 the thermocline was observed to deepen and intensify gradually. The base and top of the thermocline were observed to correspond approximately with the 8 and 18°C isotherms, respectively. During the first half (July 28 to Aug. 1) of the oscillation cycle both the base of the thermocline downwelled and the lower-layer water (below the base) warmed in the passage, indicating the presence of lower-layer water from Green Bay flowing out of the passage (Fig. 3.10). These observations were consistent with the observed (Fig. 3.10) northeasterly winds inducing northwestward transport of upper-layer water in the bay and lake (Fig. 2.9), resulting in the enhanced bay water outflow and suppressed lower-layer inflow.

During the second half (Aug 1-6) of the oscillation cycle the base of the thermocline in Rock Island Passage (Fig. 3.11) remained at an approximately constant depth while the thermocline top continued to deepen, resulting in very large temperature gradients (up to 2°C/m) between the upper and lower layers towards the end of the cycle. Also, temperatures homogenized in the lower and upper layers at around 5.5 and 20.5°C, respectively. During this period, steady southwesterly winds (Fig. 3.10) induced (Fig. 2.9) a baroclinic pressure gradient driving lower-layer inflow and a barotropic pressure gradient enhancing upper-layer outflow, producing the most intense thermocline (see Figs. 3.10 and 3.11) and the largest two-layer exchange flows (Figs. 3.4 and 3.10) observed during the entire season.

The currents and temperatures displayed in Fig. 3.12 are from Sept. 13 to Oct. 7, during which time the thermocline was degrading. Prior to Sept. 22 winds were mostly southwesterly, and during Sept. 22-23 the passage of an intense storm system resulted in strong north-northwesterly winds. Subsequently, the currents in Deaths Door

Passage showed strong two-layer exchange flow before the storm, and very strong barotropic tidal-period flows afterwards. Rock Island Passage currents were two-layered before the storm, and mostly tidal and barotropic afterwards. As seen previously, the inflowing lower-layer currents were associated with an approximate 2°C temperature difference between the records from 23(20.0) and 24(20.0). The tidal currents displayed much stronger inflow than outflow, consistent with an elevated Lake Michigan water level due to wind-induced southwestward transport (Fig. 2.9) in both the lake and bay. The tidal currents showed no significant baroclinic component because the storm destroyed the thermocline, whereas tidal currents prior to thermocline destruction (Sept. 14-18) revealed a relatively strong baroclinic component, seen as an enhancement of both the inflowing and outflowing bottom-level currents.

The storm-induced thermocline destruction during Sept. 22-23 was observed (Fig. 3.12) as a rapid homogenization of the temperatures at all three levels in Deaths Door and Rock Island Passages. After thermocline destruction, temperatures in Deaths Door Passage fluctuated between varying states of homogenization and stratification. However, the stratification was severely reduced and continued to weaken after Sept. 23. During the period Sept. 29 to Oct. 7 the lower-layer currents in both Deaths Door and Rock Island Passages were entirely into Green Bay. Rock Island currents were mostly barotropic, with a small baroclinic component suggested by occasions of increased bottom-level currents. Also, Deaths Door currents revealed a moderate two-layer exchange from Sept. 29 to Oct. 2, indicating that despite the reduced stratification, flushing near the bay mouth remains strong and efficient into the autumn months.

Fig. 3.13 shows thermistor chain recordings from Rock Island Passage during the same time period shown in Fig. 3.12. Prior to the Sept. 23 storm both the average thickness and depth of the thermocline remained relatively constant. A moderately strong oscillatory signal with a period in the range of 10-14 hours was observed in the thermocline excursions. This oscillatory signal with its poorly defined period was a

response to several forcings, including certain bay and lake surface modes (as will be seen in the following chapter) and the semidiurnal internal wave generated in nearby Deaths Door Passage (see Fig. 3.10). The Sept. 23 storm resulted in degradation of the layered structure observed in the stratification. Before the storm, the temperature gradient between the upper and lower layers averaged about 1°C/m depth, whereas immediately afterwards the gradient averaged about 0.25°C/m depth. Upper-layer waters cooled from about 17 to 13°C, while the lower-layer warmed from about 6 to 9.5°C, illustrating the homogenizing effect of the storm. Temperatures remained weakly two-layered throughout September, and in the beginning of October the two-layered structure gave way to an almost linearly stratified structure. A strong baroclinic component favoring lower-level inflow persisted into October (Figs 3.12 and 3.7), thus promoting flushing near the bay mouth even at such late dates into the stratified season.

A final sample of the raw data shows currents and temperatures recorded from moorings 22 and 23 in Deaths Door Passage (Fig. 3.14). Moorings 22 and 23 were located about 1-km apart (see Fig. 1.2) within the passage, but the considerable flow and temperature differences observed between the moorings indicate large intra-passage variability. For example, at mooring 22 temperatures at the top and middle levels were consistently warmer, and velocities at all levels were weaker than at mooring 23. Also, periods of strong flooding tidal currents at 23(20.0) and 23(29.8) were associated with periods of strong ebbing tidal currents at 22(12.0), for example during Oct. 3-6 in Fig. 3.14; this behavior persisted throughout the entire record (not shown due to size limitations), probably due to the previously-described semidiurnal internal waveform.

In summary, variability of the currents and temperatures observed during the stratified season in the passages connecting Green Bay and Lake Michigan occurs over wide ranges of time and space scales. Observed temporal fluctuations are associated with internal waves, tides, wind and barometric pressure changes, and seasonal and intra-annual thermocline variability. Large spatial variability also is observed to occur; for

example, currents sometimes are uniform across the entire mouth, and other times are oppositely directed at similar depths in neighboring passages. Also, large intra-passage variability is observed within Deaths Door Passage. Discussion of the spatial and temporal variability observed in the tidal and longer-period current fluctuations is included in the following chapter.

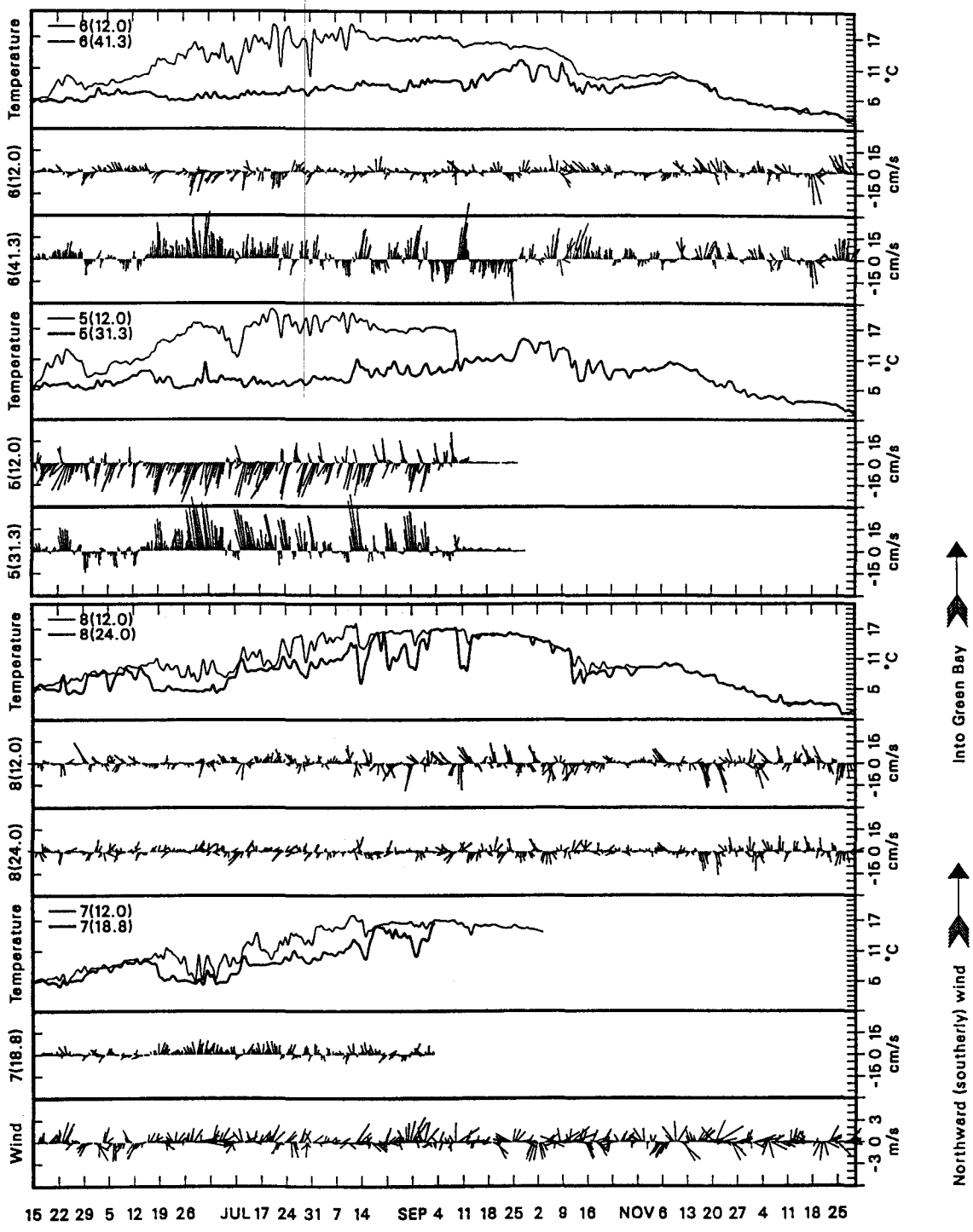

Figure 3.2. Currents and water temperatures recorded by instruments (depths indicated in meters) on moorings (Fig. 3.1) in Deaths Door (5), Rock Island (6), St. Martin Island (7), and Poverty Island (8) Passages, and winds recorded near the city of Green Bay (Fig. 1.1) during the 1977 stratified season. All data have been 40-hour low-pass filtered and averaged at a 12-hour (sticks) or 3-hour (temperatures) interval. Sticks pointing up/down represent currents flowing into/out of Green Bay, or northward/southward winds (i.e., southerly/northerly, or south/north winds). A strong lower-level Lake Michigan-water inflow persisted in Deaths Door, Rock Island, and St. Martin Island Passages during the period June 18 to July 25. Also during this period, the observed joint occurrences of relatively cool temperatures in the northern passages (St. Martin Island and Poverty Island) and warm in the southern passages (Deaths Door and Rock Island), and strong lower-layer inflow are consistent with the effects of rotation (Fig. 2.7). Two-layer estuarine exchange flow is most pronounced in Deaths Door Passage.

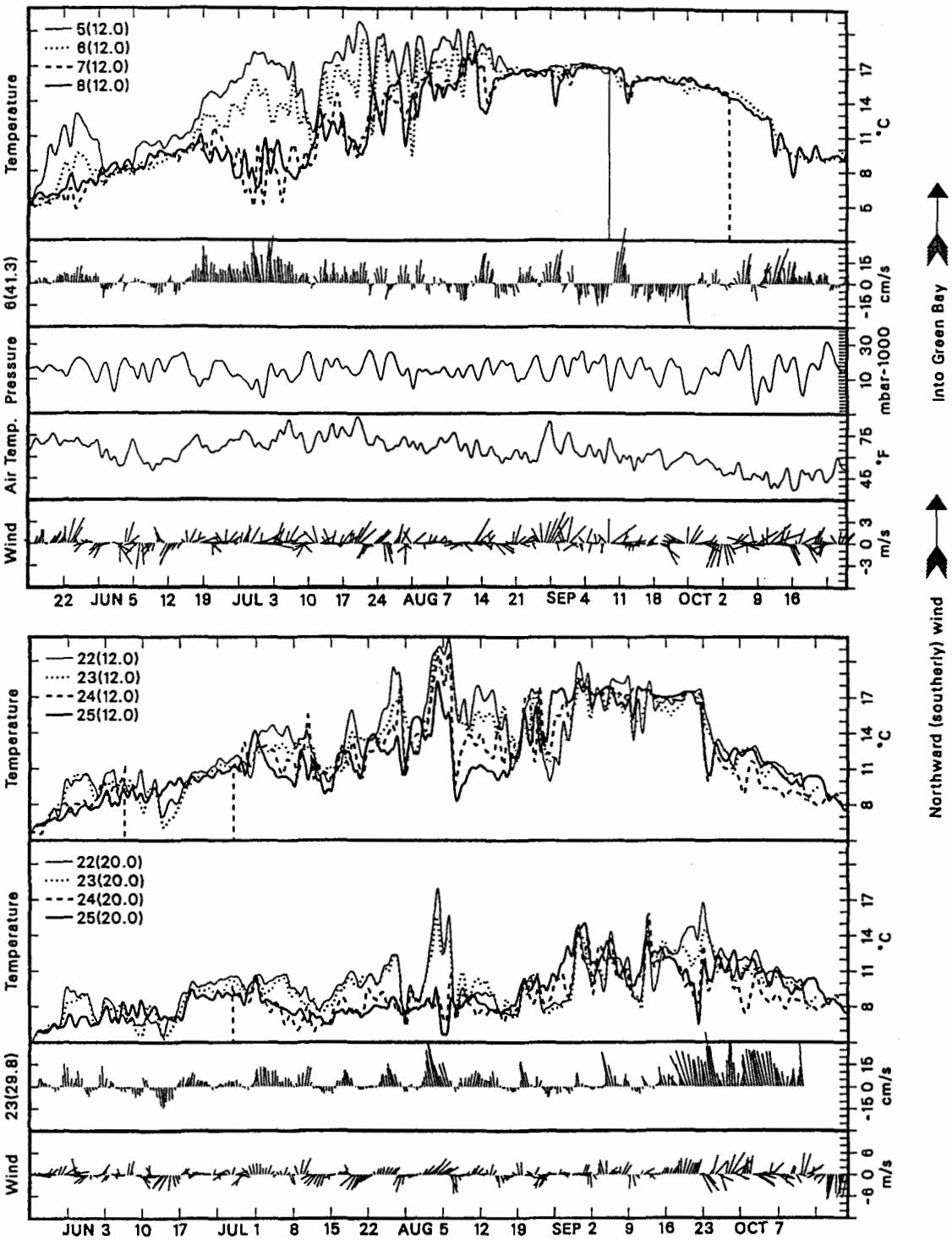

Figure 3.3. Currents, water temperatures, and meteorological data as described in Fig. 3.2 during the periods May 15 to Oct. 27, 1977 (top panel) and May 20 to Oct. 19, 1989 (bottom panel). The observed joint occurrences of strong lower-layer inflow and a tilted thermocline are consistent with rotation effects (Fig. 2.7). The thermocline tilt was such as to produce relatively warm temperatures in Deaths Door (5, 22, and 23) Passage and cool temperatures in St. Martin (7 and 25) and Poverty Island (8) Passages at similar depth levels. Joint occurrences of strong lower-layer outflow and a conversely tilted thermocline were observed much less frequently due to the prevailing pressure gradient which directs cool and dense lower-layer Lake Michigan water into Green Bay. Thermocline development during 1989 was affected by an 8-day period thermocline oscillation in Green Bay, seen during July 15 to Aug. 7 in the currents from 23(29.8) and the temperatures from 22(12.0).

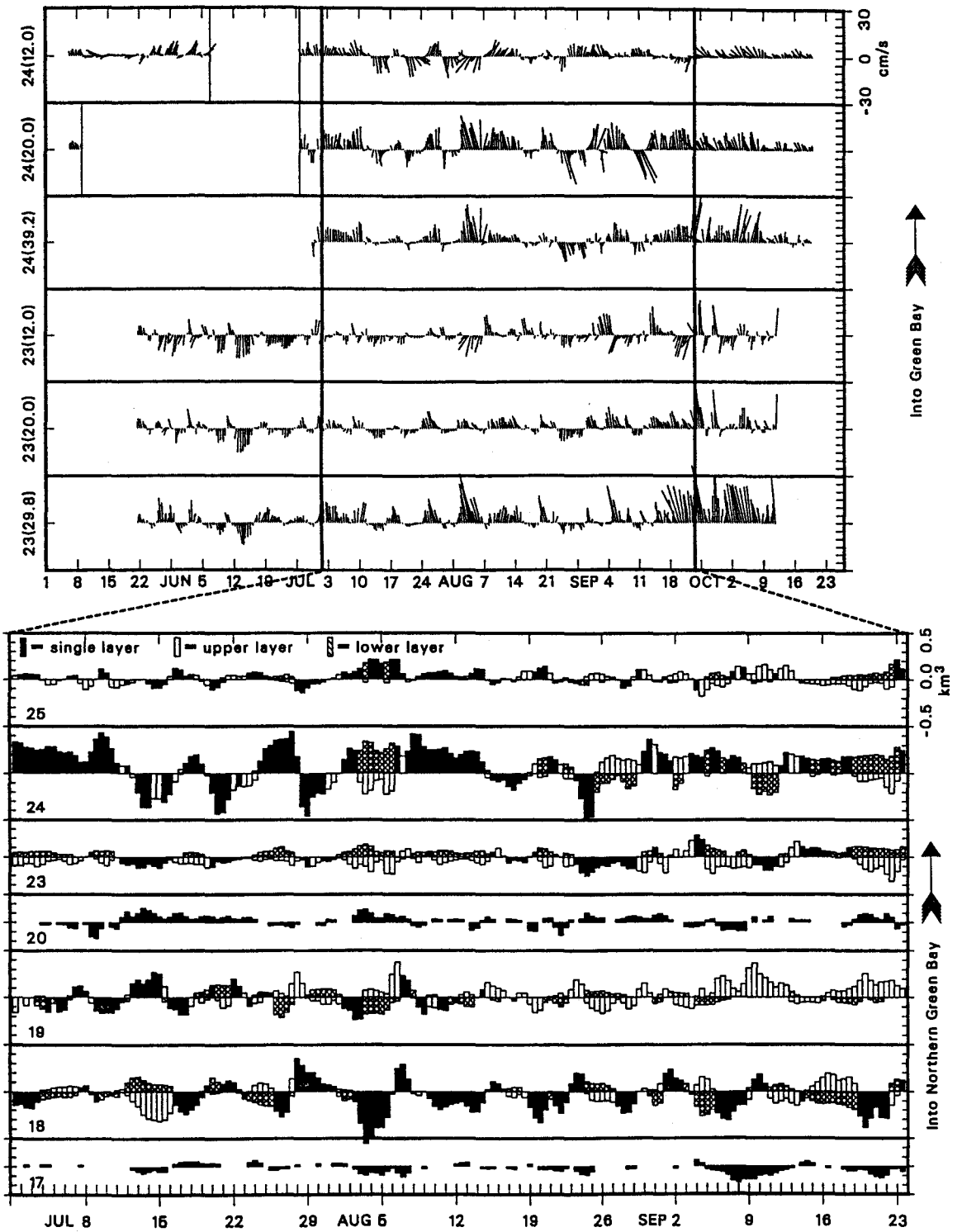

Figure 3.4. During the 1989 stratified season, low-pass filtered currents at three depth levels (12 m, 20 m, and 5 m above the bottom) in Deaths Door (23) and Rock Island (24) Passages (top panel), and bi-daily computed volume transports through all major passages in Green Bay (bottom panel). The transports, denoted by mooring number (Fig. 3.1), were divided into upper-, lower-, and single-layer components based on the zero-crossing point of the computed velocity profile, as described in the Appendix. Major two-layer exchange flow events in Deaths Door and Rock Island Passages, with lower-layer inflow and upper-layer outflow, are seen during Aug. 2-6 and Sept. 19-23, and result in water volume exchanges between Green Bay and Lake Michigan of up to one cubic km per day. Shear flow (single-layer) events with increased lower-layer speeds, as seen during July 1-11 in Rock Island Passage for example, also make a major contribution to the water volume exchange.

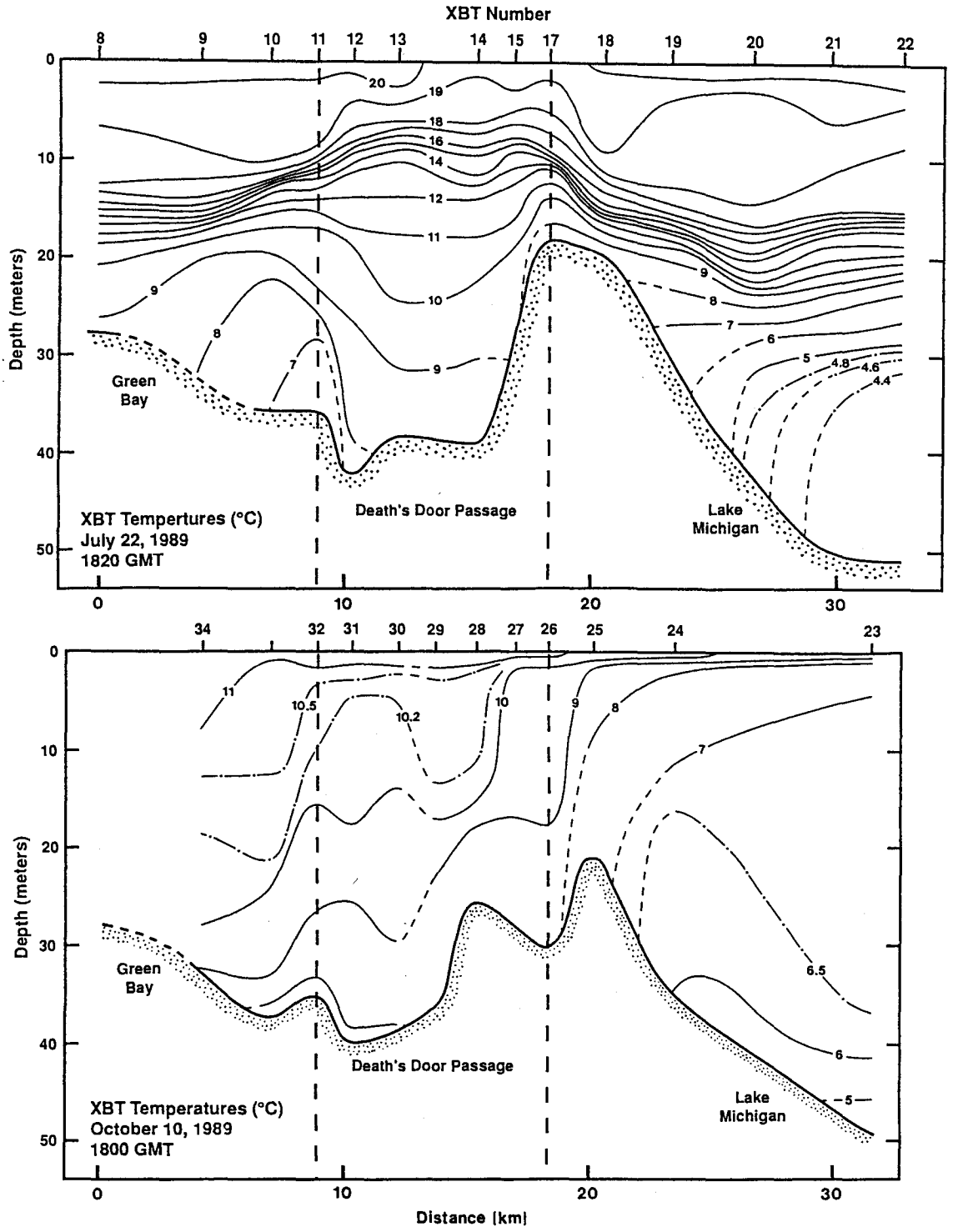

Figure 3.5. Vertical profiles of XBT temperatures during July 22 (top panel) and October 10 (bottom panel) collected along nearly the same transect (see Fig. 2.1 and Table 3.1 for XBT station locations and times) through Deaths Door Passage. In the July transect the thermocline is found between 10 and 20 m depth in Green Bay, and slightly deeper in Lake Michigan. Beneath the thermocline, water in Lake Michigan is much cooler than in Green Bay, thus providing the pressure gradient that drives Lake Michigan water into the Green Bay hypolimnion. The elevated thermocline within the passage is indicative of internal wave activity, which will be seen (Fig. 3.6) to occur primarily at the semidiurnal tidal frequency. In the October transect the thermocline is degraded but still evident, and water temperatures are cooler in Lake Michigan at all depth levels, resulting in pressure-driven Lake Michigan inflow at all depths.

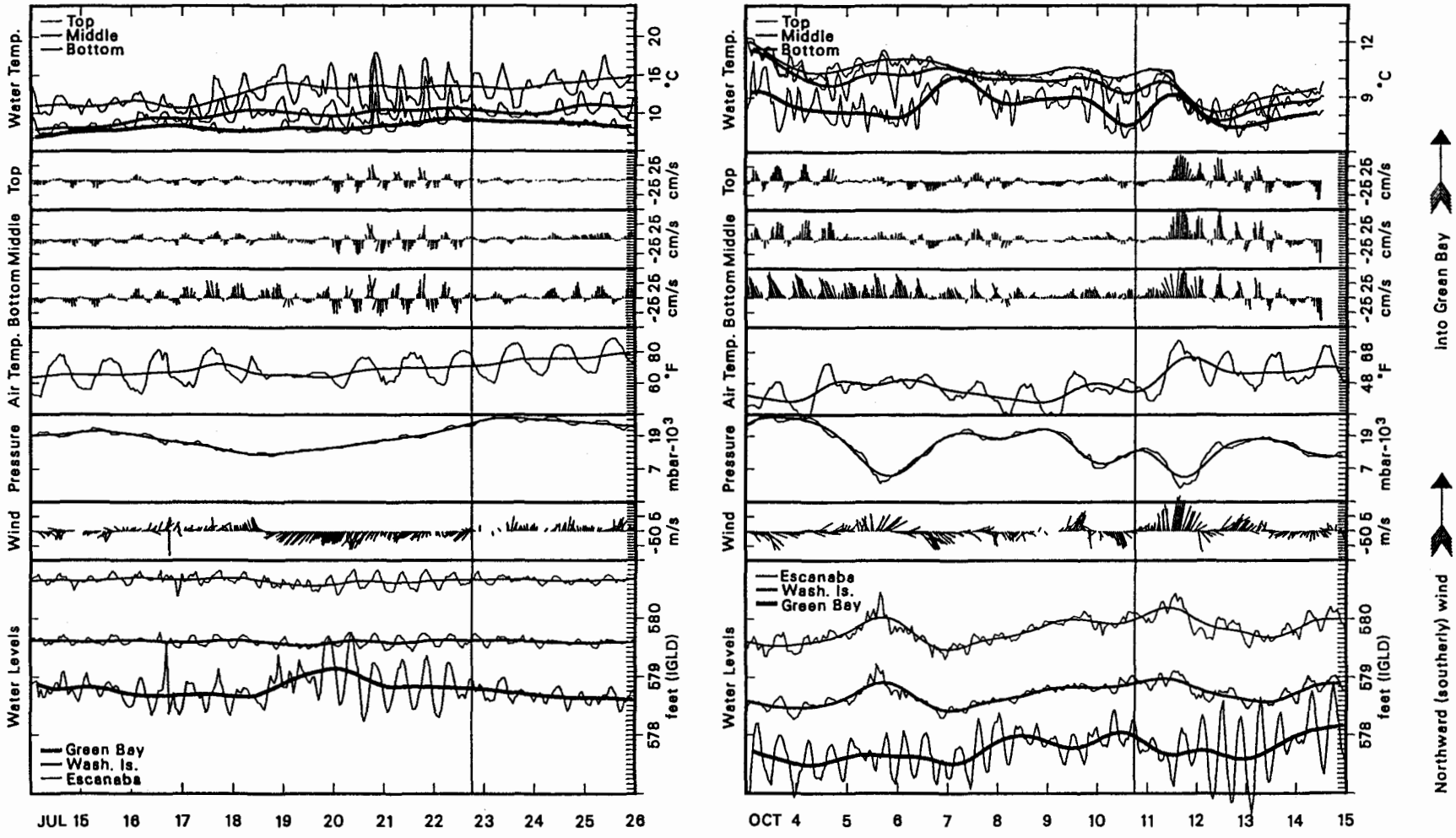

Figure 3.6. Water levels from the city of Green Bay, Washington Island, and Escanaba (offset upward by 0.8 feet), meteorological data from Green Bay, and currents and water temperatures from three depth levels (12 and 20 m, and 5 m above the bottom) in Deaths Door Passage during July 14-26 (left panel) and Oct. 3-15 (right panel). Shown is raw, hourly-averaged (thin lines and sticks) and low-pass filtered (thicker lines) data, and the vertical lines indicate the times of the XBT transects shown in Fig. 3.5. During the July transect currents were inflowing and strongest near the bottom, consistent with the observed baroclinic pressure gradient (Fig. 3.5). During October (right panel) bottom-level currents were almost entirely inflowing and middle- and top-level currents were mostly inflowing, consistent with the pressure gradient induced by the denser (colder) Lake Michigan water observed (Fig. 3.5) at all levels.

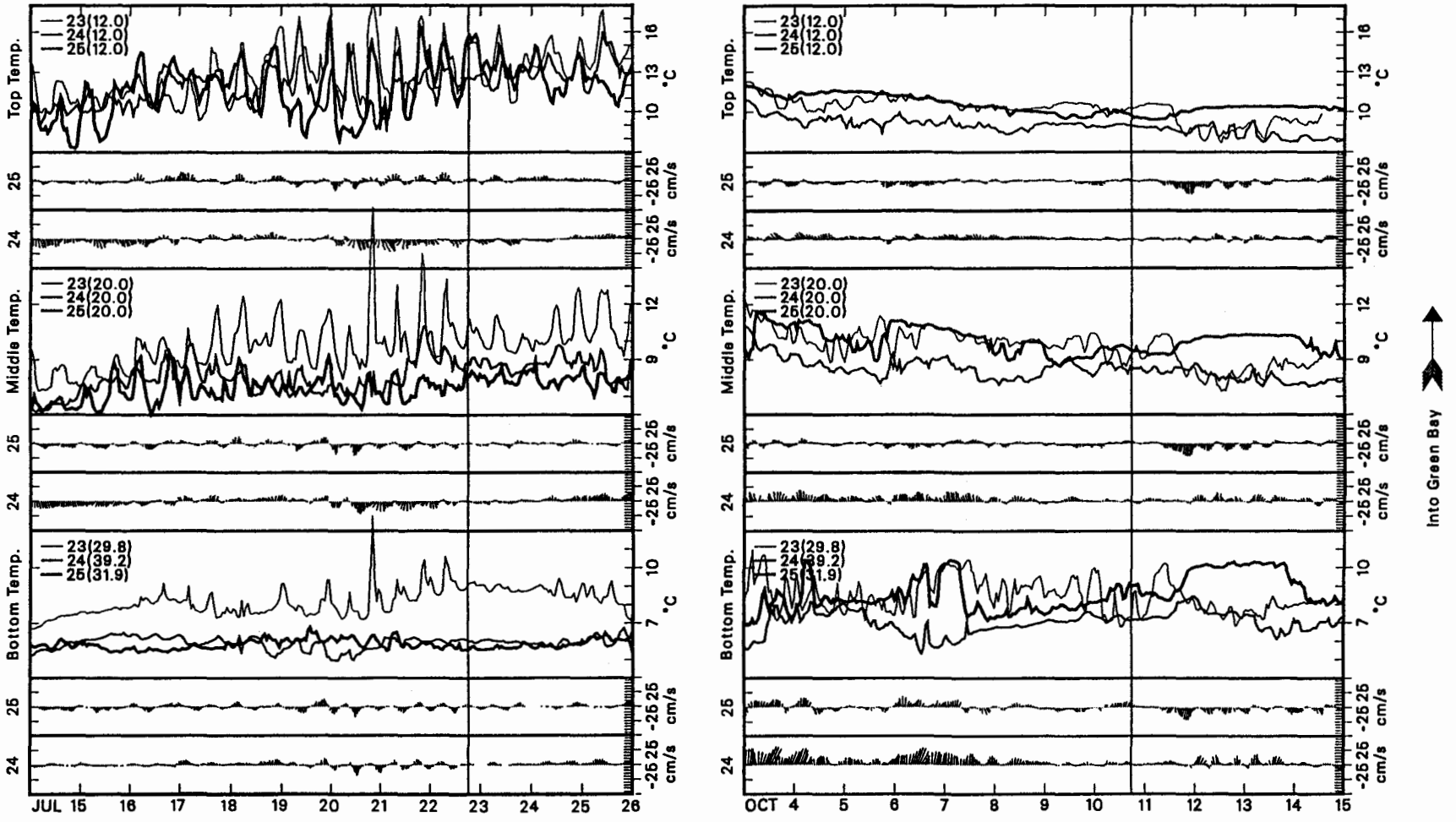

Figure 3.7. Raw, hourly-averaged currents from Rock Island (24) and St. Martin Island (25) Passages, and temperatures from all three passages at all three depth levels during July 14-26 (left panel) and Oct. 3-15 (right panel). The vertical lines indicate the times of the XBT transects shown in Fig. 3.5. During July 18-23 prominent semidiurnal temperature oscillations were observed at all depth levels in Deaths Door (23) Passage and at the top level in St. Martin Island Passage. Also, semidiurnal current oscillations were observed at all depths in all passages. During Oct. 3-9 two-layer exchange flow was very strong, as evidenced by sheared inflow with increased bottom-level currents in Rock Island Passage, and mostly outflowing currents at the top- and middle-levels in St. Martin Island Passage. Also, top- and middle-level temperatures were cooler in Rock Island Passage (the deepest passage) than in either Deaths Door or St. Martin Island Passages, indicating the cooling influence of the Lake Michigan water inflow.

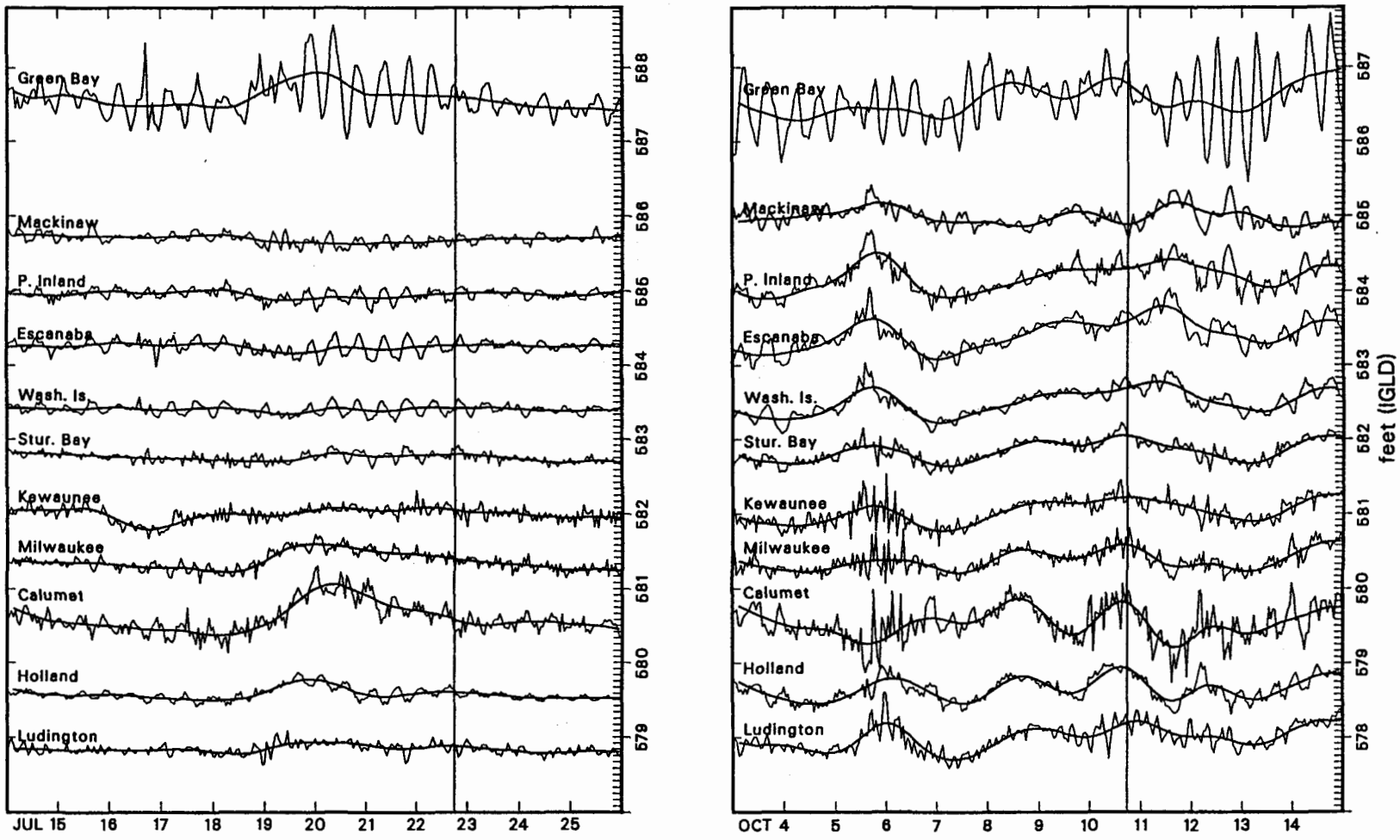

Figure 3.8. Raw, hourly (thin lines) and 40-hour low-pass filtered (thick lines) water level data recorded during July 14-26 (left panel) and Oct. 3-15 (right panel) at locations around Green Bay (city of Green Bay, WI and Escanaba, MI), from the Green Bay mouth region (Washington Island), and from around Lake Michigan (Ludington, MI, Holland, MI, Calumet, IN, Milwaukee, WI, Kewaunee, WI, Sturgeon Bay canal, Port Inland, MI, and Mackinaw City). The bottom record corresponds with the vertical axis scale, and each subsequent record is offset upward by .8 feet (1.6 feet for the top record). The vertical lines indicate the times of the XBT transects shown in Fig. 3.5. The tidal range observed at the bay mouth (Washington Island) during July 19-22 was about 4 inches, and the filtered record showed relatively steady water levels in northern Green Bay and northern Lake Michigan during this period. The large variability observed in the filtered records at all locations during October occurred over periods longer than two days, and resulted from the meteorological variability (Fig. 3.6).

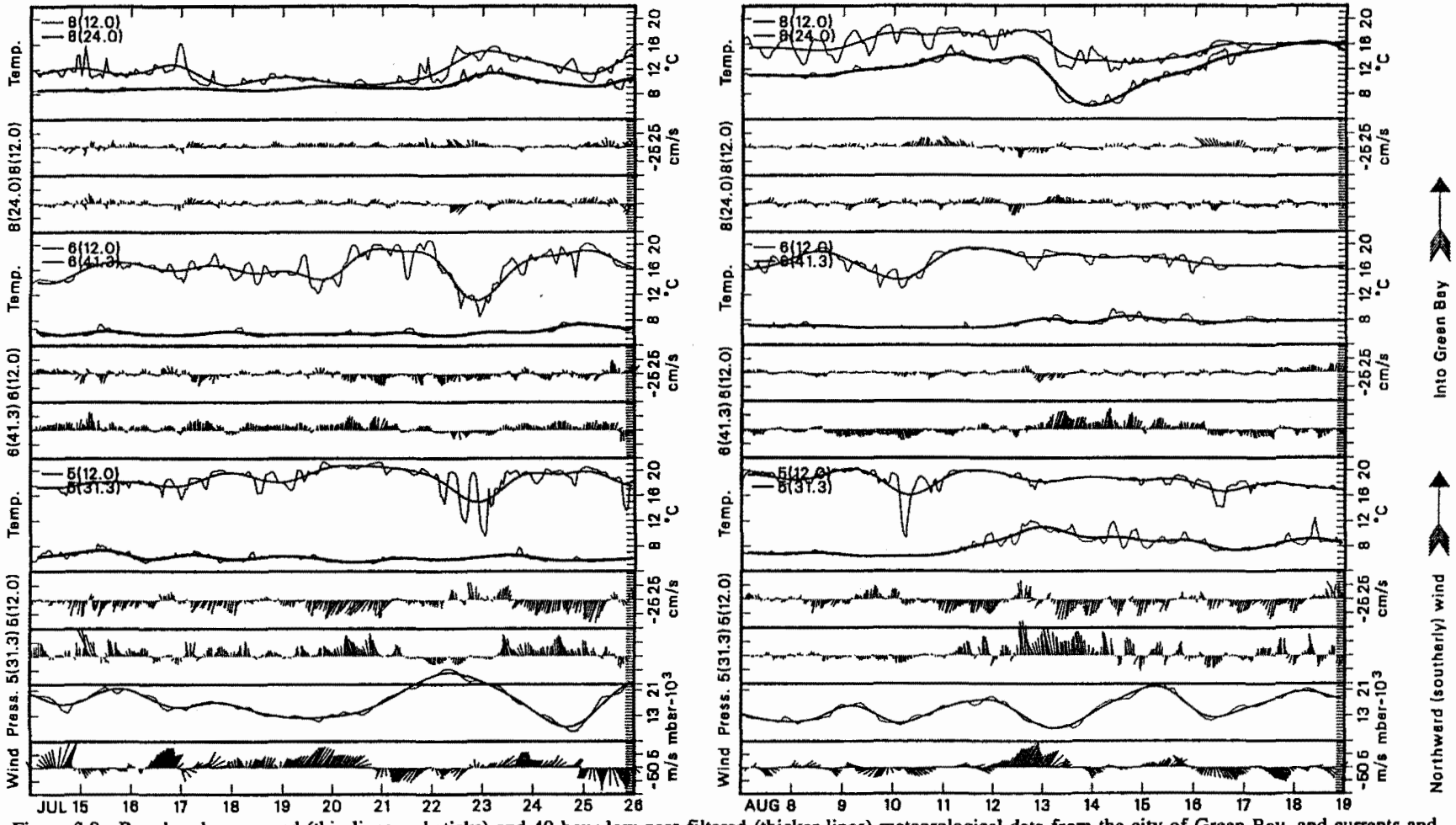

Figure 3.9. Raw hourly-averaged (thin lines and sticks) and 40-hour low-pass filtered (thicker lines) meteorological data from the city of Green Bay, and currents and temperatures from Deaths Door (5), Rock Island (6), and Poverty Island (8) Passages at two depth levels (12 m depth and 5 m above the bottom) during July 14-26 (left panel) and Aug. 7-19 (right panel), 1977. Sticks pointing up/down represent currents flowing into/out of Green Bay, or northward/southward winds (i.e., southerly/northerly). The joint occurrences of relatively cool top-level temperatures in Poverty Island Passage and intensified bottom-level inflow in Rock Island Passage (e.g., during July 18-21 and Aug. 13-16) are consistent with rotation effects (Fig. 2.7). Joint occurrences of relatively warm temperatures in Poverty Island Passage and cool temperatures in Deaths Door and Rock Island Passages and lower-layer outflow (e.g., during July 21-22) are less frequent. Also, an approximately 17-hour (i.e., inertial period) temperature oscillation was observed at the top-level in Poverty Island Passage during a period of lower-layer outflow (Aug. 7-11).

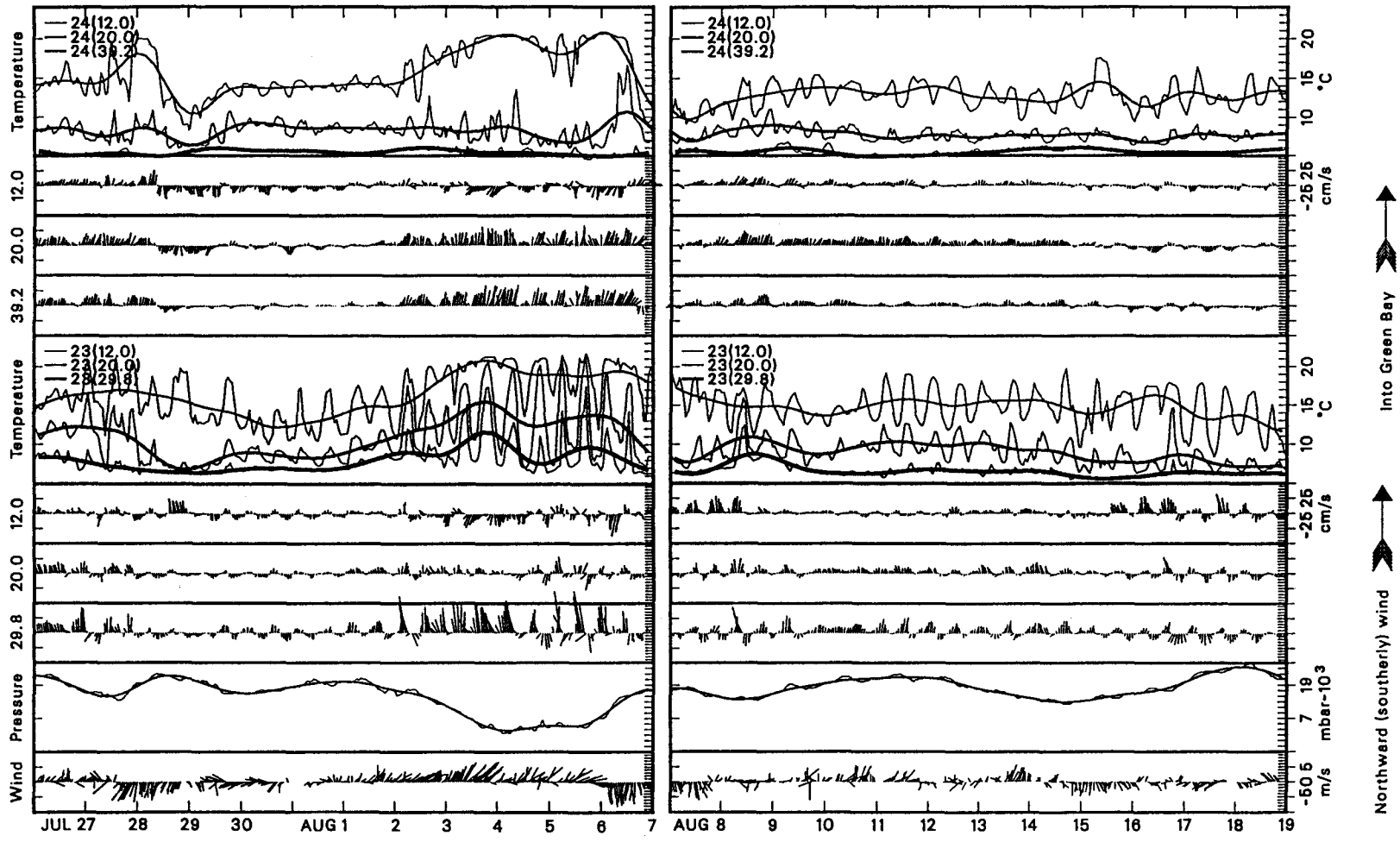

Figure 3.10. As in Fig. 3.9, for Deaths Door (23) and Rock Island (24) Passages at three depth levels (12 and 20 m, and 5 m above the bottom) during July 26 to Aug. 18, 1989. During Aug. 1-6 the largest lower-layer currents observed in Rock Island Passage were associated with the strongest cycle of the 8-day thermocline oscillation in Green Bay (see Fig. 3.3), and with a very large amplitude (≈30 m, the passage depth) semidiurnal thermocline oscillation in Deaths Door Passage. Also during this period bottom-level currents in Deaths Door Passage showed a very intense tidal signal, while the relatively steady lower-layer inflow within Rock Island Passage only revealed a very weak signal. Thus, stratified volume exchange flows in Deaths Door Passage are highly influenced by a persistent, large-amplitude, internal semidiurnal tide there, while exchange flows in Rock Island Passage are much steadier due to longer period effects (e.g., rotation and wind, Figs. 2.7 and 2.9).

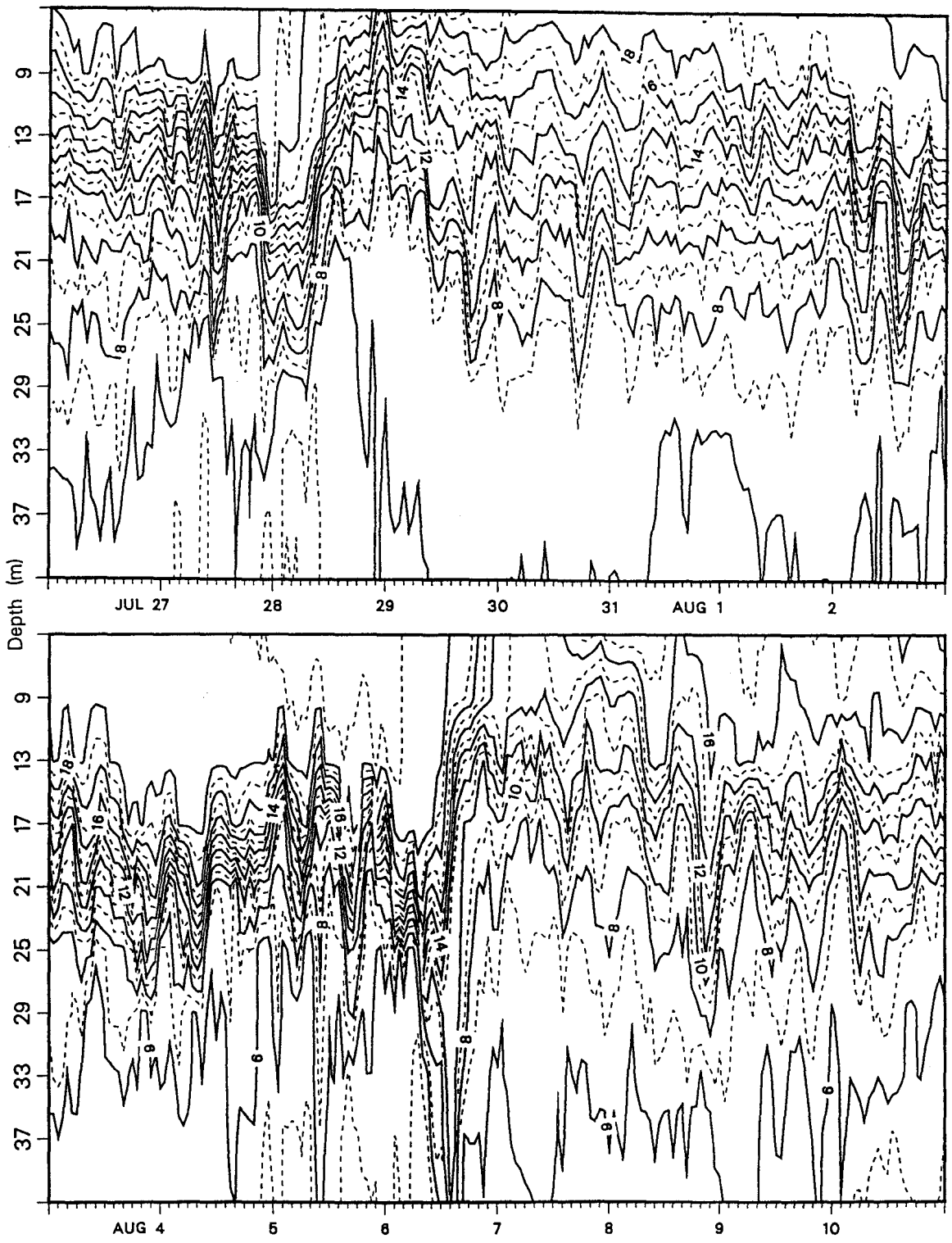

Figure 3.11. Raw, hourly thermistor chain recordings from Rock Island Passage during July 26 to Aug. 3 (top panel) and Aug. 3-11 (bottom panel), 1989. Thermistors were spaced at the 4-m intervals shown on the axis, and contour intervals are 2°C (solid lines) and 1°C (dashed lines). The thermocline is bounded by the 8 and 18°C isotherms, and displays large variability in depth and intensity (vertical temperature gradient). Each 8-day thermocline oscillation cycle in the bay (Fig. 3.10) caused a steadily deepening and intensifying thermocline at the bay mouth (e.g., from July 29 to Aug. 6), followed by a rapid upwelling and weakening of the thermocline (e.g. on Aug. 6). When the thermocline was most intense (e.g. July 26-28 and Aug. 3-6) lower-layer temperatures were coolest, and lower-layer inflow of Lake Michigan water through Rock Island Passage (Fig. 3.10) was most intense.

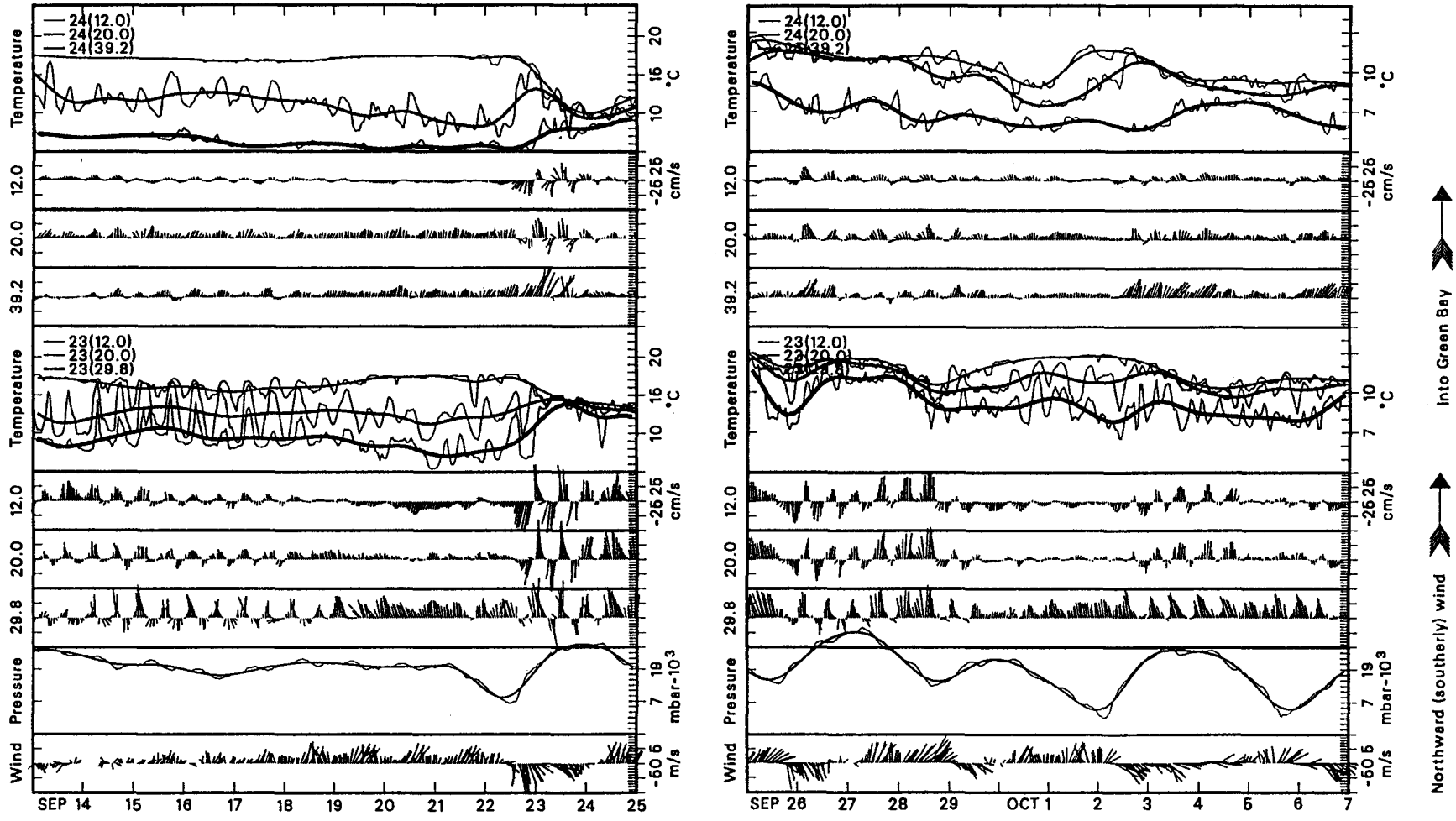

Figure 3.12. As in Fig. 3.10, during Sep. 13-25 (left panel) and Sep. 25 to Oct. 7 (right panel). The passing of an intense storm system on Sep. 22-23 abruptly initiated the autumnal storm season, and resulted in a dramatic character change in both the currents and thermal structure observed within Deaths Door (23) and Rock Island (24) Passages. In both passages the currents before the storm were relatively steady and two-layered, while afterwards currents were mostly barotropic and displayed a prominent tidal signal. The thermocline was mostly destroyed by storm-induced mixing (note the different temperature scales on the left and right panels), but strong stratification persisted well into autumn, as evidenced by the two-layer exchange event occurring Sep. 29 to Oct. 3 in Deaths Door Passage. Also after thermocline destruction, lower-layer inflows occurring as baroclinic shears were reduced, and two-layer exchange flows were non-existent in Rock Island Passage, indicating the reduced effectiveness of the autumnal pressure gradient in driving exchange flows between Green Bay and Lake Michigan.

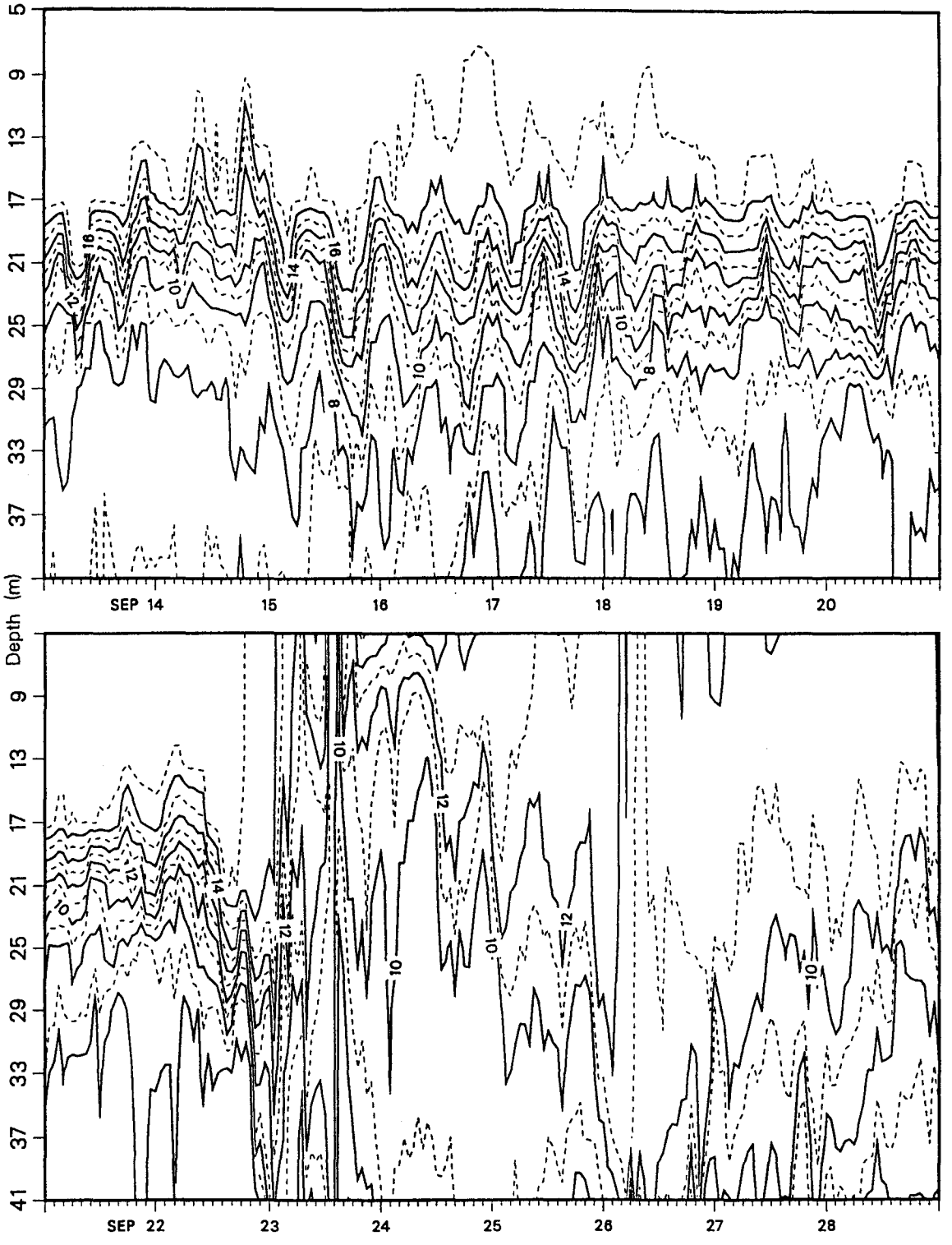

Figure 3.13. Raw, hourly thermistor chain recordings from Rock Island Passage during Oct. 13-21 (top panel) and Oct. 21-29 (bottom panel), 1989, as in Fig. 3.11. The passing of the Oct. 22-23 storm as described in Fig. 3.12 resulted in severe destruction of the thermocline. Before the storm upper- and lower-layer temperatures were about 17 and 6°C, respectively, while afterwards the temperatures were about 13 and 9°C. Before the storm, the thermocline was very steady over periods longer than a day, was found between about 17 and 29 m depth, and had an intensity (vertical temperature gradient) of about 1.0°C/m. After the storm, the weakened thermocline was highly variable, and had a greatly reduced intensity of about 0.25°C/m. Despite the greatly reduced intensity, the weakening stratification was still capable of enhancing the exchange of bay and lake waters (Fig. 3.12).

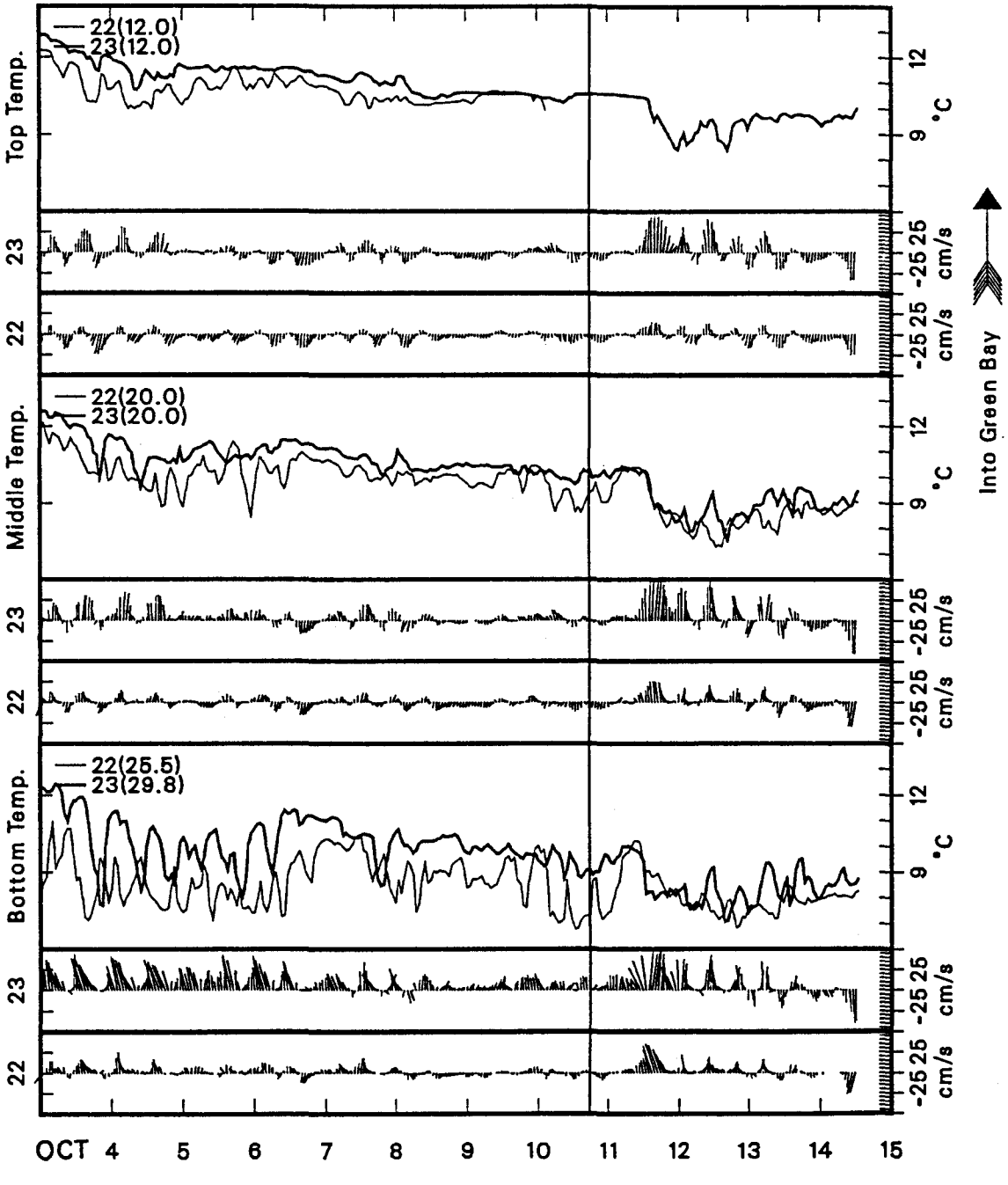

Figure 3.14. As in Fig. 3.7, showing raw, hourly currents and temperatures from two locations (moorings 22 and 23) within Deaths Door Passage. The observed variability is described in the text.

CHAPTER IV

ANALYSIS OF THE STRATIFIED VOLUME EXCHANGES

Volume Transport Computations and Results

To aid interpretation of the observed currents and temperatures from the 1989 stratified season a simple volume transport computation scheme was devised and applied to all data from moorings 17 through 25 (locations shown in Fig. 3.1). Basically, a linearly-interpolated vertical profile of the along-passage velocity component was computed using the 40-hour low-pass filtered, bidaily-averaged current values from each meter on each mooring, and then multiplied by the cross-sectional area of the corresponding passage to yield a volume transport value. The simplifying assumptions and details of the computational scheme are described in the Appendix, and the computed transports are shown in Fig. 3.4. The assumptions of no cross-passage flow structure and a linear velocity profile are less questionable for the low-pass filtered currents than for the actual (raw) currents, because the filtered currents represent the average exchanges of water through the bay mouth. However, the loss of absolute accuracy due to these assumptions is unknown because the actual flow structure is unknown (additional information would be required to determine the absolute accuracy). While the measured current velocities are accurate to within 2–3%, substantial errors probably occur in the computed transport values.

The volume transports shown in Fig. 3.4 were separated into upper-, lower-, and single-layer components based on the zero-crossing depth of the computed velocity profile (see Fig. A-1). The zero-crossing depth of the computed velocity profile presumably correlates with the two-layer interface for the case of ideal two-layer estuarine exchange,

or with some representative thermocline depth for the more general case of stratified two-layer estuarine exchange. Thus in Fig. 3.4, upper-layer transports are from above the zero-crossing, lower-layer are from below, and single-layer indicates no zero-crossing. Instances of velocity profiles with two zero-crossings were observed rarely (in less than 3% of the record) in the western Chambers Island Passage and much less frequently in the bay mouth passages, and such instances were categorized as single-layer transports. It must be noted that some of the velocity profiles categorized as single-layer showed large baroclinic shears.

The lower-layer inflowing transport can be estimated by summing the transports from all bay mouth passages in Fig. 3.4. The volume of water flowing in below the thermocline (using both lower-layer and single-layer baroclinic components) averaged at least 0.3 km^3 per day. It is seen that 0.3 km^3/day $\approx$ 10 km^3/month $\approx$ 3500 m^3/s (slightly larger than the value reported by Miller and Saylor, 1985), so that the entire volume of water in the bay (67 km^3) would be replaced in about a six-month period, which is the length of a typical stratified season (May to October). But, the lower-layer inflow must be balanced by an equal volume of upper-layer outflow, so that the water in the bay actually is replaced every three months during the stratified season. Considering this relatively high flushing rate at the bay mouth, water quality in the bay's southern end (Fig. 1.1) remains poor due to constriction of the exchange flows by the Chambers Island Passages (Fig. 1.3) and other bathymetric features to the south of these passages.

The computed transports in Fig. 3.4 show the general characteristics of the exchange flows during the 1989 stratified season. The transport values from Rock Island Passage were the largest due to the large cross-sectional area, and contributed more than half of the total exchange through the entire mouth, as suggested by Miller and Saylor (1985). The computed transports from Rock Island Passage were mostly single-layer, with two-layer exchanges occurring during only 16% of the time and inverse two-layer exchanges during 8% of the time. Other characteristics of the exchange flows in all

passages are described in the next section using scatter plots (Figs. 4.3 to 4.5) and scatter statistics.

Finally, it is necessary to at least partially justify the assumption of no cross-passage flow structure. The tidal currents seen in Fig. 3.14 during the period October 3-4 indicate that the flow varies linearly across the width of Deaths Door Passage at all depth levels, with a stronger inflow on the northern side of the passage at the lower depth levels, and a stronger outflow on the southern side at the upper levels. For such a linear cross-passage velocity distribution, a single current velocity measurement from a central location within a passage (such as mooring 24 or 25) could represent an average velocity value and thus would allow for a reasonably accurate volume transport estimation. It must be cautioned that the cross-passage velocity distributions shown in Fig. 3.14 were at times (e.g., during October 11-12) more complex than the simple nearly linear distributions indicated during October 3-4. The entire record of raw currents (not shown due to size limitations) indicates that the assumption of no cross-passage flow structure was valid at least during periods of moderate to strong tidal influence. However, both the cross-passage and vertical flow structures are mostly unknown, and thus substantial errors probably occur in the computed volume transports.

Spectral and Cospectral Analyses

Spectral and cospectral analyses show the frequency content, coherence, and phase differences for currents from different depth levels in all passages (Tables 4.1, 4.2, and 4.3, and Fig. 4.1), and for currents and temperatures from Deaths Door Passage (Fig. 4.2). All coherence, phase angle, confidence interval, and error bound values were computed as described in Jenkins and Watts (1968), and in the captions of Tables 4.1 and 4.2. Start and stop times, number of subseries, and confidence intervals for each series analyzed are listed in Table 4.1, and representative plots of spectra and cospectra from Deaths Door Passage are presented in Figs. 4.1 and 4.2.

Mooring	Water Depth (m)	Passage	Start Date of Series	Stop Date of Series	# of Points	# of Subseries	Lower C.I.	Upper C.I.
5	36.3	Deaths Door	5/16/77	9/4/77	2665	20	0.67	1.65
6	46.3	Rock Island	5/16/77	9/4/77	2665	20	0.67	1.65
8	30.0	Poverty Island	5/16/77	9/4/77	2665	20	0.67	1.65
22	30.5	Deaths Door	5/23/89	9/22/89	2929	22	0.68	1.60
23	34.8	Deaths Door	5/23/89	9/22/89	2929	22	0.68	1.60
24	44.2	Rock Island	7/1/89	9/22/89	1993	15	0.62	1.80
25	36.9	St. Martin Island	5/23/89	9/22/89	2929	22	0.68	1.60

Table 4.1. Start and stop dates, number of points, and number of subseries for each raw time series from the indicated moorings. Spectral analysis results for the series are presented in Tables 4.2 and 4.3, and Figures 4.1 and 4.2. Each series was divided into non-overlapping 128-point (128 hour) subseries, yielding 64 frequency (or period) bins with a bin width of 0.0078 cph = 0.187 cpd and a Nyquist frequency of 12.0 cpd (discussion of the analysis results is limited to frequencies lower than 6.0 cpd). Herein, individual frequency bins will be referred to by their lower bounding value (e.g., the 1.87 cpd bin ranges from 1.87 to 2.06 cpd). The 95% confidence interval (C.I.) was obtained from Jenkins and Watt (1968) using the definition (# of degrees of freedom) = 2 × (# of subseries).

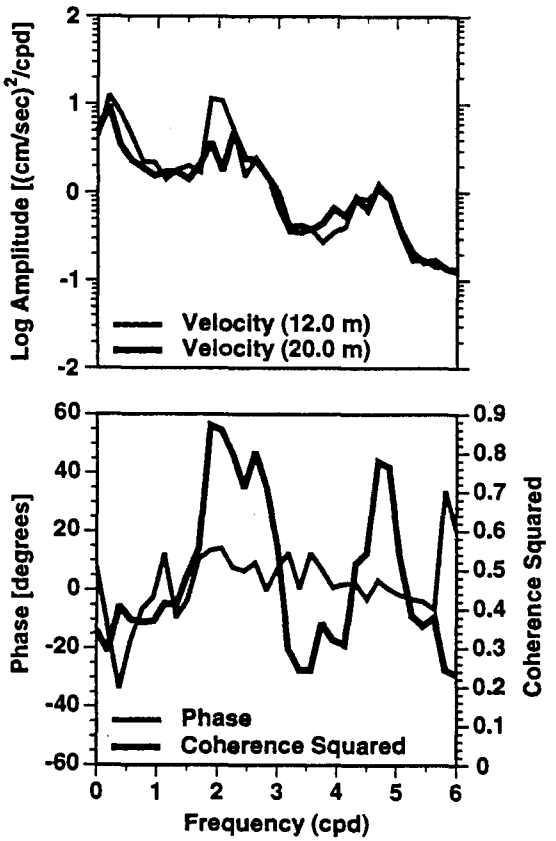

Figure 4.1. Spectra (upper panel) and cospectrum (lower panel) for middle- (20.0 m) and top-level (12.0 m) velocities from mooring 23 in Deaths Door Passage during 1989. A complete description of the spectral analysis is provided in the text and in Tables 4.1 and 4.2, and all velocity cospectra are summarized in Table 4.3.

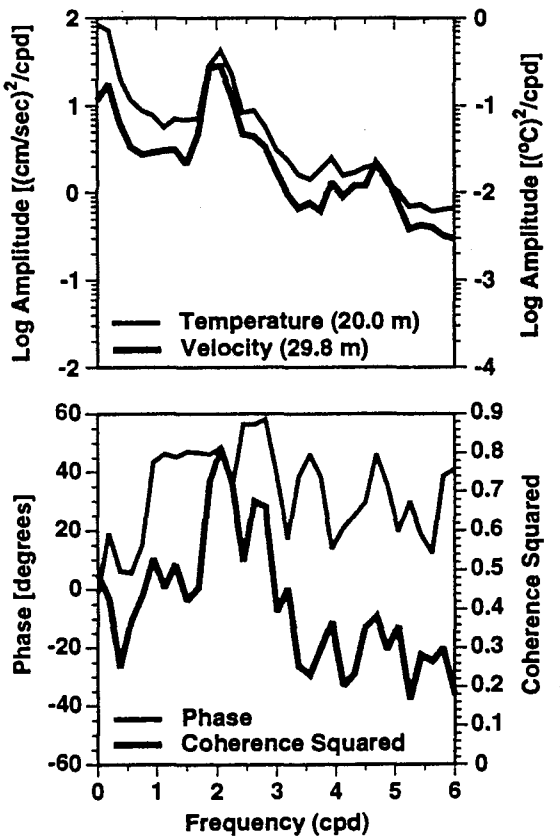

Figure 4.2. As in Figure 4.1, for middle-level (20.0 m) water temperature and bottom-level (29.8 m) velocity. At the semidiurnal peak, the coherence squared and corresponding confidence interval (from Jenkins and Watts, 1968) values are 0.81 and (0.77, 0.85), and the velocity leads the temperature by 48°.

Passage and Mooring	Depth Level	Mean (cm/s)	Trend ($\times 10^{-4}$ cm/s/hr)	Low Frequency Variance (% of total)	Semi-diurnal Variance (% of total)	1st Mode Variance (% of total)	2nd Mode Variance (% of total)
Deaths Door	TOP	-8.9	15.2	59	15	7	3
5	BOT	4.1	22.5	51	21	10	3
Rock Is.	TOP	-0.2	-2.7	47	15	9	5
6	BOT	6.0	-9.0	73	7	4	2
Poverty Is.	TOP	0.5	-2.3	54	10	9	5
8	BOT	0.6	-2.1	35	14	9	6
Deaths Door	TOP	-4.8	6.3	36	25	11	6
22	MID	-3.5	19.7	24	34	15	6
	BOT	-2.1	19.7	30	28	16	5
Deaths Door	TOP	-3.9	18.2	35	27	13	5
23	MID	-1.9	18.7	26	33	14	6
	BOT	0.8	20.4	25	35	16	5
Rock Is.	TOP	0.2	7.4	57	11	8	2
24	MID	3.9	4.5	79	5	4	1
	BOT	4.9	-18.0	60	9	8	2
St. Martin Is.	TOP	0.8	-1.0	49	13	8	5
25	MID	-0.6	6.7	40	14	8	4
	BOT	0.5	6.8	36	13	6	5

Table 4.2. Means, trends, and percent of the total variance accounted for in the low (0, 0.19, 0.37, and 0.56 cpd), semidiurnal (1.87 and 2.06), 1st mode (2.25, 2.43, 2.63, and 2.81), and 2nd mode (4.13, 4.31, 4.50, 4.69, 4.87, and 5.06) frequency bins for each along-channel velocity component series (see Table 4.1) from the indicated moorings and depth levels (TOP = 12 m, MID = 20 m, BOT = 5 m above the bottom). Each series was demeaned and detrended prior to the spectral analysis. Sample spectra plots are shown in Figure 4.1 and 4.2, and the tidal and seiche mode frequencies are listed in the text.

Passage and Mooring	Depth Levels	Peak 1 Coher. Squared	Peak 1 Freq. Bin (cpd)	Peak 1 Phase Angle (deg)	Peak 2 Coher. Squared	Peak 2 Freq. Bin (cpd)	Peak 2 Phase Angle (deg)	Peak 3 Coher. Squared	Peak 3 Freq. Bin (cpd)	Peak 3 Phase Angle (deg)
Deaths	BOTxMID	0.84	1.87	-4	0.64	2.63	-11	0.70	4.69	-8
Door	MIDxTOP	0.82	1.87	6	0.65	2.63	-1	0.81	4.69	3
22	BOTxTOP	0.77	1.87	4	—	—	—	0.68	4.69	-4
Deaths	BOTxMID	0.81	1.87	6	0.83	2.63	-1	0.75	4.87	4
Door	MIDxTOP	0.87	1.87	12	0.81	2.63	9	0.78	4.69	1
23	BOTxTOP	0.75	2.06	17	—	—	—	0.71	4.69	1
Rock	BOTxMID	0.76	2.25	16	0.76	2.63	14	0.61	4.87	14
Island	MIDxTOP	0.71	2.25	11	—	—	—	—	—	—
24	BOTxTOP	0.64	2.25	24	—	—	—	—	—	—
St. Martin	BOTxMID	0.80	1.87	6	—	—	—	0.88	4.50	0
Island	MIDxTOP	0.61	2.06	1	—	—	—	0.77	4.69	2
25	BOTxTOP	—	—	—	—	—	—	0.68	4.69	3

Table 4.3. Results of cospectral analysis for the along-channel velocity component series from each mooring during the 1989 stratified season (see also Tables 4.1 and 4.2). Three major peaks occur in the coherence squared spectra (see Figure 4.1 for example), and are indicated in the table column headings. The table only includes peaks with a coherence squared value of 0.60 or larger. See the text for the tidal and seiche frequencies, and see Figure 4.2 and the text for sample coherence squared confidence interval values.

For frequencies higher than the local inertial frequency (about 1.4 cpd), spectral energy in all passages (see Figs. 4.1 and 4.2 for example) is highest at the semidiurnal tide frequency (1.93 cpd). Various amounts of spectral energy are found at the frequencies of certain Green Bay and Lake Michigan surface seiche modes, including the 1st bay mode (2.3 cpd), 1st lake mode (2.6), 2nd lake mode (4.5), and 2nd bay mode (4.9), as computed by Rao, Mortimer, and Schwab (1976). The frequency resolution of the analysis usually was insufficient to distinguish between the 1st bay and lake modes, and the 2nd bay and lake modes, and herein these will be referred to as the 1st and 2nd modes (unless otherwise noted).

The distributions of spectral energy (or variance) in the low, semidiurnal, 1st mode, and 2nd mode frequency bins for the currents in each passage during 1977 and 1989 are listed in Table 4.2 (the following discussion mostly applies to the 1989 moorings). The largest percentage of low-frequency energy (around 70%) is found at the lower depth levels in Rock Island Passage, indicating the influence of long-period (greater than one day) forcing mechanisms (meteorological forcing, rotation effects, etc.). At the semidiurnal frequency, the energy percentage is about twice as large in Deaths Door Passage (about 30%) than in the other passages. At the 1st mode frequency, the energy percentage is small in all passages, but again is largest (about 15%) in Deaths Door Passage. At the 2nd mode frequency, the energy percentage is very small (less than about 5%) in all passages. Thus, Deaths Door Passage is the most sensitive to tidal and seiche oscillations, while lower-layer flow through Rock Island Passage is influenced more by longer-period mechanisms.

In all passages, the amount of spectral energy at the semidiurnal, 1st mode, and 2nd mode peak frequencies (Table 4.2) decreases with increasing frequency, but large coherence squared values (Fig. 4.1) are found even at the higher frequencies. The peak coherence squared values for the along-channel velocity component series from each mooring during 1989 are listed in Table 4.3. The best correlations are found between the

BOT×MID series, where coherence squared values greater than 0.70 are typical. Strong correlations between the MID×TOP series are common, especially in Deaths Door Passage, again indicating the sensitivity of this passage to the tidal and seiche oscillations. The good correlations between some of the BOT×TOP series, and the relatively small phase angles for all series (except Deaths Door Peak 1) in Table 4.3 show that the tidal and seiche currents through the passages remain mostly barotropic despite stratification.

The cospectral Peak 1 (Table 4.3) in Deaths Door and St. Martin Island Passages is the semidiurnal tide, but in Rock Island Passage is the 1st bay mode. In all passages, the cospectral Peak 2 is the 1st lake mode, and Peak 3 is the 2nd bay and lake modes. The largest coherence squared value (0.88) and corresponding confidence interval (0.85, 0.90) are noted (Table 4.3) for the BOT×MID series in St. Martin Island Passage at about the 2nd lake mode frequency. The large semidiurnal coherence squared values (from 0.75 to 0.87) for all levels from Deaths Door Passage show that the associated tidal currents are very strong, but the semidiurnal phase angles from mooring 23 are 6° to 13° greater than those from corresponding levels on mooring 22 (95% phase angle confidence band values range from ±3° to ±8° for coherence squared values ranging from 0.87 to 0.75, see Table 4.1). This phase angle difference between moorings 22 and 23 show that the strong tidal currents through Deaths Door Passage are spatially nonuniform, possibly due to the effects of the observed semidiurnal internal waveform (see Fig. 3.10).

The nature of the semidiurnal internal waveform (standing versus progressive) in Deaths Door Passage can be seen in Figure 4.2. At the semidiurnal frequency, the coherence squared value between the middle-level temperature and bottom-level currents is 0.81, and the corresponding phase angle is about 48° (the velocity leads the temperature). For a standing or progressive wave in an ideal two-layer system the velocity leads the temperature by a phase angle of 90° or 0°, respectively (for example, see Stoker, 1957, or LeBlonde and Mysak, 1980); for a wave that is half standing and half progressive, the phase angle is 45°. Thus, the semidiurnal internal waveform in Deaths

Door Passage is a combined (mixed) standing-progressive wave, with about half of the wave energy confined within the passage, and with the other half propagating away from the passage as internal waves.

Joint Occurrence Distributions and Scatter Plots

The currents and temperatures measured in the passages connecting Green Bay and Lake Michigan can be categorized based on flow directions between different passages, flow directions between upper and lower layers, and temperature (density) difference across the bay mouth. Before examining the resulting joint occurrence distributions, it is useful to examine the mean speeds observed in each passage during 1977 and 1989 (Table 4.2). In Rock Island Passage lower-layer mean speeds are strong and inflowing, while upper-layer speeds are negligible. In Deaths Door Passage, upper-layer mean speeds are strong and outflowing, the outflowing speeds decrease with increasing depth level, and some bottom-level speeds are inflowing. In St. Martin and Poverty Island Passages, mean speeds are very small. Thus, two-layer exchange between the bay and lake mostly occurs as lower-layer inflow through Rock Island Passage and upper-layer outflow through Deaths Door.

Year	Start Date	Stop Date	Depth Level	Deaths Door out /Rock Is. in (%)	Deaths Door in /Rock Is. out (%)	Both out (%)	Both in (%)	R^2 value
1977	5/16	9/4	TOP	34	7	42	17	0.20
1977	5/16	9/4	BOT	12	11	20	57	0.64
1989	7/1	9/22	TOP	29	11	27	33	0.08
1989	7/1	9/22	MID	7	5	28	60	0.63
1989	7/1	9/22	BOT	6	5	27	63	0.71

Table 4.4. Joint occurrence distributions of unidirectional and opposing flows observed through Deaths Door and Rock Island Passages from the indicated depth levels (TOP = 12 m, MID = 20 m, BOT = 5 m above the bottom) during the indicated dates using the averaged along-channel velocity component. "In" and "out" refer to flow into and out of Green Bay, respectively. Linear correlation between the Deaths Door and Rock Island along-channel velocity components is indicated by the R^2 value.

The flow directions at each depth level in Deaths Door and Rock Island Passages are categorized in Table 4.4 as both in (bayward), both out (lakeward), Deaths Door

in/Rock Island out, and Deaths Door out/Rock Island in. At the middle and bottom levels (i.e., the lower-layer), the majority of the flow (about 60%) is unidirectional and bayward, and overall the lower-layer flow is 80-90% unidirectional and 10-20% opposed in direction. At the top level the flow is more evenly distributed (about 20-40%) within the categories, but is relatively sparse (about 10%) in the Deaths Door in/Rock Island out category. The linear correlation coefficient R^2 for the flow at each depth level (Table 4.4) shows that the lower-layer flow is well correlated, while the upper-layer flow is not correlated. Thus for the two-layer estuarine exchange flows, lower-layer inflow is strong and correlated between Rock Island and Deaths Door Passages, upper-layer outflow is confined to Deaths Door Passage, and flows within the other passages and upper-layer flow within Rock Island Passage are much more variable (i.e., influenced by forcing mechanisms in addition to two-layer estuarine exchange).

Similarities and differences in the character of the two-layer exchange flows within Deaths Door, Rock Island, and St. Martin Island Passages are revealed in scatter plots (Figs. 4.3, 4.4, and 4.5, respectively) of along-channel top-level velocity versus bottom-level velocity during the a) 1977 and b) 1989 stratified seasons. In the scatter plots, positive velocities are directed into Green Bay so that points in the upper left, lower right, upper right, and lower left quadrants represent two-layer flow, inverse two-layer flow, single-layer inflow, and single-layer outflow, respectively. To create the scatter plots, the rawest (15-minute collection interval) available data were used. Percent occurrences of scatter points in each quadrant were computed using the 15-minute raw data and the averaged (low-pass filtered) data for comparison. The percentages computed using the 15-minute raw data total less than 100%, due to the exclusion of scatter points for which either the top- or bottom-level speed fell below the threshold value (about 1.0 cm/s) of the current meter rotors. For the averaged data, a threshold value was not used because the average currents can be near zero (e.g., see Table 4.2). In the following discussion,

percentages computed using the 15-minute raw data or averaged data will be referred to as % RAW or % AVG, respectively.

The exchange flow through Deaths Door Passage during 1977 (Fig. 4.3a) was mostly (48% RAW / 65% AVG) two-layered, with smaller contributions from single-layer inflow (14% RAW / 10% AVG) and outflow (17% RAW / 12% AVG). The pattern was different during 1989 (Fig. 4.3b), with a large grouping (26% RAW / 22% AVG) of points indicating single-layer outflow, and also an almost one-to-one correlation between the magnitudes of the top-level and bottom-level outflowing currents, i.e., the outflow was mostly barotropic. A second large grouping (13% RAW / 35% AVG) of points during 1989 (Fig. 4.3b) indicates two-layer flow, and a third large grouping (30% RAW / 30% AVG) indicates single layer inflow. The single-layer inflow in Fig. 4.3b (but not in Fig. 4.3a) shows that the bottom-level inflowing currents were much stronger than the top-level inflowing currents, consistent with a baroclinic shear induced by pressure-driven, dense, Lake Michigan water intruding into the lower depth levels in Green Bay. In both Figs. 4.3a and b, it is seen that occurrences of inverse two-layer flow were rare (7% RAW / 13% AVG, in each).

The 1977 Rock Island Passage scatter plot (Fig. 4.4a) reveals two groupings of points, with the majority (57% RAW / 73% AVG) indicating bottom-level inflow and a second smaller grouping (19% RAW / 27% AVG) indicating bottom-level outflow. The top-level currents were almost equally divided between inflowing (25+10=35% RAW / 29+17=46% AVG) and outflowing (32+9=41% RAW / 44+10=54% AVG), indicating the randomizing influence of the meteorological forcing, and the single-layer inflow currents revealed the pattern associated with the aforementioned baroclinic shear, again indicating the intrusion of lower-layer lake water into the bay.

In the 1989 Rock Island Passage scatter plot (Fig. 4.4b) the majority (30% RAW / 46% AVG) of the points indicate single-layer inflow with little or no baroclinic shear, and the remaining points are distributed almost evenly (11, 11, and 12% RAW / 17, 20,

and 17% AVG) around the remaining three quadrants. The 1977 Poverty Island Passage scatter points (Fig. 4.5a) are distributed almost evenly around all four quadrants (21, 15, 12, and 14% RAW / 26, 18, 30, and 27% AVG), indicating that all four exchange flows are nearly equally likely to occur. The 1989 St. Martin Island Passage scatter points (Fig. 4.5b) also appear evenly distributed, and reveal a weak but distinct one-to-one correspondence between the top- and bottom-level currents during both single-layer inflow (22% RAW / 32% AVG) and outflow (14% RAW / 16% AVG) events, indicating that the flow in this passage was primarily barotropic during at least part of the 1989 stratified season. However, also revealed in Fig. 4.5b are many occurrences of the aforementioned baroclinic shear, along with two-layer (11% RAW / 24% AVG) and inverse two-layer (12% RAW / 27% AVG) exchanges.

To summarize the scatter analysis, occurrences of single-layer inflow with a baroclinic shear were observed in all passages during the 1977 and 1989 seasons. The largest and most frequently occurring shears were observed in Death Door Passage during 1989 (Fig. 4.3b), and large and frequent shears were also observed in Rock Island Passage during 1977 (Fig. 4.4a). Two-layer exchanges occurred frequently during 1977 in Deaths Door (65%) and Rock Island (44%) Passages, and less frequently (35 and 20%, respectively) during 1989. Single-layer outflows in all passages during both seasons were generally barotropic, i.e., generally revealed a one-to-one correspondence between top- and bottom-level current magnitudes, with the best correspondence being observed in Deaths Door Passage during 1989 (Fig. 4.3b).

As a final analysis, joint occurrence distributions of lower-layer flow velocity through Rock Island Passage versus the density (temperature) difference across the bay mouth are presented for the top levels during 1977 and 1989 (Fig. 4.6), and for the middle and bottom levels during 1989 (Fig. 4.7). In each of the distributions, the majority of the points (45 to 67%) indicate lower-layer inflow corresponding with a positive density difference, i.e, with the thermocline tilted up towards the north (as in

Fig. 2.7). Except for the 1977 (Fig. 4.7) distribution, many points (17 to 23%) indicate lower-layer outflow corresponding with a negative density difference, and points in the remaining two quadrants are less common (11 to 16% in each quadrant).

During 1989 (Figs. 4.6 and 4.7), the ratio of the inflowing:outflowing lower-layer velocity was approximately equal to the ratio of the positive:negative cross-passage density difference; the top-level ratio was about 60:40, and the middle- and bottom-level ratios were about 70:30. During 1977 at the top level (Fig. 4.6), the velocity and density difference ratios were not the same; the velocity ratio was about 70:30 but the density difference ratio was 92:8. A likely reason for this disproportionately large density difference ratio is that the location of mooring 8 in Poverty Island Passage is exposed mainly to the lake (see Fig. 1.2), compared to mooring 25 in St. Martin Island Passage which is more equally exposed to both the bay and lake.

The lower-layer velocity versus cross-passage density difference distributions (Figs. 4.6 and 4.7) can be used to estimate scaling values for the geostrophic balance (Equation 6). At the middle (20.0 m) depth level (Fig. 4.6), it is seen that a 10 cm/s increase in the velocity corresponds with a 0.4 to 0.6 kg/m^3 increase in the density difference, yielding a value of $V/\Delta\rho$ = 25 to 33 (cm/s)/(kg/m^3). Similarly, at the bottom (31.3 m) level $V/\Delta\rho$ = 50 to 75 (cm/s)/(kg/m^3). In the following chapter, these values will be compared to theoretical values to demonstrate consistency with a geostrophic relationship between lower-layer velocity and cross-passage density difference. However, it also will be seen that in addition to rotation effects the lower-layer velocity and cross-passage density difference are highly influenced by other effects (e.g., wind, friction, etc.).

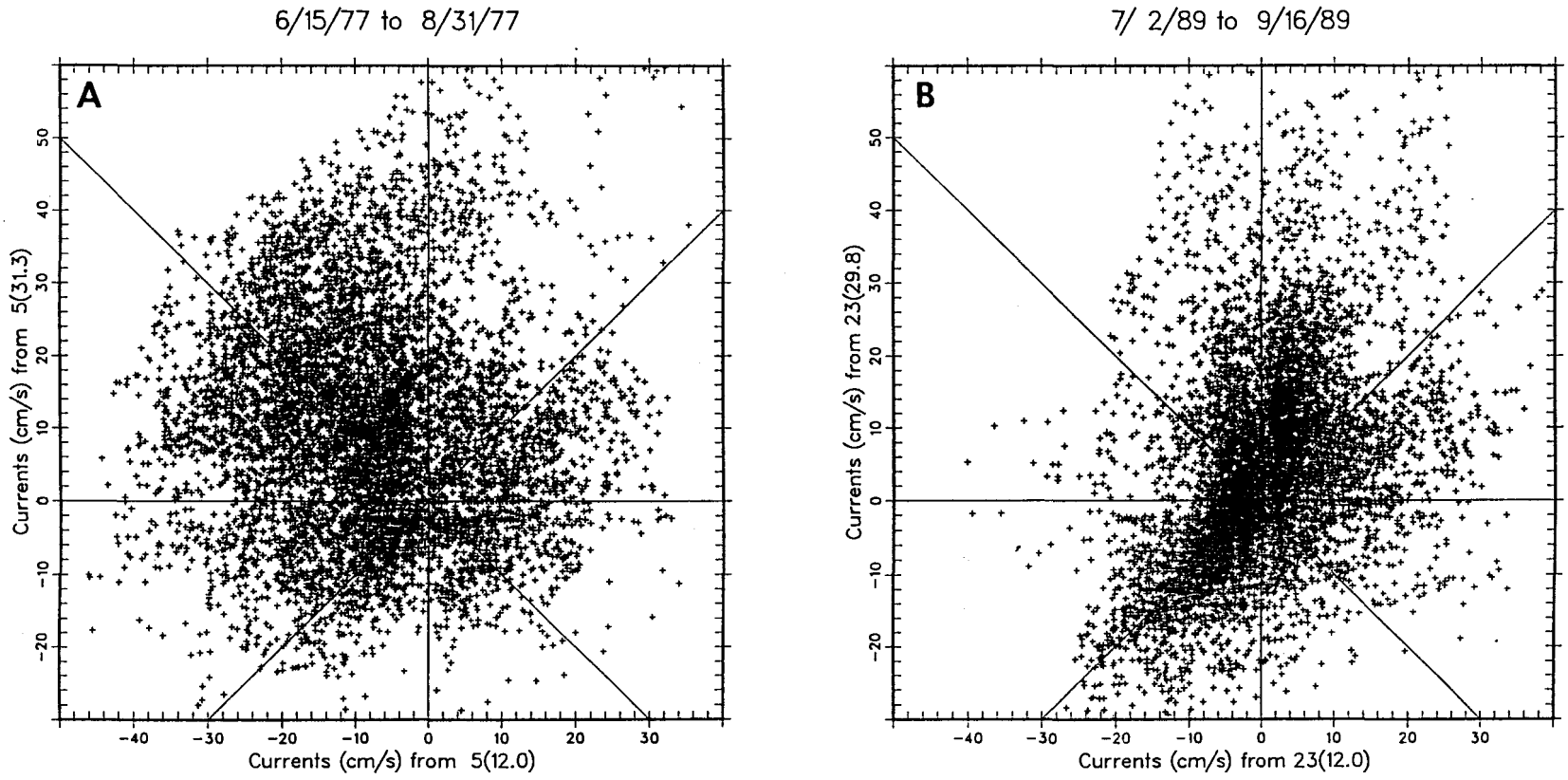

Figure 4.3. Scatter plots of top-level (x-axis) versus bottom-level (y-axis) currents from Deaths Door Passage during the a) 1977 and b) 1989 stratified seasons. Positive currents are into Green Bay, so that two-layer exchange flows are found in the upper-left quadrant, inverse two-layer exchange flows in the lower-right, and single-layer inflows and outflows in the upper-right and lower-left, respectively. See text for further description.

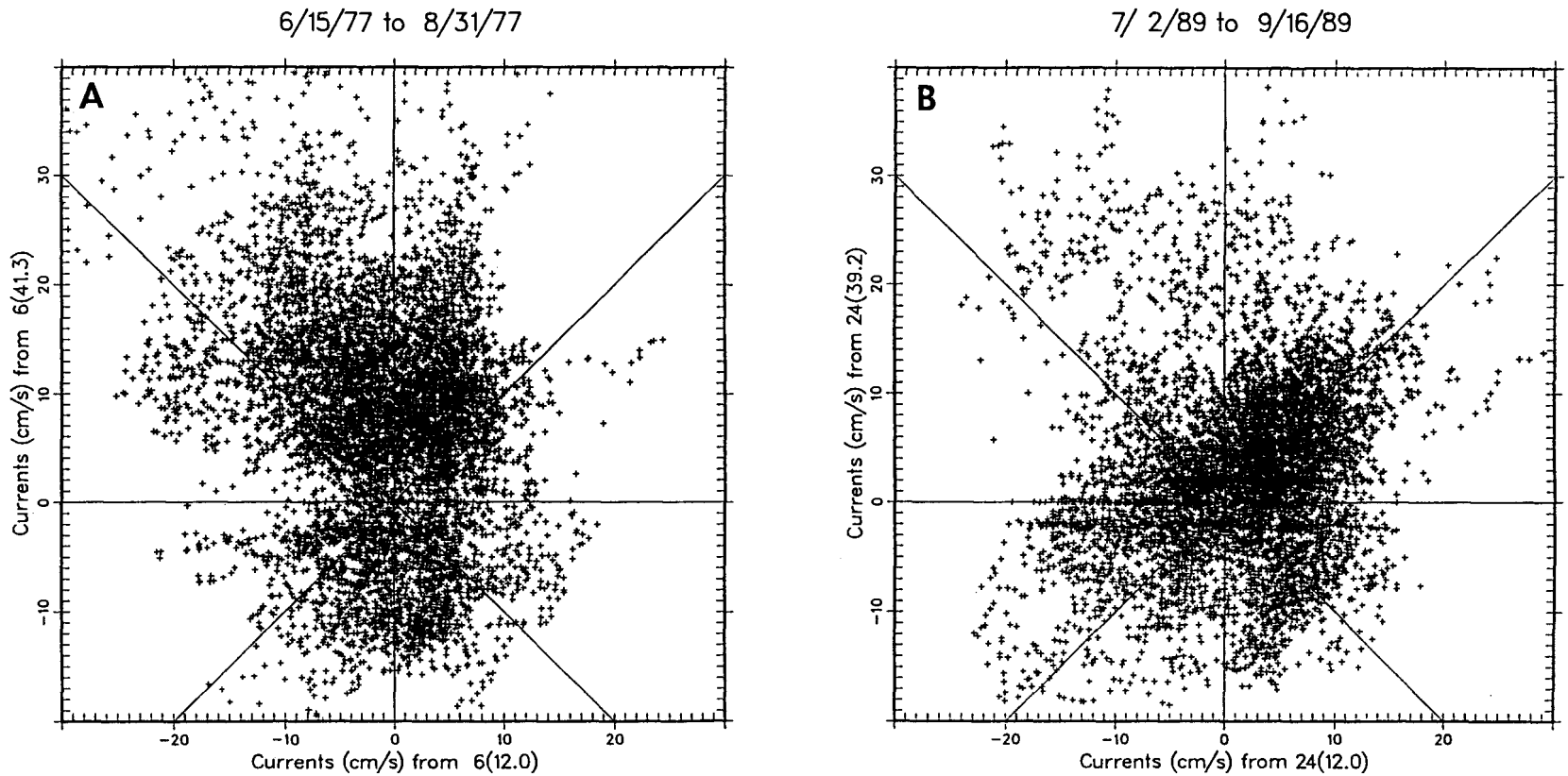

Figure 4.4. As in Fig. 4.3, from Rock Island Passage.

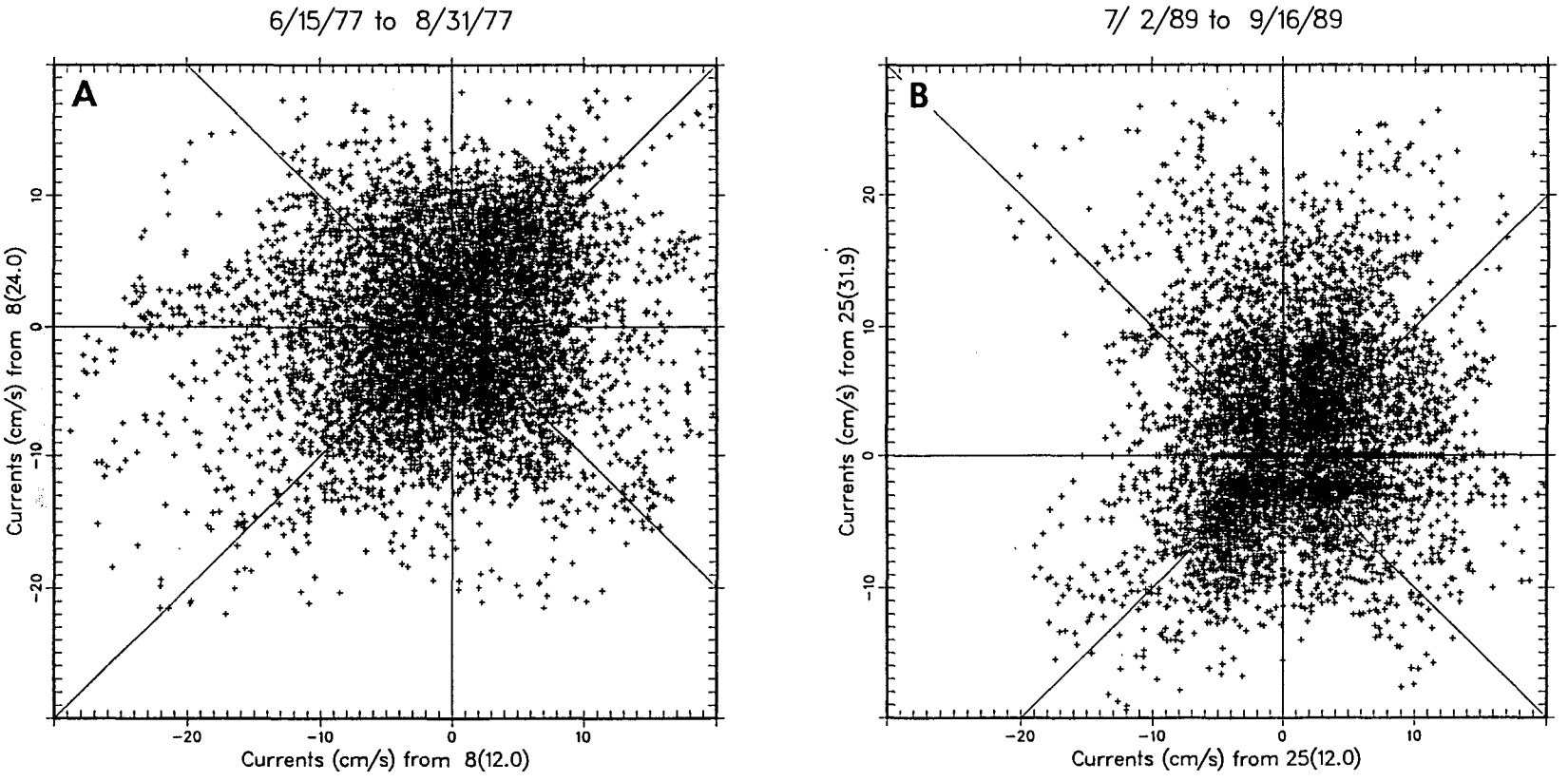

Figure 4.5. As in Fig. 4.3, from a) Poverty Island Passage during 1977 and b) St.Martin Island Passage during 1989.

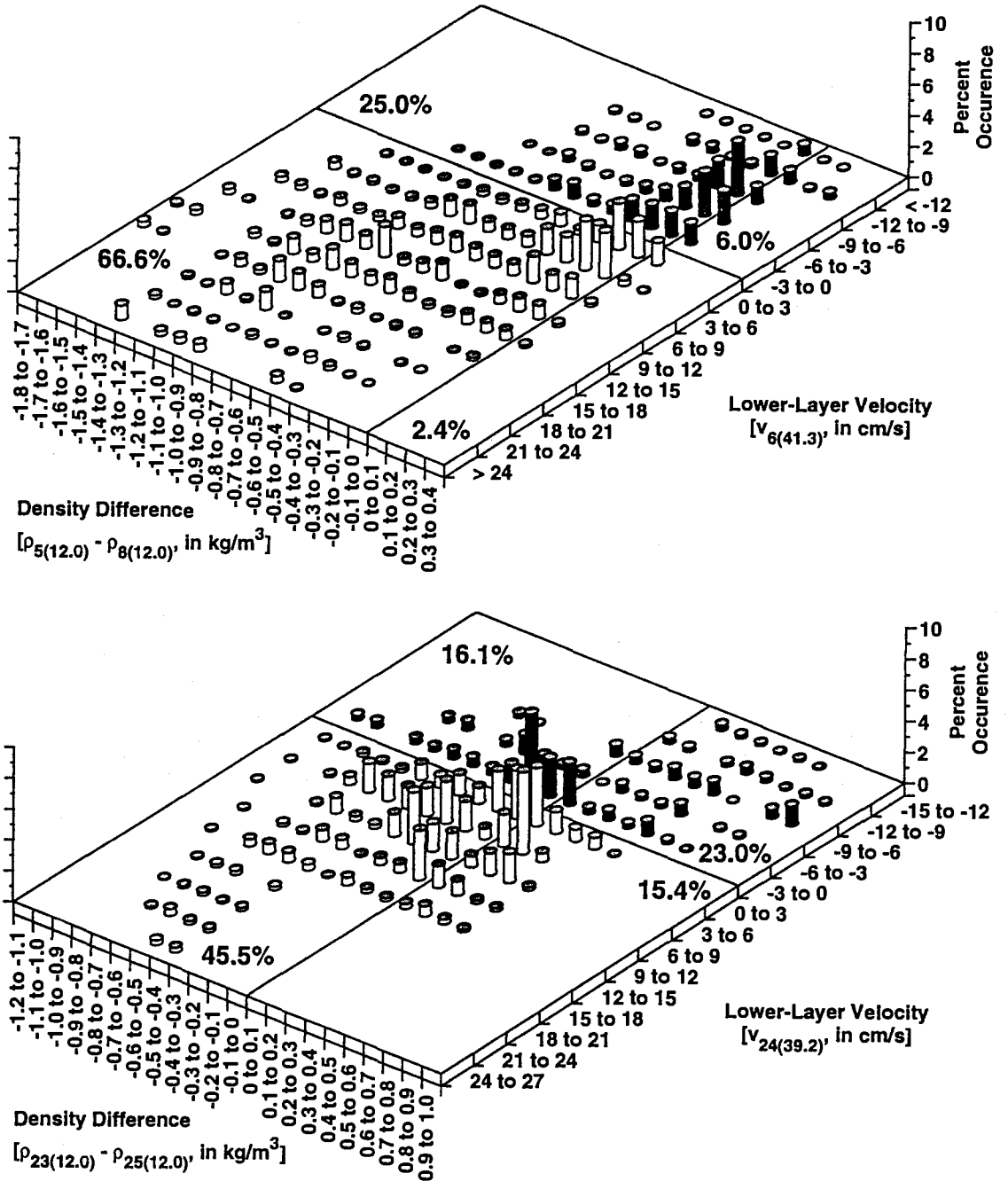

Figure 4.6. Joint occurrence distributions of lower-layer flow velocity versus density difference across the bay mouth at the top depth level (12.0 m) for 1977 (top panel) and 1989 (bottom panel), during the same dates used for the scatter plots (Fig. 4.3). The distribution plots were created using the averaged (low-pass filtered) data, which were categorized into the bins indicated on the plot axes. The lower-layer flow velocities 6(41.3) and 24(39.2) are from the bottom level in Rock Island Passage (positive velocity is inflow). The cross-mouth density differences were computed using Chen and Millero (1986) given the temperatures from the northernmost (8 and 25) and southernmost (5 and 23) moorings.

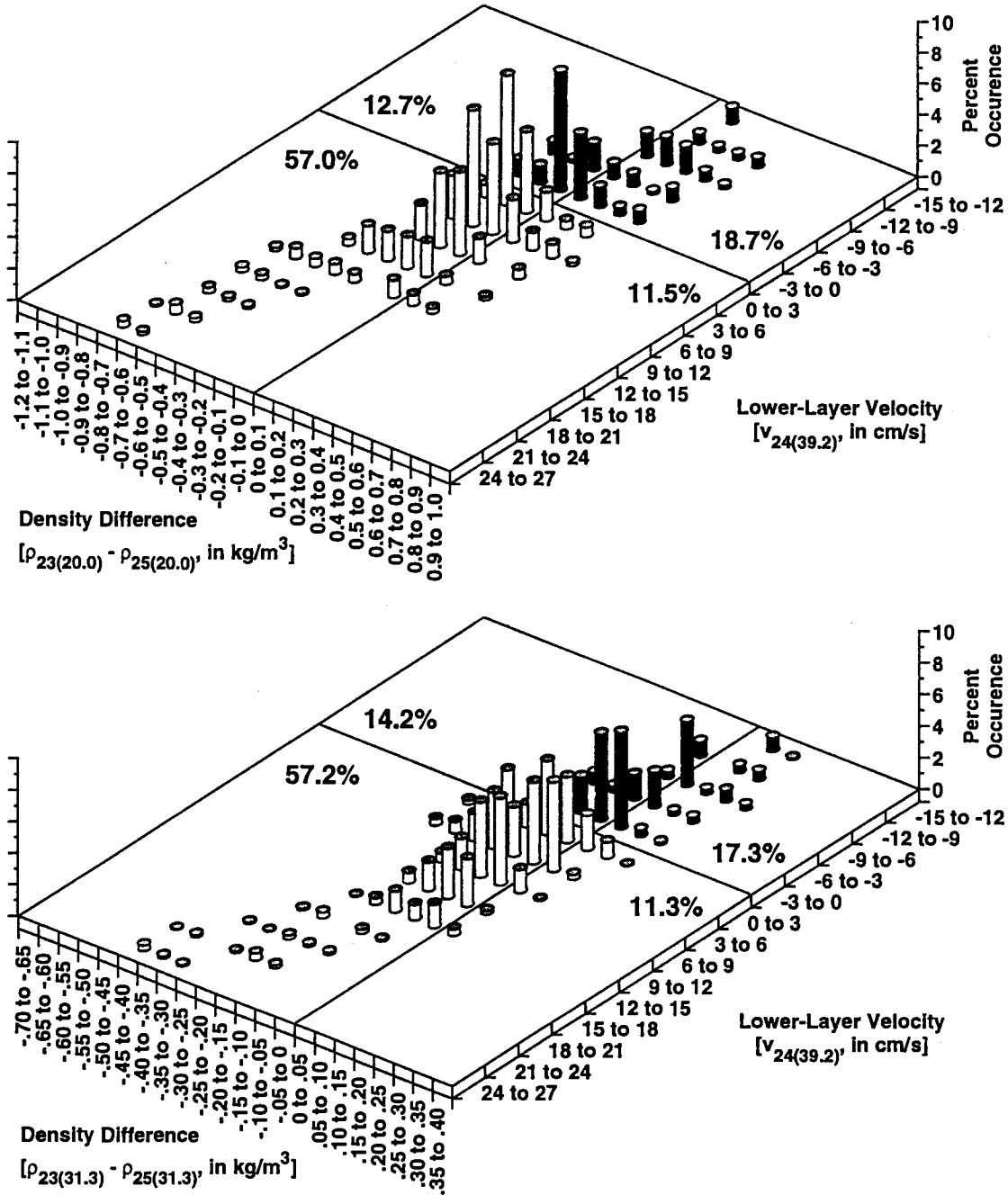

Figure 4.7. As in Fig. 4.6, at the middle (20.0 m, top panel) and bottom (31.3 m, bottom panel) depth levels during 1989. The bottom-level temperatures were recorded at slightly different depths (29.8 and 31.9 m), and were linearly interpolated to a common depth (31.3 m) for the density computation.

CHAPTER V

DISCUSSION OF THE STRATIFIED VOLUME EXCHANGES

Certainly, the major mechanism influencing the stratified volume exchanges and internal hydraulics in Deaths Door Passage is the previously-described large-amplitude semidiurnal internal waveform (Figs. 3.5 and 3.6). Using a value of 15 km = 15,000 m (estimated from Fig. 3.5) for the wavelength L indicates that such a wave would propagate as a shallow-water wave in the passage (depth ≈ 30 m). The internal wave speed c to first approximation for long waves in a two-layer fluid is (Lamb, 1932, Art. 231)

$$c^2 = g \cdot \frac{h_1 h_2}{h_1 + h_2} \cdot \frac{\rho_1 + \rho_2}{\rho_2} \qquad (7)$$

where the upper and lower layers are indicated by the subscripts 1 and 2, respectively, ρ are densities, h are layer thicknesses, and g = 10 m/s^2. From Fig. 3.5, using values of ρ_1 = .99833 (20°C), ρ_2 = .99986 (8°C), and $h_1 = h_2$ = 15 m, yields c = 0.34 m/s. The period T of the observed internal waveform (Fig. 3.5) in the passage is T = L / c = 44,100 s = 12.3 hrs, which is very close to the semidiurnal tide period (12.4) observed in the current records (Fig. 3.6, for example). Thus, the thermocline in Deaths Door Passage typically oscillates as a semidiurnal internal waveform with L ≈ 15.0 km and T ≈ 12.4 hrs, and such a thermocline oscillation would be expected to generate internal waves which would propagate at speed c = 0.34 m/s ≈ 29 km/day away from the passage.

The best example of the large-amplitude semidiurnal internal tide wave and the associated lower-layer currents in Deaths Door Passage is shown in Fig. 3.10 during Aug. 1-6. In the lower layer, the correlation of flooding tidal currents with warming

temperatures (depressed thermocline) and ebbing with cooling (elevated thermocline) can be observed during the periods between slack water, or between the peaks and troughs in the semidiurnal temperature oscillations (specifically from Fig. 4.2, the velocity leads the temperature by a phase angle of 48°). The correlations are consistent with wind and rotation effects (Figs. 2.7, 2.8, and 2.9) in the case of southwesterly winds (observed Aug. 1-6, Fig. 3.6). In this case, the upwelled thermocline in Lake Michigan and downwelled in Green Bay results in lower-layer inflow and a thermocline tilted downward towards Deaths Door Passage. In this situation, flooding (inflowing) tidal currents would strengthen the lower-layer inflow and thermocline tilt, resulting in a very depressed thermocline and thus warm temperatures in Deaths Door Passage. In the converse situation, ebbing (outflowing) tidal currents would weaken the lower-layer inflow and thermocline tilt, resulting in an elevated thermocline and cooler temperatures in the passage. Thus in Deaths Door Passage, the observed flooding-warming and ebbing-cooling correlations between the tidal currents and water temperatures are associated with the persistent internal semidiurnal thermocline oscillation (waveform) observed there.

The internal waveform in Deaths Door Passage is an internal bore (hydraulic jump) resulting from the sharp pressure drop encountered by lower-layer water as it intrudes into Green Bay from Lake Michigan. The internal bore ($G > 1$) is observed to persist in this passage during the stratified season, and thus the lower-layer inflows and two-layer exchange flows through Deaths Door Passage are maximal (when $G > 1$), as described by Armi and Farmer (1987). Another outstanding two-layer exchange event with a minimal barotropic component occurred in Deaths Door Passage during Aug. 13-14 (Fig. 3.9). During this event, the strongest lower-layer currents corresponded with the weakest upper-layer currents, and the strongest upper-layer currents corresponded with the weakest lower-layer current. This behavior is consistent with the vertical transfer of horizontal momentum between the two layers resulting from the supercritical flow ($G > 1$) generated by an internal bore. The remainder of this discussion includes sample

computations of composite Froude numbers for the observed two-layer exchange flows, and estimation of sample scaling values for the terms in the equation of motion.

The strong two-layer exchanges, homogenized layers, and intense thermocline observed in the raw data during Aug. 3-4 (Figs. 3.10 and 3.11) provide an excellent opportunity to compute sample composite Froude numbers G using Equation (4). Using values of ρ_1 and ρ_2 for pure water at 5.5 and 20.5°C, respectively, yields a value of $g' = .016$ m/s^2, and observations (Fig. 3.11) show the thermocline at about mid-depth, i.e., $y_1 = y_2 = 20$ m in Rock Island Passage. Using the approximate observed values (Fig. 3.10) of $u_1 = 0.1$ and $u_2 = -0.2$ m/s from Rock Island Passage during Aug. 3-4 yields a value of $G = 0.4$. Similarly, using approximate observed values of $y_1 = y_2 = 15$ m and $u_1 = 0.1$ and $u_2 = -0.3$ m/s from Deaths Door Passage yields $G = 0.65$. Finally, using values (data not shown) of $u_1 = 0.0$ and $u_2 = -0.2$ m/s from St. Martin Island Passage yields $G = 0.25$.

Another two-layer exchange event suited to sample composite Froude number computation is shown in Fig. 3.12 during the period Sept. 19-21. For Deaths Door, Rock Island, and St. Martin Island Passages, respectively, using values of $g' = .010$, .012, and .012, $y_1 = y_2 = 15$, 20, and 15 m, $u_1 = 0.03$, 0.05, and 0.03 m/s, and $u_2 = -0.4$, -0.15, and -0.07 m/s yields values of $G = 1.0$, 0.32, and 0.18. Thus at the narrowest section (hydraulic control point) of each passage, strong two-layer exchange flow speeds can be critical and supercritical in Deaths Door Passage, possibly approach critical in Rock Island Passage, and rarely if ever approach critical in St. Martin or Poverty Island Passages. The presence of the critical and supercritical flows indicates that the associated exchange is maximal (Armi and Farmer, 1987), but the mooring array (Fig. 1.2) was not designed specifically to test for maximal or submaximal flows. Considering the large velocities observed in Deaths Door Passage, there is reason to assume that the two-layer exchange through the passage is maximal. In Rock Island

Passage the two-layer exchange may be maximal sometimes, and in St. Martin Island Passage observations of subcritical flows suggest submaximal exchange.

As a final comparison of observations with theory, the cross-passage (x), along-passage (y), and vertical (z) momentum equations (see Fig. 2.8 for definition of axes) and the continuity equation are given respectively in Equations (8a), (8b), (8c), and (8d):

$$\frac{\delta u}{\delta t} + u\frac{\delta u}{\delta x} + v\frac{\delta u}{\delta y} + w\frac{\delta u}{\delta z} - fv = -\frac{1}{\rho}\frac{\delta P}{\delta x} + A_H\left(\frac{\delta^2 u}{\delta x^2}+\frac{\delta^2 u}{\delta y^2}\right) + A_V\frac{\delta^2 u}{\delta z^2} \quad (8a)$$

$$\frac{\delta v}{\delta t} + u\frac{\delta v}{\delta x} + v\frac{\delta v}{\delta y} + w\frac{\delta v}{\delta z} + fu = -\frac{1}{\rho}\frac{\delta P}{\delta y} + A_H\left(\frac{\delta^2 v}{\delta x^2}+\frac{\delta^2 v}{\delta y^2}\right) + A_V\frac{\delta^2 v}{\delta z^2} \quad (8b)$$

$$\frac{\delta w}{\delta t} + u\frac{\delta w}{\delta x} + v\frac{\delta w}{\delta y} + w\frac{\delta w}{\delta z} = -\frac{1}{\rho}\frac{\delta P}{\delta z} + A_H\left(\frac{\delta^2 w}{\delta x^2}+\frac{\delta^2 w}{\delta y^2}\right) + A_V\frac{\delta^2 w}{\delta z^2} \quad (8c)$$

$$\frac{\delta u}{\delta x} + \frac{\delta v}{\delta y} + \frac{\delta w}{\delta z} = 0 \quad (8d)$$

These equations govern the motions of an incompressible, rotating, frictional, non-linear fluid, assuming that the horizontal (A_H) and vertical (A_V) turbulent viscosity coefficients are much greater that the molecular viscosity coefficient (Pedlosky, 1986). Assuming the vertical velocity (w) is negligible and denoting scaling values with capital letters yields the continuity equation $\Delta U/\Delta X = -\Delta V/\Delta Y$, and the cross- and along-passage momentum equations (9a) and (9b):

$$\frac{\Delta U}{\Delta T} : U\frac{\Delta U}{\Delta X} : V\frac{\Delta U}{\Delta Y} : fV = \frac{1}{\rho}\frac{\Delta P}{\Delta X} : A_H\left(\frac{\Delta U}{\Delta X^2}+\frac{\Delta U}{\Delta Y^2}\right) : A_V\frac{\Delta U}{\Delta Z^2} \quad (9a)$$

$$\frac{\Delta V}{\Delta T} : U\frac{\Delta V}{\Delta X} : V\frac{\Delta V}{\Delta Y} : fU = \frac{1}{\rho}\frac{\Delta P}{\Delta Y} : A_H\left(\frac{\Delta V}{\Delta X^2}+\frac{\Delta V}{\Delta Y^2}\right) : A_V\frac{\Delta V}{\Delta Z^2} \quad (9b)$$

Pedlosky (1986) cites ranges (in m^2/s) of $10^1 < A_H < 10^4$ and $10^{-3} < A_V < 10^{-1}$ for estimates of the turbulent viscosity coefficients in the ocean, but estimates made from observations in lakes and oceans (Saylor, 1981, and Okubo, 1971) indicate more realistic ranges of $10^{-2} < A_H < 10^1$, and $10^{-5} < A_V < 10^{-2}$. Since both horizontal and vertical friction are expected to be important in the steeply-sloped bay mouth passages (Fig. 1.2),

values at the upper ends of these ranges ($A_H = 10^1$ and $A_V = 10^{-2}$) are used for the subsequent scale analysis.

For stratified water masses, Equations (9a) and (9b) must be separated into baroclinic (from thermocline fluctuations) and barotropic (from water surface level fluctuations) components. For two-layer exchange events, the barotropic component is assumed to be small so that the pressure gradient is associated mostly with the internal density difference (Fig. 2.8). For single-layer exchange events the barotropic component may dominate, and in this case small cross-passage surface level differences are likely to be balanced mostly by rotation effects. For example, using the values $\bar{u} = 0.2$ m/s and $w = 5000$ m in Equation (2) yields $\Delta\zeta = 0.01$ m = 1 cm, which is at or below the level of detection.

Estimation of the gradient terms in Equations (9a) and (9b) was not a consideration in the mooring array design (Fig. 1.2), but placement of the moorings at central locations within the passages allows for several simplifying assumptions (the scale values cited in the following discussion are for Rock Island Passage). The cross-passage gradients of velocity (U and V, from Fig. 3.4) are estimated by assuming the velocity ranges from zero to its maximum value over a distance ΔX (= 1000 m, Fig. 1.2) less than the distance between shore and the passage center. The along-passage gradients of velocity are estimated by assuming the velocity ranges from zero to its maximum value over the distance ΔY (= 2500 m) between open water and the passage center. The vertical gradients of velocity are estimated by assuming the velocity shear between the upper- and lower-layer velocities occurs within a layer of thickness ΔZ (= 10 m, from Figs. 3.11 and 3.13) comparable to the thermocline thickness.

The cross-passage pressure gradient ($\Delta P/\Delta X$) may be estimated using a two-layer density model (Fig. 2.8) and the hydrostatic approximation, so that $\Delta P = gh(\rho_2 - \rho_1)$. The observations (Fig. 3.3) showed large temperature differences (up to 12°C) across the

width (10 km) of the bay mouth (about 40 m depth), so a reasonable assumption is that $|h/\Delta X| \approx 20$ m/10 km. For example, using a typical value of $\rho_2-\rho_1 = 1.0$ kg/m^3 yields:

$$\frac{1}{\rho}\frac{\Delta P}{\Delta X} = \frac{gh(\rho_2-\rho_1)}{\rho\Delta X} \approx \frac{10\ \text{m/s}^2(20\ \text{m})(1.0\ \text{kg/m}^3)}{(1000\ \text{kg/m}^3)10000\ \text{m}} = 2 \times 10^{-5}\ \text{m/s}^2$$

Aside from the two XBT transects (Fig. 3.5), there is no other information about $\Delta P/\Delta Y$, so for the scaling argument it will be assumed that $\Delta P/\Delta Y = \Delta P/\Delta X$.

With all gradients defined, it is now possible to estimate magnitudes for the scale terms in Equations (9a) and (9b) using the observations. The temperatures T_1 and T_2 are from 22(20.0) and 25(20.0) in Fig. 3.3, and are converted to densities ρ_1 and ρ_2 using Chen and Millero (1986). Lower-layer velocities U and V are from 24(39.2 or 20.0), and upper-layer are from 24(12.0). For example, using values from the strong two-layer exchange event occurring during Aug. 2-8 (with $T_1 = 8$ and $T_2 = 16$°C) gives:

$$\Delta P/\rho\Delta X = \Delta P/\rho\Delta Y \approx \frac{10\ \text{m/s}^2(20\ \text{m})(0.9\ \text{kg/m}^3)}{(1000\ \text{kg/m}^3)10000\ \text{m}} = 2 \times 10^{-5}\ \text{m/s}^2$$

$$fV \approx (10^{-4}\ \text{s}^{-1})(0.25\ \text{m/s}) = 3 \times 10^{-5}\ \text{m/s}^2$$
$$fU \approx (10^{-4}\ \text{s}^{-1})(0.05\ \text{m/s}) = 5 \times 10^{-6}\ \text{m/s}^2$$

$$A_H(\Delta U/\Delta X^2) \approx 10^1\ \text{m}^2\text{/s}\ (0.05\ \text{m/s} / (1000\ \text{m})^2) = 5 \times 10^{-7}\ \text{m/s}^2$$
$$A_H(\Delta V/\Delta X^2) \approx 10^1\ \text{m}^2\text{/s}\ (0.25\ \text{m/s} / (1000\ \text{m})^2) = 3 \times 10^{-6}\ \text{m/s}^2$$

$$A_V(\Delta U/\Delta Z^2) \approx 10^{-2}\ \text{m}^2\text{/s}\ (0.03\ \text{m/s} / (10\ \text{m})^2) = 3 \times 10^{-6}\ \text{m/s}^2$$
$$A_V(\Delta V/\Delta Z^2) \approx 10^{-2}\ \text{m}^2\text{/s}\ (0.35\ \text{m/s} / (10\ \text{m})^2) = 4 \times 10^{-5}\ \text{m/s}^2$$

$$V(\Delta U/\Delta Y) \approx 0.25\ \text{m/s}\ (0.05\ \text{m/s} / 2500\ \text{m}) = 5 \times 10^{-6}\ \text{m/s}^2$$
$$V(\Delta V/\Delta Y) \approx 0.25\ \text{m/s}\ (0.25\ \text{m/s} / 2500\ \text{m}) = 3 \times 10^{-5}\ \text{m/s}^2$$

$$\Delta U/\Delta T \approx 0.05\ \text{m/s} / 2\ \text{days} = 3 \times 10^{-7}\ \text{m/s}^2$$
$$\Delta V/\Delta T \approx 0.25\ \text{m/s} / 2\ \text{days} = 1 \times 10^{-6}\ \text{m/s}^2$$

so that Equations (9a) and (9b) yield the following cross- and along-channel balances:

3×10^{-7}	:	5×10^{-6}	:	3×10^{-5}	=	2×10^{-5}	:	5×10^{-7}	:	3×10^{-6}		CROSS
1×10^{-6}	:	3×10^{-5}	:	5×10^{-6}	=	2×10^{-5}	:	3×10^{-6}	:	4×10^{-5}		ALONG
time-dependent		non-linear		rotation		pressure gradient		horizontal friction		vertical friction		

For this event, the along-passage pressure gradient is balanced by the friction and non-linear terms, while the cross-passage pressure gradient is mostly balanced by the rotation term. Rotation effects do not result in a purely "geostrophic balance" because the non-linear and friction terms are smaller by less than one order of magnitude.

The strong and relatively steady single-layer inflow event occurring during July 1-8 suggests the values V = 0.10 m/s, U = 0.02 m/s, T_1 = 11°C, and T_2 = 8°C, so that the cross- and along-channel balances for this event become:

$< 10^{-9}$	:	8×10^{-7}	:	1×10^{-5}	=	6×10^{-6}	:	2×10^{-7}	:	2×10^{-6}	CROSS
$< 10^{-9}$	:	4×10^{-6}	:	2×10^{-6}	=	6×10^{-6}	:	1×10^{-6}	:	1×10^{-5}	ALONG

All terms in the along-passage balance are of similar magnitude, but the cross-passage terms are overwhelmed by the rotation term, so in this case the along passage currents must be balanced at least in part by the cross-passage surface level tilt. For a final example, during Sept. 24-29 the exchange changed from single-layer outflow to weak inverse two-layer flow. Using the values (from the inverse two-layer portion) V = 0.10 m/s, U = 0.05 m/s, T_1 = 8°C, and T_2 = 11°C yields:

1×10^{-6}	:	2×10^{-6}	:	1×10^{-5}	=	6×10^{-6}	:	5×10^{-7}	:	5×10^{-6}	CROSS
2×10^{-6}	:	4×10^{-6}	:	5×10^{-6}	=	6×10^{-6}	:	1×10^{-6}	:	1×10^{-5}	ALONG

Again, the cross-passage terms are overwhelmed by the rotation term, and the along passage terms are similar. Also, it appears that the along-passage bottom friction term has been somewhat overestimated in all cases.

The scaling arguments suggest that during two-layer exchange events, a lower-layer, inflowing current magnitude of about V = 20 cm/s could be balanced by a thermocline tilt of about h = 20 m depth over ΔX = 10 km of distance, and that friction and non-linear effects could influence the balance. Using these scale values in Equation (6), the geostrophic relationship becomes $V/\Delta\rho = gh/\rho f\Delta X$ = 20 (cm/s)/(kg/m^3), which is very close to the range 25 to 33 (cm/s)/(kg/m^3) estimated from Fig. 4.6 for the H = 20.0 m depth level. Thus, currents through the bay mouth passages during the

stratified season are influenced by barotropic and baroclinic pressure gradients, rotation, friction, and non-linear effects, and with the present observations and analysis it is not possible to determine which force balance (if any) dominates.

In summary, two-layer exchange is a common occurrence within the mouth of Green Bay, but displays a wide degree of variability in frequency, intensity, and character, due to variability in the wind, barometric pressure, and other forcing mechanisms. Interannual variability in the exchange was exemplified by differences between the 1977 and 1989 observations. It is speculated that the 8-day thermocline oscillation in Green Bay observed during 1989 was atypical, in which case 1977 would represent a more typical stratified season. During both seasons, lower-layer inflow through Rock Island Passage and thermocline tilt across the mouth usually were observed to be consistent with rotation effects, and a persistent internal semidiurnal waveform was observed in Deaths Door Passage. Sample composite Froude numbers indicate that the internal waveform was associated with maximal exchange.

CHAPTER VI
CONCLUSIONS

The observations revealed that during the season of thermal stratification the exchange of waters between Green Bay and Lake Michigan is more complex and variable than previously believed. In Deaths Door Passage during 1977 the exchange flows ("inflow" is flow into the bay) were mostly (65%) two-layered (i.e., lower-layer inflow and upper-layer outflow). During 1989, two-layer exchange flows were observed less often (35%), but single-layer inflows revealed a much larger baroclinic component (i.e., enhanced lower-layer inflow) than during 1977. These differences were partly attributed to the effects of an 8-day period thermocline oscillation in Green Bay observed during 1989. These results indicate that the bay-lake exchange is highly variable from year to year, but the limitation of having only two observation seasons precludes more definitive conclusions about this interannual variability. Despite variability, total volume transport through the mouth passages during the 1977 and 1989 stratified seasons into and out of the lower and upper layers averaged 3500 $m^3/s \approx 0.3$ $km^3/day \approx 10$ $km^3/month$, thereby accelerating flushing of the bay.

The joint occurrences (Fig. 4.6) of strong lower-layer inflow in Rock Island Passage with relatively warm (light) water in Deaths Door and cold (dense) in St. Martin and Poverty Island Passages were common (about 60% of the season), consistent with rotation effects (Figs. 2.7 and 2.8). Joint occurrences of inverse two-layer exchange (i.e., lower-layer outflow) with relatively cold water in Deaths Door and warm in St. Martin and Poverty Island Passages also were observed (about 20% of the season). The joint occurrence distribution from the 20.0 m depth level (Fig. 4.6) indicated a geostrophic

relationship of $V/\Delta\rho = 25$ to 33 $(cm/s)/(kg/m^3)$ – where V is geostrophic velocity and $\Delta\rho$ is the cross-passage density difference – which agrees with the theoretical value. Also, periods of generally southwesterly winds were associated with enhanced inflow and two-layer exchange, qualitatively consistent with the effects of wind-induced upwelling (Fig. 2.9) in Lake Michigan outside the Green Bay mouth.

An unexpected discovery was the existence of a persistent, large-amplitude (≈20 m), semidiurnal internal waveform in Deaths Door Passage, consistent with the flooding-warming and ebbing-cooling correlations observed continuously between the semidiurnal tidal currents and temperature oscillations in that passage. The general dynamics of such a waveform were explained in terms of an internal hydraulic jump (bore) occupying the passage (due to the stratified and two-layer exchange flows occurring there), and being influenced by the barotropic semidiurnal tidal oscillation. Observations substantiated with a sample computation indicated that the semidiurnal internal waveform has a length ≈ 15 km (see Fig. 3.5) and an associated wave speed ≈ 29 km/day. Sample computations of internal Froude number revealed supercritical internal flows in Deaths Door Passage, implying that maximal two-layer exchange (Armi and Farmer, 1987) occurs in this passage.

Scatter plots and samples of the raw data showed that the frequency, intensity, and characteristics of the two-layer exchange in each passage varied widely between the 1977 and 1989 seasons. Specifically, in Deaths Door Passage occurrences of two-layer, single-layer in, single-layer out, and inverse two-layer flows respectively were 65, 10, 12, and 13% during 1977, and 35, 30, 22, and 13% during 1989. In Rock Island Passage the corresponding occurrences were 44, 29, 10, and 17% during 1977, and 20, 46, 17, and 17% during 1989. Thus, despite the interannual variability observed during the 1977 and 1989 seasons, lower-layer (baroclinic) inflows and two-layered exchange flows dominated the volume exchanges between the bay and lake during these seasons.

The results of the present investigation indicate that exchanges of bay and lake waters are substantial, promoting flushing of the bay and improving water quality there. It was noted in Chapter I that water quality in the southern half of the bay remains poor despite the substantial flushing. A likely explanation for the poor water quality is that exchanges of water between the bay and lake are much greater than exchanges between the northern and southern halves of the bay. Miller and Saylor (1992) computed a value of 900 $m^3/s \approx 0.08$ $km^3/day \approx 2.5$ $km^3/month$ for the total volume transport of lower layer water into the bay's southern half. Thus, during 1989 volume exchanges between the lake and northern bay were observed to be about four times larger than exchanges between the northern and southern halves, thereby decreasing the overall efficiency of the flushing towards the shallow bay head.

In summary, a major factor controlling the exchanges of lower-layer waters (and thus flushing of the bay) between Green Bay and Lake Michigan is the thermocline tilt (density differences) in the region of the bay mouth passages. The along-passage thermocline tilt drives inflow of cool and dense lake water into the bay hypolimnion, and the cross-passage tilt responds to this inflow via rotation (Fig. 2.7), friction, and non-linear effects. Flow variability is induced by wind-driven upwelling and downwelling (Fig. 2.9) in the bay mouth region, an 8-day thermocline oscillation in Green Bay, and a semidiurnal internal waveform in Deaths Door Passage. An average transport value of about 10 $km^3/month$ computed for the 1989 season showed that flushing of the entire volume of water in the bay with lake water occurs at least once or twice during a typical stratified season. However, the efficiency of the flushing is decreased by the bathymetric constriction between the northern and southern halves of the bay.

APPENDIX

To compute the volume transport through the passages using the measured current velocities, a simple model was derived. Basically, a computed velocity profile (Fig. A-1) is multiplied by the measured cross-sectional area of each passage (Figs. A-2 to A-6) to yield a transport value. The main simplifying assumptions are that the flow has no cross-passage structure, and the velocities can be linearly interpolated from surface to bottom to yield a velocity profile, as shown in Fig. A.1.

Passage	x_{pass} (km)	x_{sbl} (km)	x_{therm} (km)	x_{mid} (km)	z_{pass} (m)	z_{mid} (m)	A_{up} (m^2)	A_{mid} (m^2)	A_{bot} (m^2)
W. Chambers cbl	1.7	0.0	0.9	-	15	-	19500	-	-
W. Chambers	7.2	0.5	7.1	5.7	33	23	92250	47200	40350
E. Chambers	2.0	0.0	0.9	-	20	-	21750	-	-
Death's Door	2.2	0.0	1.6	1.2	34	24	28500	12600	10300
Rock Is.	4.0	0.2	3.1	2.0	44	34	47250	44650	16000
St. Martin Is.	2.5	0.1	1.9	1.3	37	27	30000	18000	10600
Poverty Is.	4.0	0.2	2.5	-	24	-	42750	-	-

Table A.1. Measured dimensions and computed areas of the passages.

The passage cross-sections shown in Figs. A.2 to A.6 were measured from navigational charts. Each passage is divided into an upper, middle, and lower layer, as shown in Fig. A.1. The widths and depths defined in Fig. A.1 were measured for each passage and are listed in Table A.1. x_{therm} is taken to be the passage width at 15 m depth, x_{mid} is taken to be the width at 10 m above the bottom, and x_{sbl} is taken to be $0.05x_{pass}$ for the passages wider than 2.2 km (see Table A.1). x_{sbl} is used to help lessen the uncertainty associated with the no cross-passage flow structure assumption, and the W. Chambers cbl (Table A-1 and Fig. A.2, mooring 17) represents the coastal boundary layer observed there.

The velocity profiles are computed by simple linear interpolation of the measured velocities to 1-m depth intervals (see Fig. A.1). The surface velocity is taken to be 10% larger than the uppermost measured velocity in order to crudely represent surface wind drag, and the bottom velocity is set equal to the lowermost measured velocity to represent a robust deep flow. The computed profiles usually indicate either a single-layer or two-layer flow structure, and thus the computed transports are separated into upper layer, lower layer, and "barotropic" (single layer) components based upon the current directions at the top and bottom levels. Since this transport computation is based entirely on velocity information, the computed single-layer flows are descriptively but incorrectly referred to as "barotropic", because they usually indicate a substantial amount of shear corresponding to the observed thermal stratification.

The passage widths at each 1-m depth interval are given by

$$L = x_{pass} - 2x_{sbl} - \frac{z}{z_{therm}}(x_{pass}-x_{therm}) \qquad \text{for } 0 \le z \le z_{therm}$$

$$L = x_{therm} - 2x_{sbl} - \frac{(z-z_{therm})}{(z_{mid}-z_{therm})}(x_{therm}-2x_{sbl}-x_{therm}) \qquad \text{for } z_{therm} < z \le z_{mid}$$

$$L = \text{measured value} \qquad \text{for } z_{mid} < z < z_{pass}$$

where all variables are defined in Fig. A.1 and listed in Table A.1. Using v_t, v_m, and v_b to represent the top, middle, and bottom measured velocities, the computed velocities at each 1-m depth interval are given by

$$V = v_t + \frac{(z_t-z)}{(z_t)} v_t\, 0.1 \qquad \text{for } 0 \le z \le z_t$$

$$V = v_t - \frac{(z-z_t)}{(z_m-z_t)}(v_t-v_m) \qquad \text{for } z_t < z \le z_m$$

$$V = v_m - \frac{(z-z_m)}{(z_b-z_m)}(v_m-v_b) \qquad \text{for } z_m < z \le z_b$$

$$V = v_b \qquad \text{for } z_b < z < z_{pass}$$

where z_t, z_m, and z_b are the depths of the measured velocities (see Figs. A.1 through A.6). Thus, for each 1-m depth interval the transport (in km^3/s) is the product of L (in km) and V (in km/sec), and the total transport is the sum of the 1-m transports from top to bottom.

The velocities used for the transport computation are 40-hour low-pass filtered and 12-hour averaged, and thus the each computed transport value represents a 12-hour period. For W. Chambers Island Passage (Fig. A.2), transports are computed for moorings 18 and 19 using half the indicated cross-sectional area, thus helping to lessen uncertainty associated with the computation. For Deaths Door Passage (Fig. A.4), top velocities are used from mooring 22 and middle and bottom velocities from mooring 23, because lower-layer inflow is stronger at mooring 23 and upper-layer outflow is stronger at mooring 22, as described in Chapter III. For Poverty Island Passage (Fig. A.6), half the velocity from mooring 25 is used for the transport computation, and thus the transports computed for this passage probably should be disregarded. Due to this lack of confidence, similar estimates were not performed for other shallow regions (e.g. Fig. A.6)

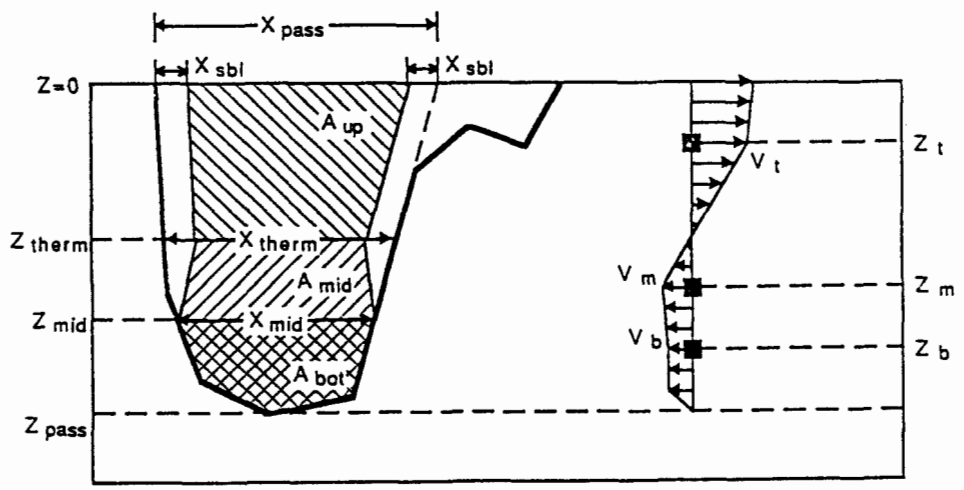

Figure A.1.

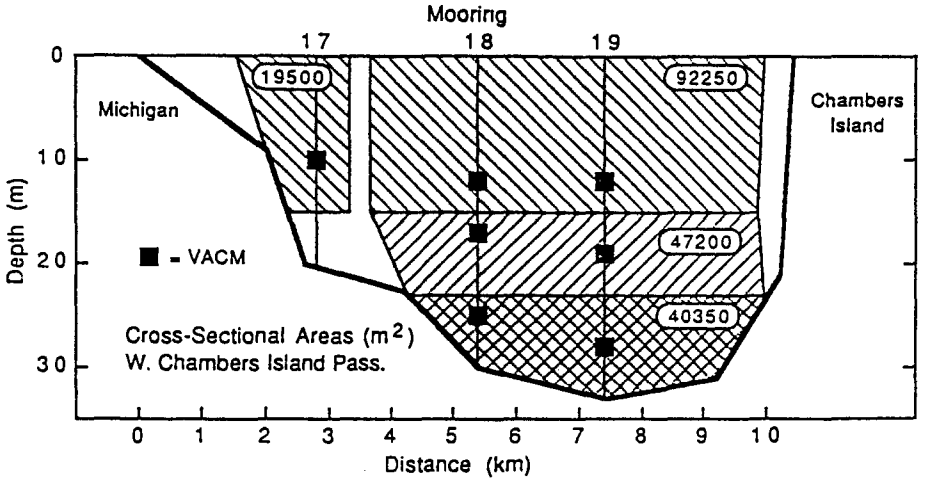

Figure A.2

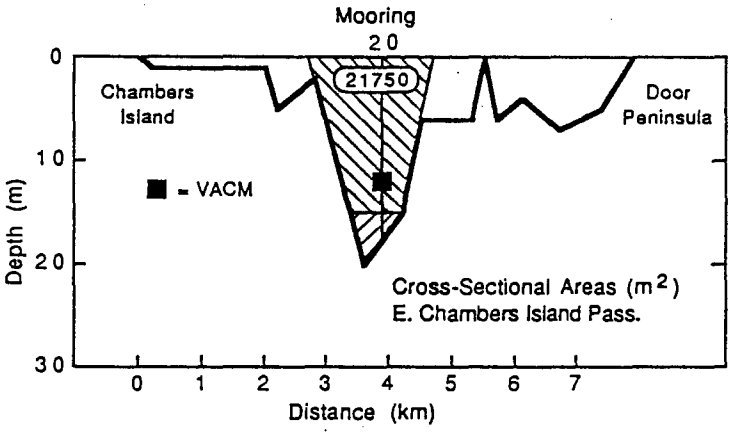

Figure A.3.

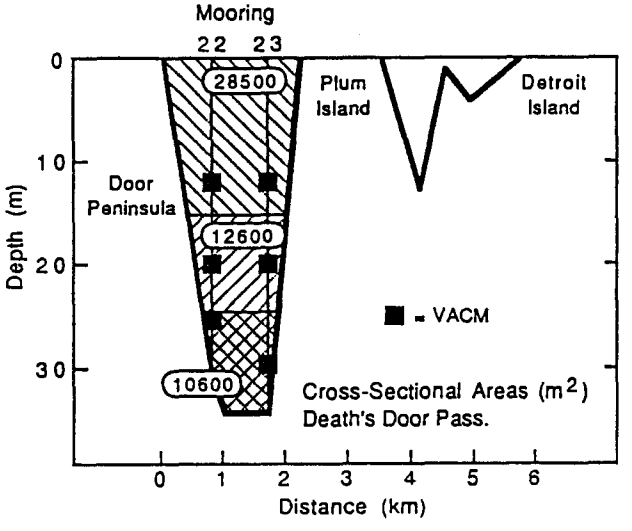

Figure A.4.

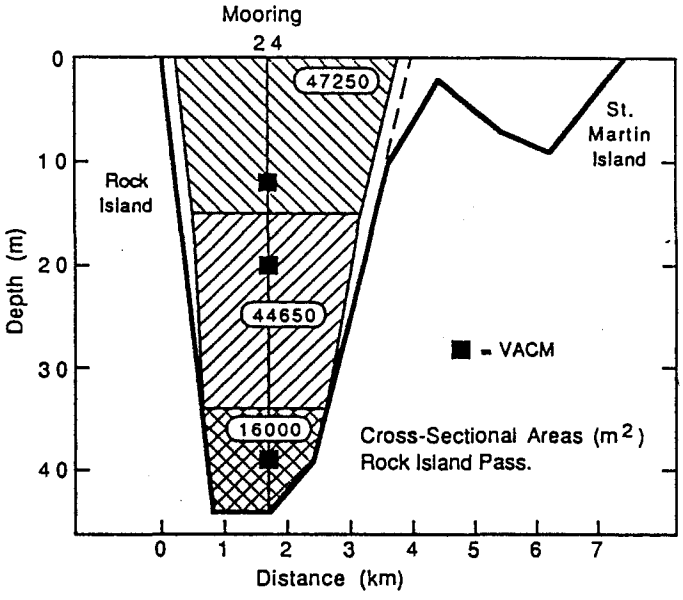

Figure A.5

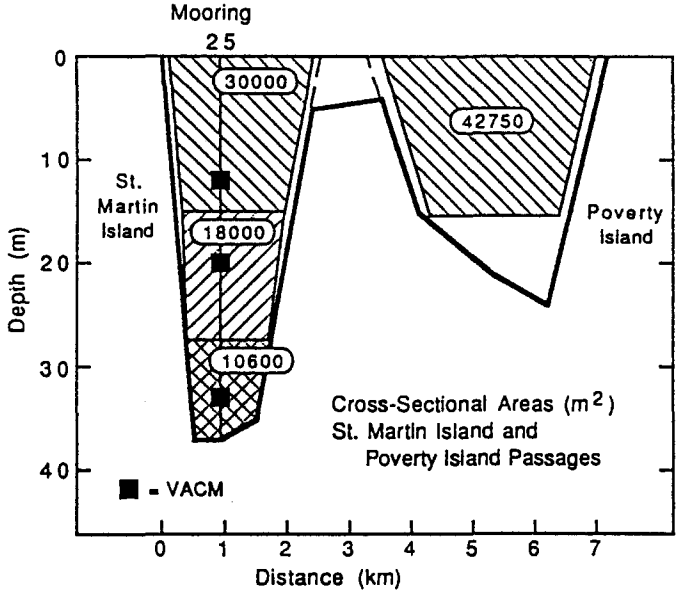

Figure A.6.

BIBLIOGRAPHY

Armi, L. The hydraulics of two flowing layers with different densities. Journal of Fluid Mechanics **163**:27-58 (1986).

Armi, L., and D.M. Farmer. Maximal two-layer exchange through a contraction with barotropic net flow. Journal of Fluid Mechanics **164**:27-51 (1986).

Armi, L., and D.M. Farmer. A generalization of the concept of maximal exchange in a strait. Journal of Geophysical Research **92**(C13):14679-14680 (1987).

Baines, P.G. Internal tides, internal waves, and near-inertial motions. in Baroclinic Processes on Continental Shelves. ed. C.N.K. Mooers, American Geophysical Union, Washington, DC, 19-32 (1986).

Bennett, J.R. The circulation of large lakes. in Upwelling Ecosystems, ed. R. Boje and M. Tomczak, Springer-Verlag, Berlin, 223-234 (1978).

Chen, C.T., and F.J. Millero. Precise thermodynamic properties for natural waters covering only the linmological range. Limnology and Oceanography **31**(3):657-662 (1986)

Clarke, A.J. Application of a frictional channel flow theory to flow in the Prince of Wales Channel, Torres Strait. Journal of Physical Oceanography **20**(6):890-899 (1990).

Csanady, G.T. Lateral momentum flux in boundary currents. Journal of Physical Oceanography **5**(4):705-717 (1975).

Eid, B.M.F. Investigation into interfacial transports and exchange flows for lake models. Ph.D. thesis, McMaster University, Hamilton, Ontario (1981).

Farmer, D.M., and L. Armi. Maximal two-layer exchange over a sill and through the combination of a sill and contraction with barotropic flow. Journal of Fluid Mechanics **164**:53-76 (1986).

Farmer, D.M., and J.S. Møller. Measurements and modelling in the Great Belt: a unique opportunity for model verification. in The Physical Oceanography of Sea Straits, ed. L.J. Pratt, Kluwer Academic Publishers, Netherlands, 125-152 (1990).

Garrett, C., and B. Petrie. Dynamical aspects of the flow through the Strait of Belle Isle. Journal of Physical Oceanography **11**(3):376-393 (1981).

Garrett, C., and B. Toulany. Sea level variability due to meteorological forcing in the northeast Gulf of St. Lawrence. Journal of Geophysical Research **87**(C3):1968-1978 (1982).

Gill, A.E. Adjustment under gravity in a rotating channel. Journal of Fluid Mechanics **77**(3):603-621 (1976).

Gill, A.E. The hydraulics of rotating channel flow. Journal of Fluid Mechanics **80**(4):641-671 (1977).

Gill, A.E. Atmosphere-Ocean Dynamics, Academic Press, Inc., New York, 662 pp., (1982).

Gottlieb, E.G., J.H. Saylor, and G.S. Miller. Currents and water temperatures observed in Green Bay, Lake Michigan, part I: winter 1988-1989, part II: summer 1989. NOAA Technical Memorandum ERL GLERL Contribution No. 713, NOAA Great Lakes Environmental Research Laboratory, Ann Arbor, 90 pp., (1990).

The Great Lakes Reporter. The Center for the Great Lakes, Chicago, IL, **6**(3):5-7 (1989).

Heaps, N.S., F.R.S. Mortimer, and E.J. Fee. Numerical models and observations of water motion in Green Bay, Lake Michigan. Philosophical Transactions of the Royal Society of London **A306**:371-398 (1982).

Hermann, A.J., P.B. Rhines, and E.R. Johnson. Nonlinear Rossby adjustment in a channel: beyond Kelvin waves. Journal of Fluid Mechanics **205**:469-502 (1989).

Ippen, A.T. Channel transistions and controls. in Engineering Hydraulics, ed. H. Rouse, John Wiley and Sons, New York, 496-570 (1950).

Jacobs, S.J. On wind-driven lake circulation. Journal of Physical Oceanography 4(3):392-399 (1974).

Jenkins, G.M., and D.G. Watts. Spectral Analysis and Its Applications, Holden-Day, San Franscisco, 525 pp., (1968).

Ketchum, B.H. The exchanges of fresh and salt waters in tidal estuaries. Journal of Marine Research **10**(1):18-38 (1951).

Kraus, E.B., and J.S. Turner. A one-dimensional model of the seasonal thermocline. Tellus **19**(1):98-105 (1967).

LeBlond, P.H., and L.A. Mysak. Waves in the Ocean, Elsevier Scientific Publishing Company, New York, 602 pp., (1980).

Lamb, H. Hydrodynamics, Dover Publications Inc., New York, 738 pp. (1945).

Lawrence, G.A. On the hydraulics of Boussinesq and non-Boussinesq two-layer flows. Journal of Fluid Mechanics **215**:457-480 (1990).

McCormick, M.J., and G.A. Meadows. An intercomparison of four mixed layer models in a shallow inland sea. Journal of Geophysical Research 93(C6):6774-6788 (1988).

Miller, G.S., and J.H. Saylor. Currents and temperatures in Green Bay, Lake Michigan. Journal of Great Lakes Research **11**(2):97-109 (1985).

Miller, G.S., and J.H. Saylor. Water volume transport calculations in central Green Bay. NOAA Technical Memorandum, NOAA Great Lakes Environmental Research Laboratory, Ann Arbor (expected publication, 1992).

Modlin, R.F., and A.M. Beeton. Dispersal of Fox River water in Green Bay, Lake Michigan. Proceedings, 13th Conference on Great Lakes Research, Buffalo, NY, April 1970. International Association for Great Lakes Research, Ann Arbor, 468-476 (1970).

Mohammed-Zaki, M.A. Time scales in wind driven lake conditions. Journal of Geophysical Research **85**(C3):1553-1562 (1980).

Mooers, C.N.K., and R.L. Smith. Continental shelf waves off Oregon. Journal of Geophysical Research **73**(2):549-557 (1968).

Mortimer, C.H. Spectra of long surface waves and tides in Lake Michigan and at Green Bay, Wisconsin. Proceedings, 8th Conference of Great Lakes Research, Toronto, Canada,1965. Great Lakes Research Division Publ. No. 13, Ann Arbor, 304-325 (1965).

Mortimer, C.H. Lake hydronamics. Mitteilungen Internationale Vereinigung fuer Theoretishe und Angewandte Limnologie **20**:124-197 (1974)

Mortimer, C.H. Water movement, mixing, and transport in Green Bay, Lake Michigan. Proceedings, Green Bay Research Workshop, Green Bay, WI, September 1978. WIS-SG-78-234, University of Wisconsin Sea Grant Program, Green Bay, 10-56 (1978).

Munk, W.H., and E.R. Anderson. Notes on a theory of the thermocline. Journal of Marine Research **7**(4):276-295 (1948).

Neumann, G., and W.J. Pierson. Principles of Physical Oceanography, Prentice-Hall, Inc., Englewood Cliffs, NJ, 545 pp., (1961).

Oguz, T., E. Ozsoy, M.A. Latif, H.I. Sur, and U. Unluata. Modeling of hydraulically controlled exchange flow in the Bosphorus Strait. Journal of Physical Oceanography **20**(7):945-965 (1990).

Okubo, A. Oceanic diffusion diagrams. Deep Sea Research **18**(8):789-802 (1971).

Okubo, A., and M.J. Karweit. Diffusion from a continuous source in uniform shear flow. Limnolongy and Oceanography **14**(4):514-520 (1969).

Pickard, G.L., and W.J. Emery. Descriptive Physical Oceanography, Pergamon Press, New York, 249 pp. (1982).

Pedlosky, J. Geophysical Fluid Dynamics, Springer-Verlag, New York, 624 pp., (1984).

Pollard, R.T., P.B. Rhines, and R.O.R.Y. Thompson. The deepening of the wind mixed layer. Geophysical Fluid Dynamics **3**:381-404 (1973).

Pond, S., and G.L. Pickard. Introductory Dynamic Oceanography, Pergamon Press, New York, 241 pp. (1978).

Price, J.F., and R.A. Weller. Diurnal cycling: Observations and models of the upper ocean response to diurnal heating, cooling, and wind mixing. Journal of Geophysical Research **91**(C7):8411-8427 (1986).

Pratt, L.J. Geostrophic versus critical control in straits. Journal of Physical Oceanography **21**(5):728-732 (1991).

Rao, D.B., C.H. Mortimer, and D.J. Schwab. Surface normal modes of Lake Michigan. Calculations compared with spectra of observed water level fluctuations. Journal of Physical Oceanography **6**(4):575-588 (1976).

Rocha C., C.A., and A.J. Clarke. Interaction of ocean tides through a narrow single strait and narrow multiple straits. Journal of Physical Ocreangraphy **17**(12):2203-2218 (1987).

Saylor, J.H. Survey of Lake Michigan harbor currents. Proceedings, 7th Conference of Great Lakes Research, Toronto, Canada, April 1964. Great Lakes Research Division Publ. No. 11, Ann Arbor, 366-367 (1964).

Saylor, J.H., J.R. Bennett, P.C. Liu, R.L. Pickett, F.M. Boyce, C.R. Murthy, and T.J. Simons. Water Movements. in The International Field Year for the Great Lakes, ed. E.J. Auberts and T.L. Richards, NOAA Great Lakes Environmental Research Laboratory, Ann Arbor, 247-319 (1981).

Saylor, J.H., G.S. Miller, and E.S. Gottlieb. Near-resonant wind forcing of internal seiches in Green Bay, Lake Michigan. Journal of Marine Systems (expected publication, 1992).

Schwab, D.J. Storm Surge Studies on the Great Lakes. American Society of Civil Engineers Convention, Chicago, October 1978. ASCE Preprint no. 3353 (1978).

Shen, C.Y. The rotating hydraulics of the open-channel flow between two basins. Journal of Fluid Mechanics **112**:161-188 (1981).

Stern, M.E., J.A. Whitehead, and B.L. Hua. The intrusion of a density current along the coast of a rotating fluid. Journal of Fluid Mechanics **123**:237-265 (1982).

Stoker, J.J. Water Waves, Interscience Publishers, Inc., New York, 567 pp., (1957).

Stigebrandt, A. On the effect of barotropic current fluctuations on the two-layer transport capacity of a constriction. Journal of Physical Oceanography **7**(1):118-122 (1976).

Stommel, H., and H.G. Farmer. Abrupt change in width in two-layer open channel flow. Journal of Marine Research **11**(2):205-214 (1952).

Stommel, H., and H.G. Farmer. Control of salinity in an estuary by a transition. Journal of Marine Research **12**(1):13-20 (1953).

Tang, B. Fluctuating flow through straits of variable depth. Journal of Physical Oceanography **20**(7):1077-1086 (1990).

Toulany, B., and C. Garrett. Geostrophic control of fluctuating barotropic flow through straits. Journal of Physical Oceanography **14**(4):649-655 (1984).

United States Environmental Protection Agency. Green Bay/Fox River mass balance study. Great Lakes National Program Office Report No. 06-89, Chicago, IL, (1989).

Wang, P.F., and M. Zakikhani. "Hydrodynamic transport modeling of Green Bay, WI - two- and three-dimensional simulations". 34th Conference of the International Association of Great Lakes Research, State University of New York at Buffalo, June 1991 (unpublished conference presentation, 1991).

Whitehead, J.A., A. Leetmaa, and R.A. Knox. Rotating hydraulics of strait and sill flows. Geophysical Fluid Dynamics **6**:101-125 (1974).

Whitehead, J.A. Flow of a homogeneous rotating fluid through straits. Geophysical and Astrophysical Fluid Dynamics **36**:187-205 (1986).

Wood, I.R. A lock exchange flow. Journal of Fluid Mechanics **42**(4):671- 688 (1970).

Wright, D.G. Comments on "Geostrophic control of fluctuating barotropic flow through straits. Journal of Physical Oceanography **17**(12):2375-2377 (1987).